Title
Dynamic Regulation of Mammalian Cell Signaling through Optical Protein Clustering

Author
Bugaj, Lukasz Jan

Publication Date
2014

Peer reviewed|Thesis/dissertation

Dynamic Regulation of Mammalian Cell Signaling through Optical Protein Clustering

By

Lukasz Jan Bugaj

A dissertation submitted in partial satisfaction of the

requirements for the degree of

Joint Doctor of Philosophy

with the University of California, San Francisco

in

Bioengineering

in the

Graduate Division

of the

University of California, Berkeley

Committee in Charge:

Professor David Schaffer, Chair
Professor Ehud Isacoff
Professor Patricia Babbitt
Professor John Dueber

Spring 2014

Abstract

Dynamic Regulation of Mammalian Cell Signaling through Optical Protein Clustering

by

Lukasz Jan Bugaj

Joint Doctor of Philosophy in Bioengineering

with the University of California, San Francisco

University of California, Berkeley

Professor David Schaffer, Chair

Dynamic regulation of cell signaling can drive cellular decisions, whereby a cell can choose divergent fates based on the strength, timing, or location of even an individual protein signal. However, the chemical and genetic tools widely used to probe cell signaling suffer from poor spatiotemporal resolution and cannot easily recapitulate the dynamics with which protein signals affect cell fate choices. Optogenetic techniques have recently enabled rapid and reversible cellular protein activation through light inducible protein heterodimerization, homodimerization, and gene transcription within living cells. Protein oligomerization, however, represents a distinct and important mode of activation for numerous cell signaling events, yet its study and control remain challenging due to the lack of tools to inducibly modulate a protein's oligomeric state. In this dissertation, I will describe the discovery and characterization of a novel method to optically regulate protein oligomerization within cells. This discovery has allowed us precise control over intracellular signaling pathways and cell fate decisions that are a consequence of these signals.

Cryptochrome2 (Cry2) is a light sensitive protein that forms light-dependent oligomeric "photobodies" in *Arabidopsis thaliana*. We demonstrated that these photobodies can be formed inducibly, reversibly, and tunably in mammalian cells, and we co-opted Cry2 oligomerization to optically regulate mammalian signaling cascades. Using end-to-end protein fusions of Cry2 to specific signaling proteins, we first enabled optical control over the β-catenin pathway, achieving a higher transcriptional response than obtained with the natural pathway ligand Wnt 3a. We then used Cry2 clustering to robustly and dynamically activate RhoA signaling with light. To our knowledge this is the first demonstration of clustering as a mode of activation for this well-studied protein. We have also shown conservation of activation *via* clustering among Rho family members Rac1 and Cdc42, enabling photoactivation of all three GTPases through identical Cry2 fusions.

In subjecting multiple distinct signaling pathways to optical regulation *via* Cry2, we showed that Cry2 may be abstracted as a clustering module capable of regulating numerous signaling networks at nodes sensitive to clustering. Supporting and expanding on this hypothesis, we developed an extension of this method called Clustering Indirectly with Cryptochrome 2, or CLICR. CLICR enables Cry2-mediated clustering of binding partners, which can be applied to regulate both cytoplasmic and membrane-bound signaling proteins and, excitingly, can be engineered to modulate *endogenous* protein activity through fusion of an appropriate adapter molecule to the Cry2 module. We used this generalizable approach to optically cluster and regulate endogenous transmembrane receptor tyrosine kinase (RTK) and β-integrin activity with high spatiotemporal precision, enabling inducible and reversible control of transmembrane receptors without overexpression of exogenous signaling molecules. This methodology broadly extends optogenetic capabilities to a large class of endogenous intracellular and transmembrane signaling proteins important in cell fate decisions and disease progression.

In developing optogenetic Cry2 clustering, we demonstrated its utility in uncovering oligomerization as a mode of regulation for certain signaling proteins. Since the Rho GTPases were not known to be modulated in this manner, we further examined the mechanism by which clustering enhances Rho GTPase membrane translocation. We found that, although cluster-induced membrane translocation is dependent on interaction with its activating GEF enzyme, GEF catalysis is not necessary for this localization, while the presence of the C-terminal lipid tail is critical. We propose a model of activation based on these findings. Further, we developed sensitive methods for detection of cluster-induced GTPase activation, and we identify and test the role of putative elements postulated to enhance GTPase activity and inactivation upon oligomerization.

In addition to uncovering novel mechanistic protein activity, the Cry2 optogenetic tool has tremendous potential for studying the dependence of signaling dynamics on cell fate decisions. Adult neurogenesis is of great interest for ameliorating numerous neurodegenerative diseases, and β-catenin signaling plays a central role in this process. We demonstrated that, upon further protein engineering and illumination-hardware optimization, Cry2 clustering could be used to strongly induce β-catenin signal within neural stem cells and enable optogenetic neurogenesis. We further showed that neurogenesis could be tuned by modulating the activating light source, setting the stage for studies interrogating the neural stem cell response to defined timing and intensity of the β-catenin pathway, yielding insight into how these cells may integrate neurogenic cues in their native stem cell niche.

In summary, we have developed a modular, single-construct, and genetically encoded method to rapidly and reversibly induce oligomerization within mammalian cells, and we have shown its utility and portability in regulating several diverse proteins pathways on fast timescales in response to blue light illumination. We have used Cry2 to both uncover novel protein signaling properties and to regulate and interrogate important cell fate decisions, and we anticipate its modularity will allow broad expansion of the optogenetic toolbox to a large class of signaling proteins important in cell fate decisions and disease progression.

Table of Contents

Table of Figures

Chapter 2

Chapter 3

Chapter 4

Chapter 5

Acknowledgements

It has been a rich and fulfilling six years at Berkeley, and I would like to acknowledge and thank those most responsible for having made this part of my life so remarkable.

My immense gratitude goes to David Schaffer, who has been an exemplary advisor and mentor over the years. He provided me the freedom to be creative and explore, but with the focus necessary to achieve, and his ever-present support and advice was crucial to the ultimate success of both the work and my graduate experience.

Many thanks also go to my Qualifying Exam and Dissertation Committees, comprising Ehud Isacoff, Patricia Babbitt, and John Dueber. They have both challenged me and guided me through the more rigorous grad school milestones. In particular, John has been a wonderful source of feedback and advice through numerous conversations over the years.

Thank you to Atri Choksi, Colin Mesuda, and Shalmalee Pandit, my undergraduate helpers who helped me with realizing many of the experiments within this dissertation, but who also taught me many lessons in patience, teaching, and effective mentorship.

Outside of the lab, my great thanks go to my wife Ivel Morales, whom I affectionately refer to as my best result from graduate school. Aside from generally improving all aspects of my life, her understanding, patience, and support during the many failures and trying days were essential.

Thank you also to my mom Magdalena, my dad Jerzy, and my sisters Agata and Kasia, who, despite my sporadic (at best) attempts at communication, have remained understanding and supportive. Particular thanks also to my mother for lending her expertise for my many questions in statistical methodology, helping both me and other members of the lab. And thanks are in order to the newest family members Noah and Staś (and their parents) for brightening my daily life with adorable pictures and videos.

Thanks to all of the great and talented friends I have made in the in the Schaffer Lab and the Bay Area. Among the numerous people whom I have met, Alex Hughes, Tim Downing, Albert Keung, Priya Shah, Prashanth Asuri, Ashley Fritz, Noem Ramey, Melissa Kotterman, Dawn Spelke, Prajit Limsirichai, and Sisi Chen have all been excellent friends and have made the experience particularly colorful. The same is true of Grey Ballard, Vivek Gopalan, and Daniel Balke, who have enriched my life both through their friendship and through re-introducing me to the game of tennis.

To the above and the many, many others whom I could not name here, thank you!

Chapter 1

Optogenetic Tools for Probing Signaling Dynamics within Mammalian Cells

1.1 Introduction

Cellular behavior is regulated by protein and nucleic acid interactions within cells, where signaling cascades propagate and interact with each other in complex networks. In order to effect an astonishing number of cell behavioral programs with a relatively limited repertoire of signaling proteins, the cell can select combinations of signaling pathways as well as quantitatively vary the levels of activation of each in order to regulate or choose specific behaviors. Thus, the duration, strength, and context of a single signaling molecule are able to influence the system response and lead to differing cellular phenotypes and fates (*1*). For example, oscillations in the Hes1 transcription factor determine somite segmentation in developing vertebrate embryos (*2, 3*), transient versus sustained ERK1/2 signaling determines cell fate in differentiation of a model neural cell line (*4*), and the bi-stable nature of sonic hedgehog signaling allows the detection of threshold levels of signal to determine cell fate in an all-or-none fashion (*5-7*). The encoding and decoding of cell signaling dynamics has been reviewed (*8*). Such input-output relationships are of broad interest in many fields, including regenerative medicine, cancer, and immunology, among others, where understanding the precise cues that direct cell fate choices is critical for developing novel therapies. Unfortunately, it is challenging to make progress in learning how signaling dynamics instruct cellular processes due to the lack of tools with sufficient spatiotemporal resolution. Standard techniques are cumbersome and involve measuring cell response after static biochemical or genetic signal stimulation on the timescale of hours to days. Additionally, promiscuity of the stimulus may activate peripheral pathways and obscure the signal transmitted through a particular receptor of interest. Thus, developing new techniques to help elucidate the effect of signaling dynamics on cell behavior may both advance basic biological knowledge of signal transduction as well as provide information on how to best target and control signaling pathways for the next generation of targeted therapeutics.

Towards these aims, there exists great interest in developing photoactivatable protein systems to modulate cell signaling in real-time. Successful design of a light-controllable signaling protein – and thus a light-controllable signaling pathway – allows unparalleled control of the intensity, duration, and location of a signaling stimulus. Further, the stimulus would be highly orthogonal to natural cellular signaling pathways, as most mammalian cells possess no known light-responsive elements. Pioneering work by Miessenboeck, Isacoff, Boyden and Deisseroth demonstrated the power of this concept by successfully engineering light responsive neurons through the expression of light-sensitive ion channels in neural cells (*9-13*). The ability

to isolate the function of one cell type within a complex neural network *in vivo* has revolutionized the field of neurobiology (*14*). These advances ushered in the new field of optogenetics, a term that has now evolved to include any class of genetically encodable protein whose activity can be manipulated with light. Though seminal papers launching the field were published in 2005, the impact was immediate, and by 2010, Nature Methods recognized the field as for its annual "Method of the Year" award. In 2013, Miesenboeck, Deisseroth, Boyden, and others received the Brain Prize recognizing the impact of optogenetics in decoding complex neuronal networks. Analogously, there is anticipation that the development of tools to dissect complex networks of signaling proteins may yield similar advances in basic systems biology and in the application thereof throughout biological studies.

In this chapter, we review the current state of the art in genetically encodable optogenetic tools that have been engineered or co-opted for manipulating signaling phenomena in living mammalian cells. Categorized by mode of regulation, these tools fall into four main groups: allosteric or steric modulators, heterodimerizers, homodimerizers, and oligomerizers. Below we discuss each, including their mode of activation, their optical properties, and the strategies with which they've been implemented to regulate cell signaling within living mammalian cells.

1.2 Steric regulators

1.2.1 As LOV1

The Light-Oxygen-Voltage 2 (LOV2) domain from the *A. Sativa* phototropin1 protein is a naturally blue light sensitive domain that was among the first used for the development of optogenetic tools to study mammalian cell signaling. This small domain folds around the blue-light absorbing flavin mononucleotide (FMN), which, upon illumination, forms a covalent adduct with a reactive cysteine in the FMN binding pocket of LOV2 (*15*). Upon binding to the FMN, LOV2 undergoes a conformational change which propagates out to the surface of the protein, where a C-terminal helix (the Jα helix) is docked. This conformational change disrupts the interaction between the Jα helix and the LOV2 surface, and the helix unfolds (*16*). Light state conversion takes place within microseconds of illumination, and dark state reversion happens with a half-life on the order of 30s (*15*). The large light-induced conformational change coupled with fast temporal properties makes LOV2 an attractive photosensing/actuating module for regulation of mammalian signaling proteins. A number of groups have co-opted this protein for optogenetic control through steric regulation, as described below.

The first demonstration of a cytoplasmic optogenetic signaling protein was a photoactivatible Rac1 (PA-Rac1) by Wu, Hahn and colleagues (*17*). Here, the authors fused a constitutively active Rac1 to the C-terminus of the LOV2-Jα helix, with the hypothesis that in the dark state, the LOV2 domain would sterically block the Rac1 from downstream signal activation. Upon blue light illumination, the unfolding of the Jα helix would release this inhibition, allowing blue light defined Rac1 activity. The authors demonstrated the success of this design by inducing light-dependent membrane ruffles and lamellipodial extension within cells. Upon focal illumination, cells were induced to extend and move in a particular direction as defined by the light. This ability to spatially and temporally define Rac1 activation and cellular

movement has since been used in many *in vitro* and *in vivo* studies, including ones studying the *Drosophila* ovary (*18*), neutrophil motility in zebrafish (*19*), as well as mouse neuronal changes upon cocaine addiction (*20*).

Though successful, the engineering effort in creating PA-Rac1 required trial-and-error generation of numerous fusion positions between LOV2 and Rac1, as changing the final fusion position by a single amino acid rendered the PA-Rac1 light insensitive and constitutively active (*17*). The authors further uncovered a serendipitous but critical interaction of a Rac1 tryptophan residue with the LOV2 domain core, which stabilized the dark-state inhibition of Rac1. Upon introduction of this tryptophan into Cdc42, the authors were able to demonstrate regulation of Cdc42 in an analogous manner as PA-Rac1 (*17*).

This initial success in co-opting LOV2 for optogenetic regulation inspired numerous other efforts to use the light-induced LOV2 conformational change to gate specific peptides or proteins within mammalian cells. Pham, Truong, and colleagues developed a method for light-inducible Ca2+ signaling by using Jα-helix gating to sterically hinder a peptide from the STIM1 C-terminus which, upon binding Orai1 calcium channels, stimulates Ca2+ influx into the cytoplasm (*21*). Similarly, the same group used an analogous strategy to modulate caspase-7 and thus apoptosis via LOV2-gated steric occlusion of the caspase-7 catalytic domain (*22*).

LOV2 has also been engineered for modular control of protein function. Bonger, Wandless and colleagues developed a method for light-induced protein degradation using Jα-mediated steric occlusion of a short, RRRGN degradation peptide, which targets proteins to the proteasome upon Jα-helix unfolding. Termed the B-LID for "blue-light inducible degradation" domain, this fusion was able to mediate fluorescent protein degradation 5-10 fold in cell culture, and it demonstrated efficacy in zebrafish embryos (*23*). In another example, Strickland, Glotzer, and colleagues developed a method for light-inducible heterodimerization mediated *via* LOV2-based steric occlusion of a peptide. In this method, a short 7 amino acid peptide that possessed affinity for an engineered PDZ domain (ePDZ) was overlapped with the Jα helix in a manner that allowed peptide:ePDZ interaction in the light, but inhibited it in the dark state. This method was called "Tunable, light-controlled interacting protein tags," or TULIPS, and it allowed spatiotemporally defined protein translocation within HeLa cells (*24*). Due to the well-characterized and engineered binding interaction used in this method, the binding kinetics and thermodynamics may, in principle, be readily altered, offering a heterodimerizing system with easily tunable properties.

1.3 Dimerizers

Protein colocalization is a common mechanism of signal induction. For instance, translocation of a guanine nucleotide exchange factor to the membrane can induce Rho GTPase activity, and colocalization of a kinase with its substrate can induce substrate phosphorylation. Thus, many efforts in optogenetic protein engineering have centered around developing methods for light-induced hetero- and homo-dimerization. Four main heterodimerizing pairs have developed and implemented in mammalian systems: PhyB/PIF, FKF1/Gigantea, Cry2/CIB1 and

Dronpa145N/Dronpa145K. Currently, only three reported homodimerizing pairs exist: VVD, UVR8, and a modified variant of the photoswitchable Dronpa protein.

1.3.1 PhyB-PIF6

The *Arabidopsis thaliana* Phytochrome B (PhyB) protein interacts with phytochrome interacting factor 6 (PIF) in a light-dependent manner (*25*). The PhyB/PIF pair have two unique properties: 1) PhyB has a red-absorbing and far-red absorbing state, termed the "Pr" and "Pfr" states that absorb 650 nm and 750 nm light, respectively, and 2) PhyB can transition between Pr and Pfr states inducibly via red or far-red illumination within seconds. The Pfr state is the conformation in which PhyB binds to PIF (*25*). To date this is the only optogenetic system that responds within the red and far-red region, which is advantageous since longer wavelength light is less toxic towards cells and can penetrate tissues better than blue-shifted light. Further, the ability to rapidly toggle between the Pr and Pfr states allows the highest precision of temporal but also spatial signal modulation within cells. For instance, if only a small region of activation is desired, focal illumination with activating 650 nm light may be superimposed over whole-field illumination of inactivating 750 nm light, ensuring that any active signaling molecule that diffuses out of the defined region of activation will be rapidly inactivated. Despite these advantages, one significant disadvantage is the reliance of PhyB sensitivity on the phycocyanobilin (PCB) chromophore. This chromophore is not naturally produced within mammalian cells, and must be purified from *Spirulina* and supplemented to the cells exogenously. Though cells appear to rapidly take up PCB and no cytotoxic effects have been reported (*26*), this system is not fully genetically encodable, presenting a significant obstacle for potential *in vivo* studies. One further disadvantage is that the PhyB/PIF system shows cell-type specificity in expression and in function (O. Weiner, personal communication), though the factors contributing to this variability remain unexamined.

Initial use of the PhyB/PIF system in mammalian cells demonstrated the ability of a membrane-tethered PhyB to rapidly and reversibly induce membrane recruitment and release of PIF over an indefinite number of cycles owing to the fast photoswitching kinetics (*26*). Further, membrane recruitment in precise subcellular-scale spatial patterns was demonstrated using patterned illumination of 650 nm light on a background of inactivating 750 nm light, demonstrating the unrivaled spatial precision of the PhyB/PIF optogenetic system. This initial report then proceeded to enable spatially defined Rac1 activation through membrane recruitment of the Rac1 activating GEF Tiam, leading to directed lamellipodial protrusions. Analogous strategies for activation of the Rho GTPases RhoA and Cdc42 were also implemented, though these were not characterized as thoroughly as for Rac1 activation (*26*).

Subsequent work by Toettcher, Lim and colleagues took further advantage of the rapid switchability of the PhyB/PIF system and designed an imaging-based feedback controller to precisely regulate the amount of PIF membrane recruitment to buffer against noise from cell-to-cell expression heterogeneities (*27*). Here, a fluorescently tagged PIF was recruited to the membrane towards a target set-value, as indicated by fluorescence recruitment. Fluorescence intensity was read out in real time through microscopy, and the error between the set point and the actual fluorescence value was fed back to the illumination device, which adjusted the ratio of activating/inactivating light, recursively bringing the recruited PIF levels towards the desired set point value. Upon successful demonstration and characterization, the authors then reported the

ability to regulate intracellular PI3-kinase signaling with similar feedback precision. PI3-kinase (PI3K) activity was induced through PhyB/PIF membrane recruitment of the PI3K catalytic domain, and using a PH-BFP fluorescent biosensor reporting PI3K activity as the feedback control node, precise levels of PIP3 production could be controlled and buffered against both expression heterogeneities and pharmacological perturbation (*27*).

This same group then exhibited the ability to elucidate cellular responses to highly dynamic signal modulation (*28*). By adapting the PhyB/PIF system to regulate MAPK activation through recruitment of the Ras-GEF Sos catalytic domain to the cell membrane, MAPK activity could be activated in response to red light and inactivated in response to far-red light. Using cells expressing this system and a fluorescently labeled Erk1, the authors were able to observe Erk1 translocation dynamics as a function of dynamic Ras activation. A frequency response analysis uncovered that the MAPK signaling is buffered against stimulation shorter than ~4 minutes, but transmits longer duration signals faithfully over a wide range of timescales. The authors proceeded to stimulate cells for varying periods of time and interrogated differential proteomic and transcriptional responses that effectively decoded the Erk activation dynamics. This report provides a convincing proof-of-principle that optogenetics can be an effective tool to rigorously study the effects of signaling dynamics on cell fate decisions.

1.3.2 FKF1-Gigantea

The first published blue-light induced heterodimerizing pair used the FKF1 and GIGANTEA (GI) proteins from *Arabidopsis thaliana (29, 30).* FKF1 is a LOV domain containing protein that requires a FMN cofactor to sense blue light. Though this optogenetic system is entirely genetically encoded, both the FKF1 and GI are large proteins (68 and 129 kDa, respectively), yielding difficulties with expression on some systems. Further, kinetics of this system are relatively slow, requiring ~30 minutes for maximal binding within cells as observed through a membrane translocation assay (*30*). Further, withdrawal of light yielded no observable dissociation between the binding partners for > 1.5 hours, rendering this system too slow for use in dynamic cell signaling studies in its current form. However, this system may be more suitable for inducing irreversible or slower physiological processes, such as protein complementation or gene transcription.

Initial demonstration of FKF1/GI as an optogenetic tool (*30*) involved membrane translocation of a constitutively active Rac1 protein missing its C-terminal CaaX tail, which acts as a signal for addition of a lipid moiety that allows membrane localization of the activated native protein. In the absence of this tail, Yazawa, Dolmetsch and colleagues used the light-mediated interaction to induce membrane Rac1 translocation and activation. The authors further showed that by fusing GI to a Gal4 DNA binding domain and FKF1 to the VP16 transactivator, an optogenetic two-hybrid system could be developed that allowed five-fold induction of reporter gene expression in blue light vs. dark. Polstein, Gersbach and colleagues expanded on this method by replacing the Gal4 binding domain with DNA-binding zinc finger domains, which in principle would allow light-induced targeting of any endogenous gene as defined by the engineered zinc finger specificity (*31*). Using transient transfection of the heterodimerizing

components and a luciferase reporter downstream of nine repeated zinc finger binding sites, the authors achieved a maximal 53-fold induction in light vs. dark conditions.

1.3.3 Cryptochrome 2-CIB1

Cryptochrome 2 (Cry2) and cryptochrome interacting basic helix-loop-helix 1 (CIB1) represent another blue light responsive heterodimerizing protein pair from *Arabidopsis thaliana* that has been co-opted for optogenetic purposes (*32*). Cry2, responding maximally to 450 nm light via a flavin adenine dinucleotide (FAD) cofactor, undergoes a rapid light-induced conformational change and interacts with CIB1 (*32*), and this interaction decays with a half-life of about 5 minutes within mammalian cells (*33, 34*). Though Cry2 and CIB1 are transcription factors and display strong nuclear localization within plants, variants with mutated NLS sequences allowed cytoplasmic localization and activation of this pair. Further, truncated versions of these proteins (Cry2PHR and CIBN) were identified (*33*) and often display more optimal expression and kinetic properties than the full length proteins.

In the initial optogenetic implementation of Cry2/CIB1, Kennedy, Tucker and colleagues first demonstrated rapid and reversible membrane translocation of a cytoplasmic Cry2 to a membrane-tethered CIB1. With success here, Cry2/CIBN were then used in a novel implementation enabling light-mediated Cre recombination. In this demonstration, Cry2 and CIBN were co-expressed fused to either the C- or N-terminal fragment of a split Cre recombinase. With as little as 15 minutes of illumination, detectable levels of Cre complementation and recombination were observed as assayed by excision of a stop codon in a GFP reporter construct.

Due to its rapid kinetics, genetic encodability without need for additional cofactors, and ease of engineering, the Cry2/CIBN system has gained traction among investigators wishing to employ optogenetics in their studies. Cry2/CIBN has since been engineered to regulate both membrane $PI(3,4,5)P_3$ generation and its reversion to $PI(4,5)P_2$ (*35*), light-induced transcription of a luciferase reporter in zebrafish (*36*), MAPK signaling in mammalian cells *via* membrane translocation of c-Raf (*37*), translational control (*38*), and TALEN-directed optogenetic regulation of endogenous gene expression and chromatin modification within primary neurons and brains of freely-moving mice (*39*).

An important consideration in designing experiments with Cry2/CIB1 is the conserved ability for Cry2 to self-associate into large, dynamic oligomers in both plant and mammalian cells (*34, 40*). Although this behavior has been shown to not interfere with many Cry2/CIB1 heterodimerization-dependent applications, and in some cases may conceivably enhance observed light-induced effects, this dual nature of Cry2 is important to appreciate if designing interactions that require a strict 1:1 stoichiometry, or if troubleshooting a failed experiment. Indeed, we have shown that Cry2 clustering alone can be utilized to robustly manipulate mammalian cell signaling in a highly modular fashion (see Section 1.4) (*34*).

1.3.4 Dronpa145N-Dronpa145K

Dronpa is a monomeric photoswitchable protein that is derived from a tetrameric parent (*41*). It was recently discovered that a Dronpa mutant with a K145N mutation (Dronpa 145N) can transition between a tetrameric and monomeric state in response to 400 nm and 500 nm light, respectively (*42*). Further, it was shown that a tandem dimer of the wild-type (Dronpa 145K) and mutant Dronpa 145N can be toggled between a heterodimerized and dissociated state using 400 nm and 500 nm light, respectively.

In order to minimize the tetrameric Dronpa 145N homointeraction and favor the heterodimeric Dronpa-145N/Dronpa-145K interaction, this tool was implemented exclusively with single-chain fusions of the N- and K- mutants, and the heterodimerization was used to sterically or allosterically regulate signaling effectors (*42*). Zhou, Lin and colleagues first demonstrated the ability of this tandem heterodimer to regulate the Cdc42 activating guanine nucleotide exchange factor (GEF) Intersectin (ITSN) in fibroblasts, which allowed spatially defined relief of ITSN inhibition upon illumination with 490 nm light and concomitant activation of Cdc42-induced filopodial extensions. As a second example, Dronpa-145N dimerization inhibited a protease, which upon light induced inhibition release was able cleave a fluorescent protein from the membrane.

1.3.5 VVD

The 186 amino acid protein Vivid (VVD) from the filamentous fungus *Neurospora crassa* is the smallest LOV-domain containing protein (*43*). Blue light absorption by the internal FAD cofactor induces FAD interaction with an internal cysteine, which induces a conformational change that propagates out to an N-terminal helix, consequently inducing a rapidly-exchanging homodimerization of the VVD LOV domain (*43*).

The VVD protein was used to create a successful, single-construct optogenetic transcription system. To do this, the authors replaced the homodimerization domain of the Gal4 transcription factor (Gal4(65)) with the VVD protein (*44*). Gal4 only recognizes its cognate DNA in dimeric form, and the authors were able to demonstrate that the Gal4(65)-VVD protein only binds DNA in response to light. After further optimization, the authors created GAVPO, an optimized Gal4-VVD fusion that can induce transcription of a gene roughly 100-fold in light vs. dark conditions. The authors further demonstrated the feasibility of using GAVPO within living mice. GAVPO was also used by a different group studying neural stem cells, where various dynamic profiles of Asc1 expression were induced to observe effects of Asc1 on stem cell fate decisions (*45*).

1.3.6 UVR8

The *A. thaliana* UVR8 protein is a unique optically active protein in many regards. First, this protein forms a constitutive, non-covalent homodimer in the dark, which dissociates upon UV-B absorption. This “light-off” behavior is opposed to most other optically active proteins,

where light induces an interaction. Secondly, UVR8 does not require a cofactor for light sensing but rather senses UV-B illumination via two tryptophan residues near the dimer interface (*46*). Finally, the UV-B exciting light is spectrally distinct from other optogenetic activating wavelengths, potentially allowing multiplexing of UVR8-based tools with numerous other optically-sensitive tools. UVR8 was implemented in an initial demonstration as a tool enabling light-dependent protein secretion (*47*). In this strategy, UVR8 is fused to a secreted protein, and the dark-promoted homoassociation prevents proper secretion. Upon UV-B illumination, the proteins dissociate and secretion can proceed. The authors also used this tool to study intracellular secretory trafficking through neurons.

1.4 Oligomerizers

1.4.1 Cryptochrome 2

In addition to hetero- and homo-dimerization, oligomerization is another method by which signaling proteins may be activated. Though well appreciated as a mode of activation for transmembrane receptors, protein oligomerization also plays a significant role in cytoplasmic signaling proteins as well. Only one optogenetic clustering protein has been described to date, and it was first observed, characterized, and implemented in mammalian cells by the author of this dissertation (See Chapter 2 for a detailed description). Interestingly, this protein is the *Arabidopsis thaliana* Cryptochrome 2 (Cry2), which was initially used in the Cry2/CIB1 heterodimerizing pair (See section 1.3.3). Cry2 has a dual nature, able to both bind CIB1 and itself in response to blue light illumination. However, in the absence of CIB1, Cry2 strongly and rapidly binds itself in response to blue light, and upon light withdrawal, the clusters decay with a half-life of about 5 minutes. Though both full-length and the truncated Cry2PHR have been observed to cluster, the Cry2PHR exhibits stronger expression and clusters with faster kinetics, and so this truncation has been used instead of the full-length protein for optogenetic applications (*34*).

Cry2 clustering was initially used to activate the canonical Wnt/β-catenin pathway, giving robust activation of a pathway reporter to levels higher than observed with natural pathway ligand (*34*). Cry2 was then used to cluster and activate RhoA, revealing an unknown mode of activation (clustering) for this well-studied protein. Implementation and application of Cry2 clustering is described in detail in Chapters 2-5 of this dissertation. Ozkan-Dagliyan, Sancar, and colleagues further characterized *A. thaliana* Cry2 nuclear clustering and showed that end-to-end fusion of Cry2 with the TopBP1 DNA damage checkpoint protein can activate a DNA damage signaling pathway in response to light (*48*). Importantly, the authors also uncovered that *Arabidopsis* Cry2 forms a light-promoted complex with the human E3 ubiquitin ligase COP1, an important reminder that these heterologously expressed tools may not be entirely orthogonal to the desired system of study. Finally, Wend, Radziwill, and colleagues activated mammalian MAPK signaling *via* a single construct c-Raf-Cry2 fusion (*49*). Though the authors report having used Cry2 to homodimerize Raf to greater effect (i.e. greater pathway activation) than using Cry2-CIBN heterodimerization, the possibility exists that the authors were in fact forming higher order oligomers with Cry2 to see strong pathway activation, something that would not be

possible with the Cry2/CIB1 pair. Oligomerization of c-Raf1 has been reported to be a strong method of Raf1 activation (*50*).

1.5 Conclusion

The above represent the current state of the art in applying optical tools to perturb and study cell biology, though new optogenetic tools and implementations continue to become available. In this dissertation, I will detail the discovery, implementation, engineering, and biological application of one particularly powerful optogenetic methodology: the light-induced clustering of *Arabidopsis thaliana* Cryptochrome2.

1.6 References

1. J. E. Purvis, G. Lahav, Encoding and Decoding Cellular Information through Signaling Dynamics. *Cell* 152, 945 (2013).
2. H. Hirata *et al.*, Oscillatory expression of the bHLH factor Hes1 regulated by a negative feedback loop. *Science* 298, 840 (2002).
3. G. Tiana, S. Krishna, S. Pigolotti, M. H. Jensen, K. Sneppen, Oscillations and temporal signalling in cells. *Phys Biol* 4, R1 (2007).
4. S. Traverse *et al.*, EGF triggers neuronal differentiation of PC12 cells that overexpress the EGF receptor. *Current Biology* 4, 694 (1994).
5. K. Lai, M. J. Robertson, D. V. Schaffer, The sonic hedgehog signaling system as a bistable genetic switch. *Biophys J* 86, 2748 (2004).
6. J. Ericson, S. Morton, A. Kawakami, H. Roelink, T. M. Jessell, Two Critical Periods of Sonic Hedgehog Signaling Required for the Specification of Motor Neuron Identity. *Cell* 87, 661 (1996).
7. J. Ericson *et al.*, Sonic hedgehog induces the differentiation of ventral forebrain neurons: A common signal for ventral patterning within the neural tube. *Cell* 81, 747 (1995).
8. Jeremy E. Purvis, G. Lahav, Encoding and Decoding Cellular Information through Signaling Dynamics. *Cell* 152, 945 (2013).
9. S. Wang *et al.*, All optical interface for parallel, remote, and spatiotemporal control of neuronal activity. *Nano Lett* 7, 3859 (2007).
10. S. Szobota *et al.*, Remote control of neuronal activity with a light-gated glutamate receptor. *Neuron* 54, 535 (2007).
11. E. S. Boyden, F. Zhang, E. Bamberg, G. Nagel, K. Deisseroth, Millisecond-timescale, genetically targeted optical control of neural activity. *Nature neuroscience* 8, 1263 (2005).
12. S. Q. Lima, G. Miesenböck, Remote Control of Behavior through Genetically Targeted Photostimulation of Neurons. *Cell* 121, 141 (2005).
13. B. V. Zemelman, G. A. Lee, M. Ng, G. Miesenböck, Selective Photostimulation of Genetically ChARGed Neurons. *Neuron* 33, 15 (2002).
14. K. M. Tye, K. Deisseroth, Optogenetic investigation of neural circuits underlying brain disease in animal models. *Nat Rev Neurosci* 13, 251 (2012).
15. M. Salomon, J. M. Christie, E. Knieb, U. Lempert, W. R. Briggs, Photochemical and Mutational Analysis of the FMN-Binding Domains of the Plant Blue Light Receptor, Phototropin†,‡. *Biochemistry* 39, 9401 (2000).
16. S. M. Harper, L. C. Neil, K. H. Gardner, Structural basis of a phototropin light switch. *Science* 301, 1541 (2003).
17. Y. I. Wu *et al.*, A genetically encoded photoactivatable Rac controls the motility of living cells. *Nature* 461, 104 (2009).
18. X. Wang, L. He, Y. I. Wu, K. M. Hahn, D. J. Montell, Light-mediated activation reveals a key role for Rac in collective guidance of cell movement in vivo. *Nat Cell Biol* 12, 591 (2010).

19. S. K. Yoo *et al.*, Differential Regulation of Protrusion and Polarity by PI(3)K during Neutrophil Motility in Live Zebrafish. *Developmental Cell* 18, 226 (2010).
20. D. M. Dietz *et al.*, Rac1 is essential in cocaine-induced structural plasticity of nucleus accumbens neurons. *Nat Neurosci* 15, 891 (2012).
21. E. Pham, E. Mills, K. Truong, A Synthetic Photoactivated Protein to Generate Local or Global Ca2+ Signals. *Chemistry & Biology* 18, 880 (2011).
22. E. Mills, X. Chen, E. Pham, S. Wong, K. Truong, Engineering a Photoactivated Caspase-7 for Rapid Induction of Apoptosis. *ACS Synthetic Biology* 1, 75 (2011).
23. K. M. Bonger, R. Rakhit, A. Y. Payumo, J. K. Chen, T. J. Wandless, General Method for Regulating Protein Stability with Light. *ACS Chemical Biology* 9, 111 (2013).
24. D. Strickland *et al.*, TULIPs: tunable, light-controlled interacting protein tags for cell biology. *Nat Meth* 9, 379 (2012).
25. M. Ni, J. M. Tepperman, P. H. Quail, Binding of phytochrome B to its nuclear signalling partner PIF3 is reversibly induced by light. *Nature* 400, 781 (1999).
26. A. Levskaya, O. D. Weiner, W. A. Lim, C. A. Voigt, Spatiotemporal control of cell signalling using a light-switchable protein interaction. *Nature* 461, 997 (2009).
27. J. E. Toettcher, D. Gong, W. A. Lim, O. D. Weiner, Light-based feedback for controlling intracellular signaling dynamics. *Nat Meth* 8, 837 (2011).
28. Jared E. Toettcher, Orion D. Weiner, Wendell A. Lim, Using Optogenetics to Interrogate the Dynamic Control of Signal Transmission by the Ras/Erk Module. *Cell* 155, 1422 (2013).
29. M. Sawa, D. A. Nusinow, S. A. Kay, T. Imaizumi, FKF1 and GIGANTEA Complex Formation Is Required for Day-Length Measurement in Arabidopsis. *Science* 318, 261 (2007).
30. M. Yazawa, A. M. Sadaghiani, B. Hsueh, R. E. Dolmetsch, Induction of protein-protein interactions in live cells using light. *Nat. Biotech.* 27, 941 (2009).
31. L. R. Polstein, C. A. Gersbach, Light-Inducible Spatiotemporal Control of Gene Activation by Customizable Zinc Finger Transcription Factors. *Journal of the American Chemical Society* 134, 16480 (2012).
32. H. Liu *et al.*, Photoexcited CRY2 Interacts with CIB1 to Regulate Transcription and Floral Initiation in Arabidopsis. *Science* 322, 1535 (2008).
33. M. J. Kennedy *et al.*, Rapid blue-light-mediated induction of protein interactions in living cells. *Nat. Meth.* 7, 973 (2010).
34. L. J. Bugaj, A. T. Choksi, C. K. Mesuda, R. S. Kane, D. V. Schaffer, Optogenetic protein clustering and signaling activation in mammalian cells. *Nature methods* 10, 249 (2013).
35. O. Idevall-Hagren, E. J. Dickson, B. Hille, D. K. Toomre, P. De Camilli, Optogenetic control of phosphoinositide metabolism. *Proceedings of the National Academy of Sciences* 109, E2316 (2012).
36. H. Liu, G. Gomez, S. Lin, S. Lin, C. Lin, Optogenetic Control of Transcription in Zebrafish. *PLoS ONE* 7, e50738 (2012).

37. K. Aoki *et al.*, Stochastic ERK Activation Induced by Noise and Cell-to-Cell Propagation Regulates Cell Density-Dependent Proliferation. *Molecular Cell* 52, 529 (2013).
38. J. Cao *et al.*, Light-inducible activation of target mRNA translation in mammalian cells. *Chemical Communications* 49, 8338 (2013).
39. S. Konermann *et al.*, Optical control of mammalian endogenous transcription and epigenetic states. *Nature* 500, 472 (2013).
40. P. Mas, P. F. Devlin, S. Panda, S. A. Kay, Functional interaction of phytochrome B and cryptochrome 2. *Nature* 408, 207 (2000).
41. R. Ando, H. Mizuno, A. Miyawaki, Regulated Fast Nucleocytoplasmic Shuttling Observed by Reversible Protein Highlighting. *Science* 306, 1370 (2004).
42. X. X. Zhou, H. K. Chung, A. J. Lam, M. Z. Lin, Optical Control of Protein Activity by Fluorescent Protein Domains. *Science* 338, 810 (2012).
43. B. D. Zoltowski, B. R. Crane, Light Activation of the LOV Protein Vivid Generates a Rapidly Exchanging Dimer†‡. *Biochemistry* 47, 7012 (2008).
44. X. Wang, X. Chen, Y. Yang, Spatiotemporal control of gene expression by a light-switchable transgene system. *Nat Meth* 9, 266 (2012).
45. I. Imayoshi *et al.*, Oscillatory Control of Factors Determining Multipotency and Fate in Mouse Neural Progenitors. *Science* 342, 1203 (2013).
46. W. Di *et al.*, Structural basis of ultraviolet-B perception by UVR8. *Nature* 484, 214 (2012).
47. D. Chen, E. S. Gibson, M. J. Kennedy, A light-triggered protein secretion system. *The Journal of Cell Biology* 201, 631 (2013).
48. I. Ozkan-Dagliyan *et al.*, Formation of Arabidopsis Cryptochrome 2 Photobodies in Mammalian Nuclei: APPLICATION AS AN OPTOGENETIC DNA DAMAGE CHECKPOINT SWITCH. *Journal of Biological Chemistry* 288, 23244 (2013).
49. S. Wend *et al.*, Optogenetic Control of Protein Kinase Activity in Mammalian Cells. *ACS Synthetic Biology*, (2013).
50. Z. Luo *et al.*, Oligomerization activates c-Raf-1 through a Ras-dependent mechanism. *Nature* 383, 181 (1996).

Chapter 2

Optogenetic Protein Clustering and Signaling Activation in Mammalian Cells

This chapter is in part a postprint of a paper submitted to and accepted for publication as

Bugaj, L.J., Choksi, A.T., Mesuda, C.K., Kane, R.S. & Schaffer, D.V. Optogenetic protein clustering and signaling activation in mammalian cells. *Nature Methods* 10, 249-252 (2013).

2.1 Introduction

The regulation of cellular function involves precise modulation of signal intensity, location, and duration (*1*). Protein oligomerization – the assembly of proteins into multimers – is a particularly powerful mechanism for modulating cellular signaling and is used to activate broad classes of proteins including membrane receptors, receptor ligands, kinases, transcription factors, and numerous other cytosolic signaling effectors. Within such systems, protein oligomerization enables ultra-sensitive digital signaling responses, connects nanoscale protein activity to microscale control of cellular structures, provides scaffolds for assembly of enzymatic activities, and participates in disease pathologies (*2*).

Studying the impact of protein oligomerization on cell behavior is challenged, however, by the lack of approaches to exert tunable control over a protein's oligomeric state. Transmembrane receptors can be clustered with antibodies, and intracellular targets can be oligomerized with small-molecule dependent dimerization of repeated inducible dimerizing domains (*3*). Due to their reliance on biochemical agents to mediate clustering, however, such techniques suffer from limited spatial resolution and are incapable of dynamic protein regulation.

Optogenetic systems (*4*) have recently demonstrated precise and reversible control of signaling pathways through photo-control of protein heterodimerization (*5-9*) and homodimerization (*10*). These are important modes for regulating protein activity, but they are distinct from the assembly of proteins into higher order oligomers. In this chapter, we present a genetically encoded platform for modular and tunable control of protein oligomerization, and we demonstrate its broad utility for controlling diverse intracellular signaling cascades.

2.2 Results

Arabidopsis thaliana Cryptochrome 2 (Cry2, GenBank NM_179257) forms oligomeric "photobodies" in plant cells in response to blue light (*11*), but this property has not been reported in mammalian cells. Upon transfection into HEK 293T cells, we observed that the photolyase homology region (PHR) of Cry2 fused to mCherry (Cry2-mCh) rapidly formed distinct fluorescent puncta within 10 seconds of blue light illumination (Figure 2.1A,B). Upon blue light withdrawal, the clusters dispersed to their original state within minutes (Figure 2.1B). Notably, clustering was not observed with a light-insensitive Cry2 mutant harboring a D387A mutation (*12*) (Figure 2.1C). From a diffuse initial condition, Cry2-mCh fluorescence could be repeatedly clustered and unclustered with similar kinetics (Figure 2.1D, Figure 2.2). FRAP analysis of individual clusters demonstrated rapid fluorescence recovery (Figure 2.2), suggesting that in the light state the oligomers dynamically exchange Cry2-mCh subunits with the bulk and/or one another (Figure 2.4).

Cry2 clustering was not reported in a recent study that focused on light-dependent Cry2-CIB1 interactions in mammalian cells (*5*). In the presence of cytosolic CIB1, we find that Cry2 can still cluster (Figure 2.5) and that CIB1 colocalizes with these clusters, which indicates that CIB1 interaction does not preclude Cry2 clustering and may even offer a means to assemble two proteins into a cluster.

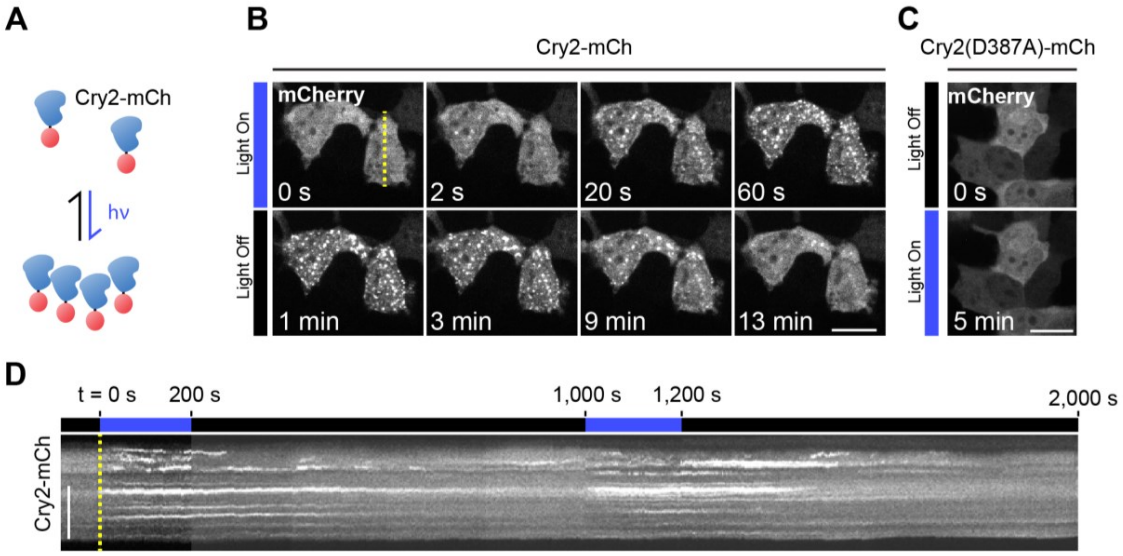

Figure 2.1 Cry2-mCh oligomerizes under blue light in mammalian cells. A) Schematic depicting light-induced protein clustering. B) Stills of Cry2-mCh cluster formation in HEK 293Ts in response to 488 nm laser light (top), as well as dissociation (bottom) after light withdrawal. Scale bar, 20 µm. C) Clustering does not occur with the light-insensitive mutant Cry2(D387A)-mCh. Scale bar = 20 µm. D) Kymograph of mCherry fluorescence corresponding to the dashed line in (B). Scale bar = 20 µm.

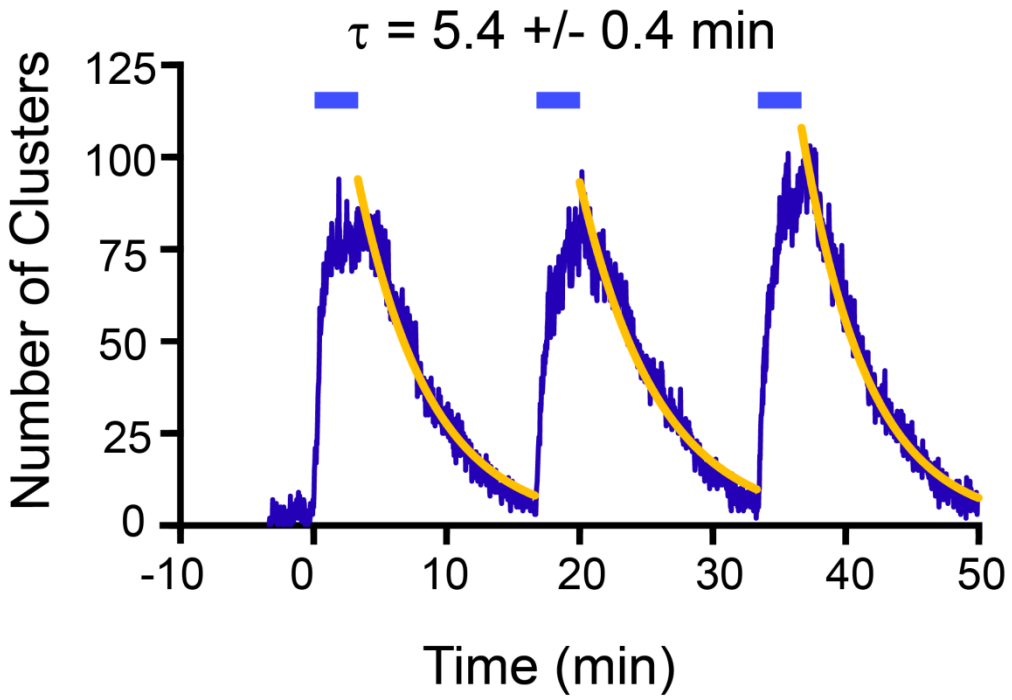

Figure 2.2 Measurement of cluster number over multiple light/dark cycles demonstrates repeatable, rapid clustering and de-clustering with consistent kinetics. Single exponential decay fit of cluster number allows measurement of cluster decay constant τ (mean +/- 1 s.d., n = 3 decay cycles).

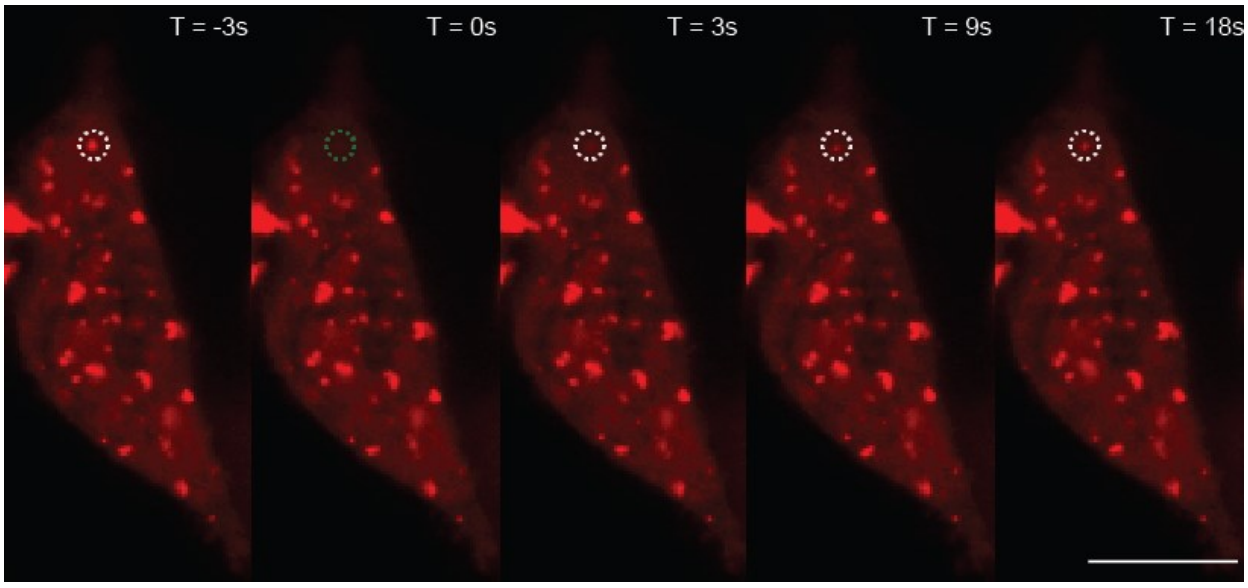

Figure 2.3 FRAP analysis shows Cry2-mCh clusters are highly dynamic. HEK 293T cells were transfected with Cry2-mCh and illuminated to form clusters. In this representative series, the indicated cluster was photobleached at T = 0 s and its recovery observed. The cluster regained fluorescence within seconds, suggesting that Cry2-mCh clusters are dynamic. Scale bar = 10 μm.

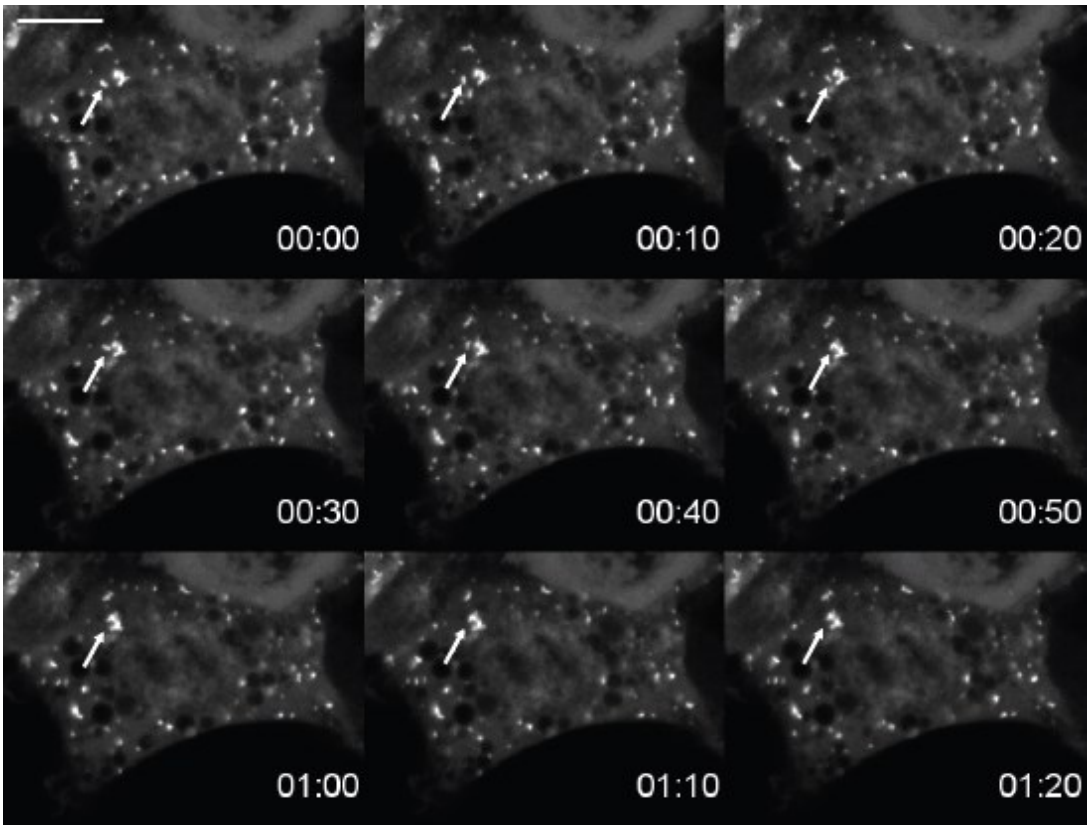

Figure 2.4 Cry2-mCh oligomers combine into higher order oligomers. HEK 293T cells expressing Cry2-mCh were illuminated to induce cluster formation. In the representative sequence above, a cluster (arrow) is tracked over time as it diffuses through a cell and encounters a larger cluster at 50 s. These clusters then remain associated, suggesting that individual Cry2-mCh oligomers bind to create higher order oligomers. Time given in minutes:seconds. Scale bar, 10 μm.

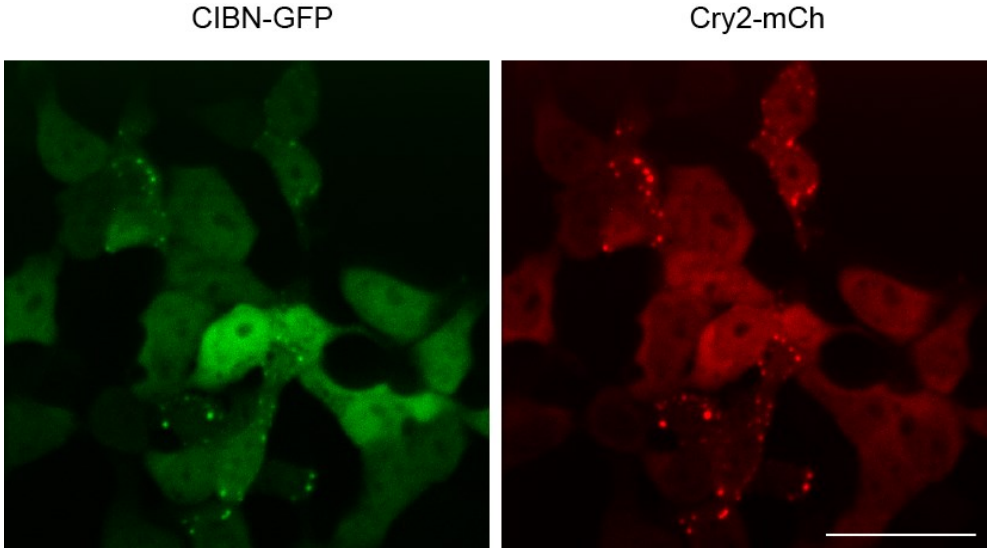

Figure 2.5 Oligomerized Cry2 retains heteroaffinity for CIBN. HEK 293Ts were transfected with a 1:2 molar ratio of CIBN-GFP:Cry2-mCh plasmid constructs and illuminated with 488 nm laser within a confocal microscope. Cytoplasmic CIBN-GFP colocalized with cytoplasmic Cry2-mCh clusters, suggesting that light-induced Cry2-CIBN affinity is retained when Cry2 is in clustered form. Scale bar, 50 μm.

In parallel with an increase in oligomer size upon illumination, the number of visible clusters in a cell increased sigmoidally over time (Figure 2.6). Fitting this relationship to a sigmoidal function allowed extraction of $T_{1/2}$, the time at which a half maximal number of visible clusters was detected. This metric of association kinetics was dependent on light intensity (Jonckheere-Terpstra trend analysis (*13*) (see Methods), $p = 0.004$, $n = 4$, Figure 2.7). Upon light withdrawal, cluster number followed a single exponential decay with a time constant of ~5.5 minutes (Figure 2.2), consistent with a previous report of the lifetime of the activated Cry2 photo-isomer in mammalian cells ($t_{1/2} \sim 5.5$ min) (*5*).

We next investigated whether inducible Cry2-mCh clustering could be harnessed to induce oligomerization-dependent signaling. Canonical Wnt/β-catenin signaling is triggered by Wnt ligand binding to Frizzled and LRP6 co-receptors, which then form higher order clusters (*14, 15*) and activate β-catenin. Upon activation, β-catenin translocates to the nucleus and functions as a transcriptional cofactor to activate key targets. Recently, constitutive clustering of just the LRP6 C-terminal domain (LRP6c) was shown to robustly activate β-catenin signaling (*16*). Using chemically induced dimerizing domains, we found that LRP6c oligomerization is indeed necessary – and dimerization insufficient – to activate β-catenin signaling (Figure 2.8, Figure 2.9). To determine whether the LRP6c endodomain could be oligomerized in response to light, and thus offer spatiotemporally precise control over canonical Wnt signaling (Figure 2.10), we fused it to the C-terminus of Cry2-mCh (Cry2-mCh-LRP6c). After introduction of this construct into HEK 293T cells, visible puncta appeared within two seconds of blue light illumination, and these clusters dissociated upon light withdrawal with somewhat slower kinetics than observed with Cry2-mCh (Figure 2.11). To assess whether this clustering could induce pathway activation, cells carrying a β-catenin responsive luciferase reporter (*17*) were transfected with Cry2-mCh-LRP6c. Blue light illumination led to elevated levels of active β-catenin,

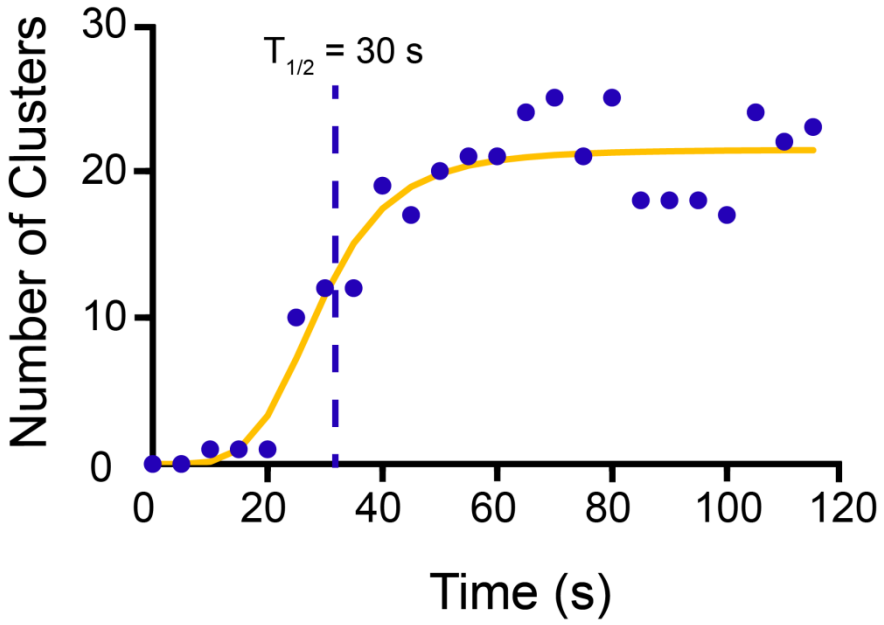

Figure 2.6 Representative plot of single cell cluster formation over time. Similar behavior was observed in all cells whose cluster formation was measured.

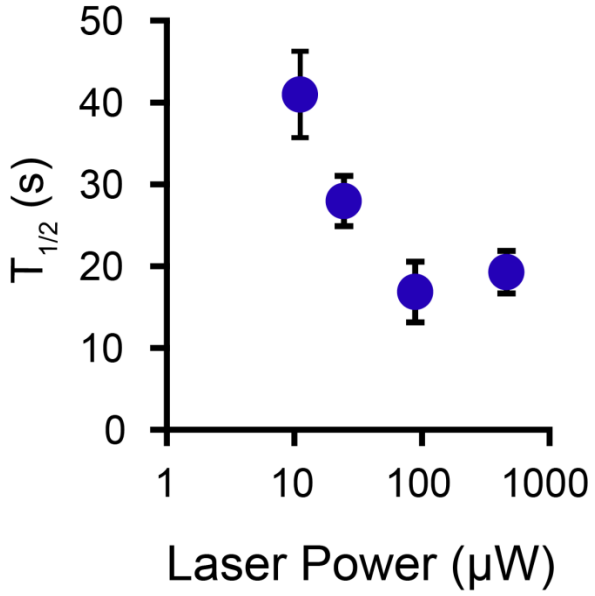

Figure 2.7 Clustering kinetics are a function of illuminating intensity. Representative plot of concentration-normalized $T_{1/2}$ increase with decreased illuminating intensity (see Methods). Plot shows mean +/- 1 s.e.m., n = 4 cells for each condition.

accompanied by considerably higher levels of luciferase activity, in Cry2-mCh-LRP6c cells relative to unilluminated or untransfected controls (Figure 2.12A,B). The β-catenin and luciferase signals were attenuated through co-expression of constitutively active GSK-3β, a β-catenin signaling antagonist, indicating specificity of pathway activation. Furthermore, the light-induced Cry2-mCh-LRP6c transcriptional response was similar to that observed using the strong pathway agonist CHIR99021, suggesting a large dynamic range of activation (Figure 2.12A,B). Despite the similar transcriptional response, these two conditions exhibited differentially elevated levels of active β-catenin (Figure 2.12B), potentially due to a non-linear or dynamic relationship between active β-catenin levels and induced luciferase expression or activity.

To generalize these results to another cell type, and to determine whether low genetic copy numbers of the construct could yield similar results, Cry2-mCh-LRP6c was introduced via a retroviral vector into neural stem cells (NSCs) harboring the β-catenin luciferase reporter. Upon illumination with a custom-built device allowing control of pulse width and frequency (Figure 2.13), cells demonstrated a strong dose responsiveness to increased blue light pulse frequency ($p = 0.0051$, $n = 2$ replicates, Jonckheere-Terpstra trend analysis, Figure 2.14), whereas cells kept in the dark yielded a negligible readout. Maximal light-induced signaling increased luciferase expression ~200-fold over unilluminated controls and greatly exceeded reporter expression induced by high levels of pathway agonist Wnt3a (Figure 2.14), further demonstrating tunability of β-catenin activity through a large signaling range. The ability to dynamically control β-catenin activity may enable novel insights throughout the numerous biological systems where this molecule plays a central role.

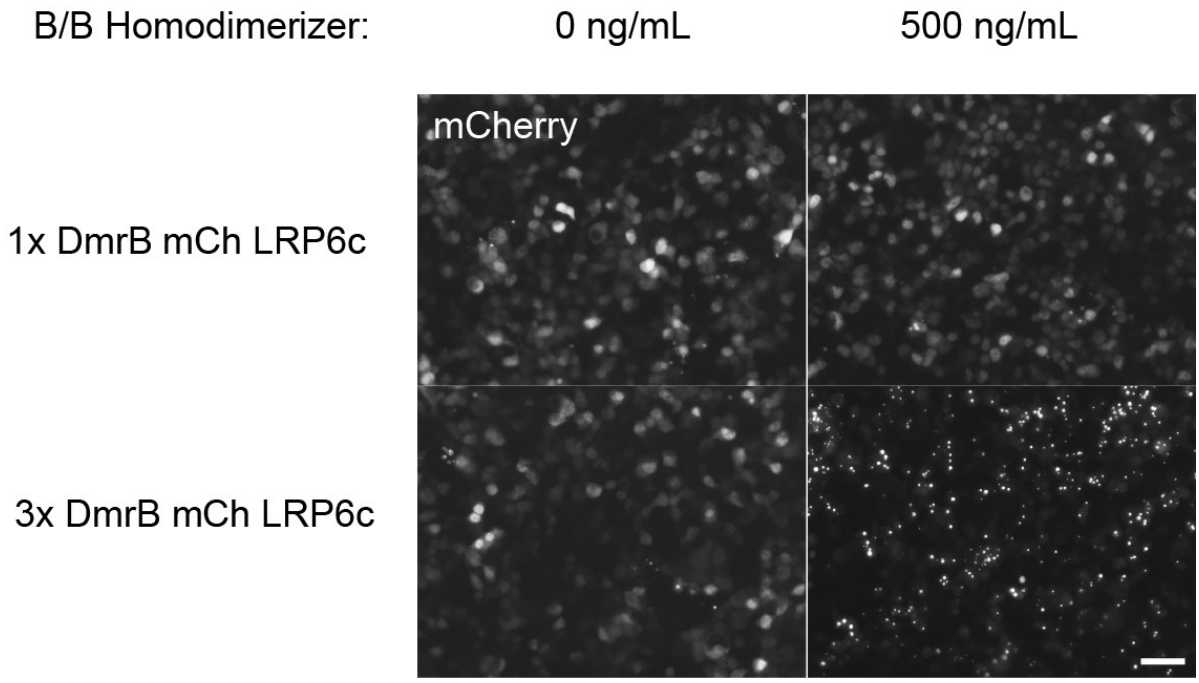

Figure 2.8 Oligomerization is necessary for LRP6c-induced β-catenin activity. To demonstrate that LRP6c oligomerization is necessary for LRP6c-mediated activation of β-catenin, mCherry-LRP6c was fused to either one (1x) or three (3x) repeats of the chemically-inducible dimerizing DmrB domain (originally FKBP). Addition of the small molecule B/B Homodimerizer (Clontech) induces higher order oligomerization of the 3x construct but not the 1x construct, where it presumably only induces homodimerization. Scale bar = 50 um.

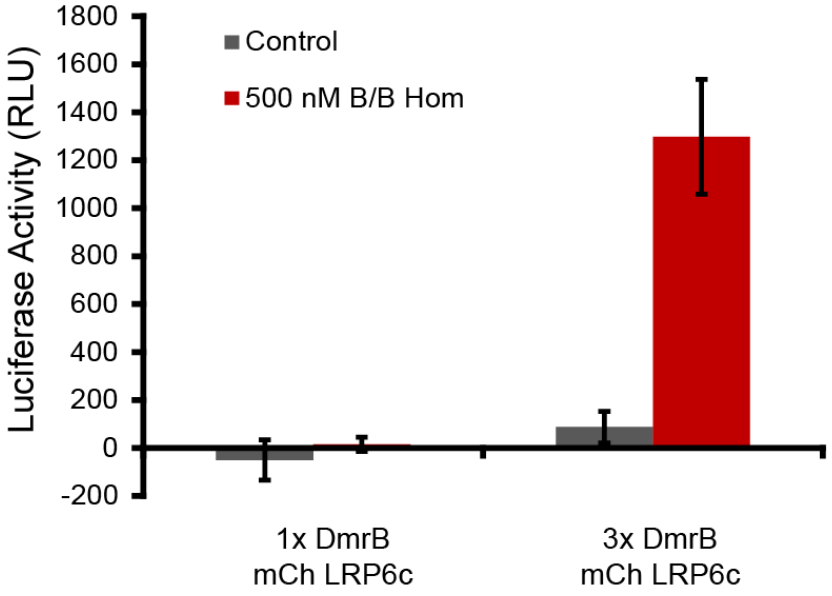

Figure 2.9 Oligomerization is necessary for LRP6c-induced β-catenin activity. Representative experiment showing that addition of B/B Homodimerizer elicits a β-catenin transcriptional response in 293T TFP luciferase reporter cells transfected with the 3x construct but not with the 1x construct, suggesting that oligomerization is necessary for LRP6c-mediated β-catenin signaling activity. Graph shows baseline subtracted means +/- 1 s.d., n = 3 replicates. RLU, relative light units.

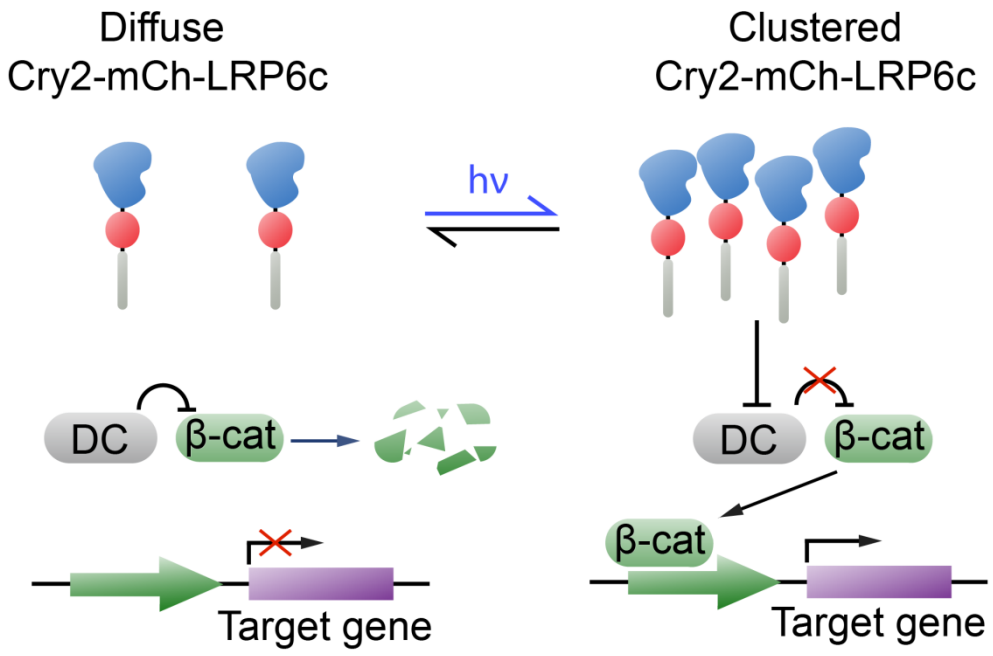

Figure 2.10 Schematic of β-catenin photoactivation strategy. Upon light (hυ) activation, clustering of the LRP6c domain inhibits the destruction complex (DC), relieving β-catenin inhibition and allowing its translocation to the nucleus and regulation of target gene transcription.

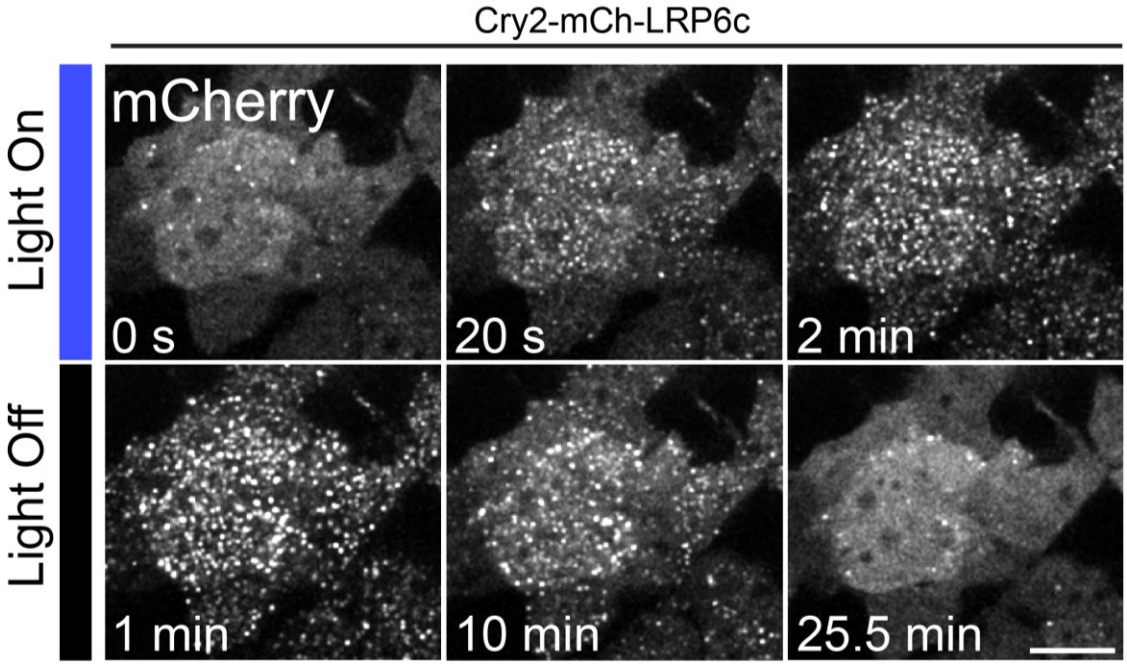

Figure 2.11 Cry2-mCh-LRP6c retains the ability to reversibly cluster in HEK 293T cells. Scale bar, 20 μm.

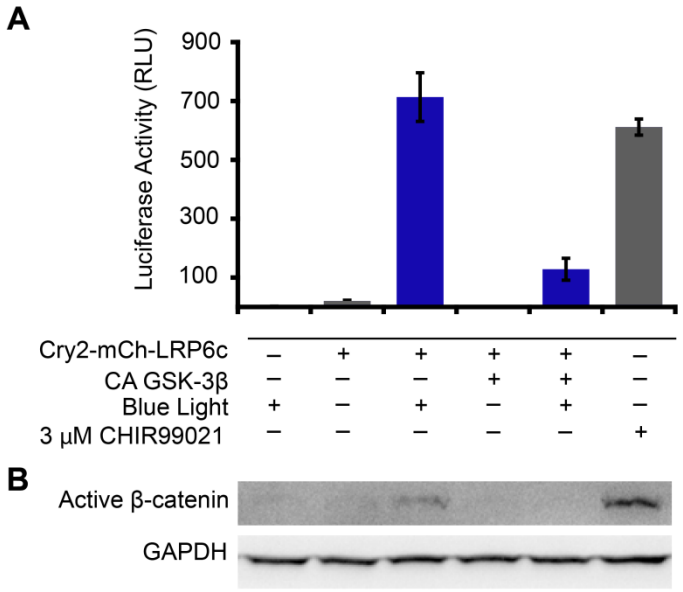

Figure 2.12 Light induced Cry2-mCh-LRP6c clustering modulates the Wnt/β-catenin pathway. A) Light-induced β-catenin transcriptional activity assayed in HEK 293T cells carrying Cry2-mCh-LRP6c and a luciferase reporter shows strong β-catenin activity after 16 hr exposure to blue light pulses (500 ms pulse every 10 seconds). The light induced signal was attenuated in the presence of a β-catenin pathway inhibitor, i.e. constitutively active GSK-3β, and was comparable to that observed with small molecule pathway agonist CHIR99021 (3 μM). Graph shows mean +/- 1 s.d., n = 3 replicates. B) Western blot for active β-catenin levels in HEK 293T cells under the same conditions as in (A).

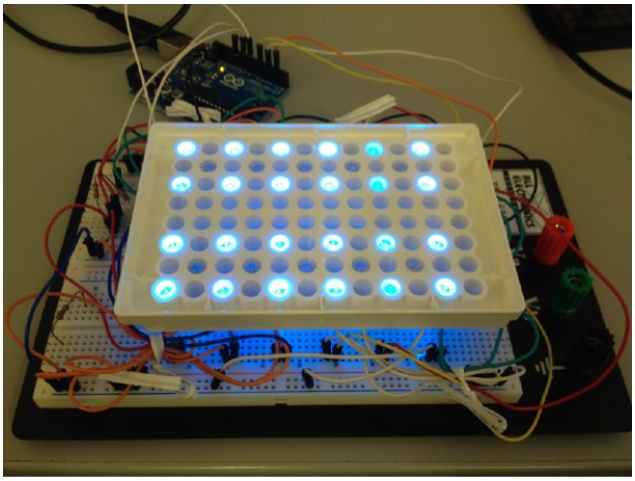

Figure 2.13 Device for illuminating live cells with 1-13 independent channels in a cell culture incubator. The above device consists of 5 mm blue LEDs arranged in a breadboard to fit into wells of an inverted, clear-bottom, 96 well plate. The LEDs are driven by the Arduino open-source electronics prototyping platform (www.arduino.cc), which allows independent control of up to 13 channels. The image depicts 6 independent channels. Pulse frequency and pulse width of light are controlled through a custom-written script in the Arduino language (2.6.2 Appendix B). For experiments, cells were seeded in the appropriate wells in a clear-bottom, black-walled plate, which is placed on top of the depicted assembly to align the LED light with the wells and subsequently illuminate the cells therein. The entire device was small and could be placed into a standard cell culture incubator for long-term illumination of living cells. By changing the LED placement, this approach could be used for illuminating cells in non-96-well cell culture formats as well.

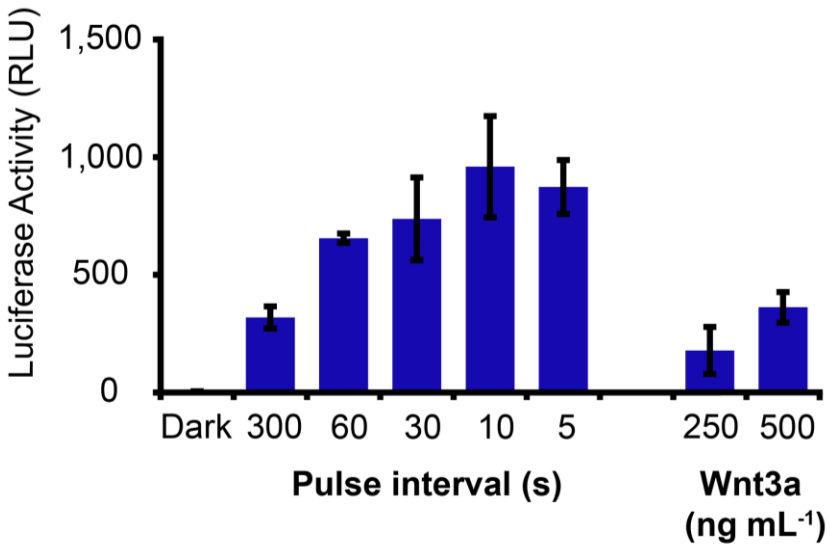

Figure 2.14 Light-induced β-catenin activity in neural stem cells. Neural stem cells carrying the luciferase reporter and expressing Cry2-mCh-LRP6c strongly upregulated luciferase in response to Wnt3a protein or to 500 ms light pulses for 16 hours, with the interval between pulses varying from 5-300 s. Graph is representative of three independent experiments, and error bars show the range of duplicate samples. RLU, relative light units.

We next investigated the modularity of Cry2-mCh as a general tool for clustering proteins and activating other signaling pathways. Rho GTPases are small proteins involved in actin polymerization, cell motility, and mechanotransduction (*18*). Oligomerization of the Rho GTPase Rac1 has been reported to enhance its enzymatic activity and effector activation within *in vitro* assays (*19*), though the functional significance of Rac1 oligomerization in living cells has to our knowledge not been studied. Within 2 seconds of illumination, HEK 293T cells expressing a fusion of Cry2-mCherry with Rac1 (Cry2-mCh-Rac1) demonstrated translocation of mCherry fluorescence from the cytoplasm to the membrane, a hallmark of Rho GTPase activation, accompanied by apparent cell spreading, suggesting Rac1 activation (*20*) (Figure 2.15, Figure 2.17).

Since a different strategy has recently been utilized to generate a photoactivatible Rac1 (*21*), we investigated whether our inducible clustering approach could be harnessed to activate a distinct Rho GTPase family member. RhoA is a small GTPase primarily responsible for mediating cellular tension and cytoskeletal contraction. However, photocontrol of RhoA has as yet not been achieved, and oligomerization has not been linked to RhoA activity. Intriguingly, a fusion of mCherry-RhoA protein to a constitutively oligomerizing DIX domain was membrane-localized (Figure 2.16). Analogously, Cry2-mCherry-RhoA was initially diffuse but rapidly translocated to membranes and vesicles within seconds of activation with 458 nm or 488 nm laser light (10 μW) in HEK 293Ts (Figure 2.15, Figure 2.17) and NIH 3T3 fibroblasts (Figure 2.18). This translocation did not occur in cells expressing RhoA and Cry2 on separate peptide chains (not shown), suggesting it was not due to non-specific effects of Cry2 photoisomerization. Furthermore, within minutes of single cell illumination, cellular membrane retraction was evident (Figure 2.19), suggesting that the RhoA translocation coincided with RhoA activation. Finally, both membrane retraction and Cry2-mCherry-RhoA membrane localization were reversible within minutes, and cells could be repeatedly activated and inactivated.

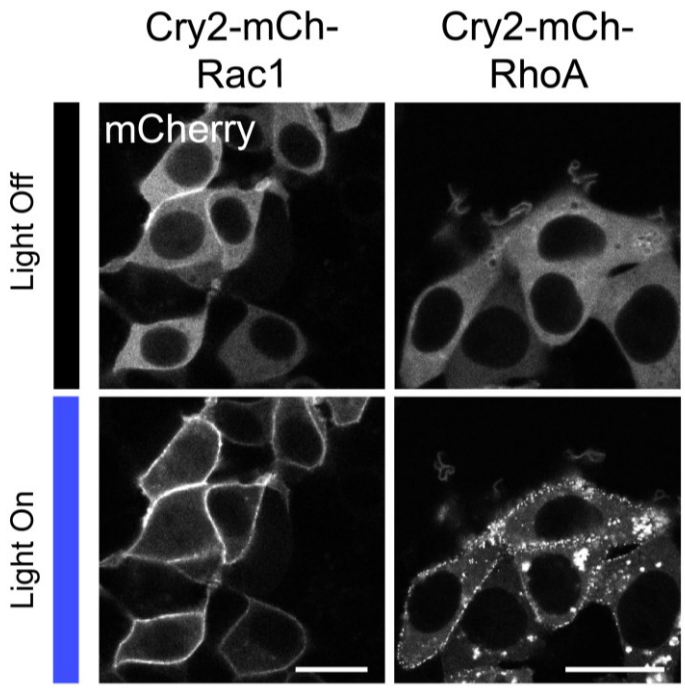

Figure 2.15 Light-induced clustering induces Rac1 and RhoA membrane translocation. Cry2-mCh-Rac1 translocates to the cell membrane, and Cry2-mCh-RhoA translocates to the cell membrane and vesicles upon light illumination of HEK 293Ts. Scale bars = 25 μm.

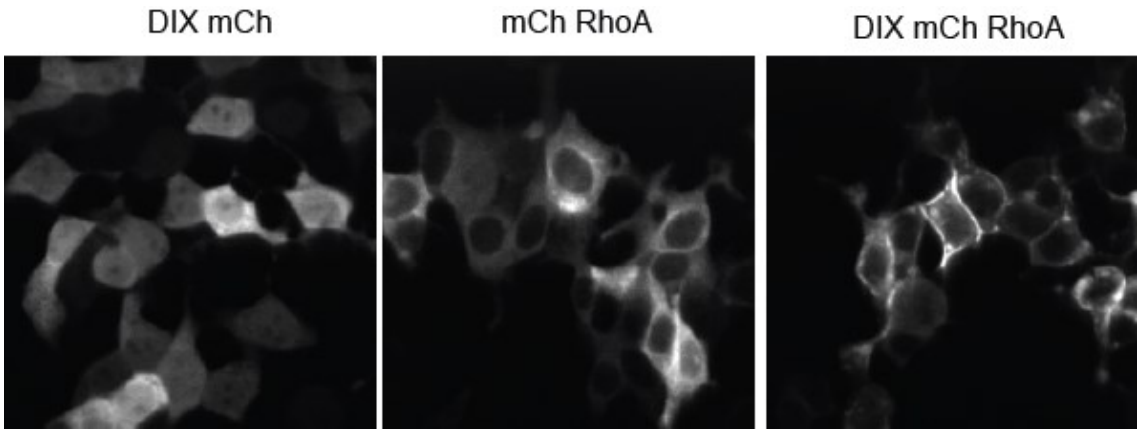

Figure 2.16 Constitutively oligomerized RhoA localizes to the membrane. A fusion of mCherry-RhoA to a constitutively oligomerizing DIX domain localizes to the membrane of transfected HEK 293Ts, whereas DIX-mCh or mCh-RhoA fusions do not. The DIX domain is a weakly oligomerizing domain, so no large clusters appear at this protein expression level in the DIX-mCh panel, though punctate fluorescence can be observed in highly-expressing cells.

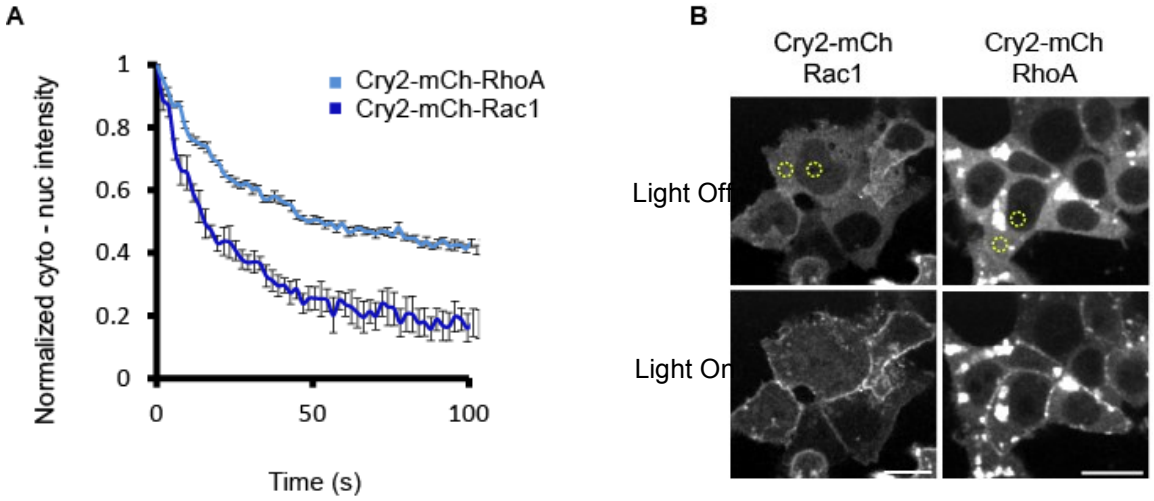

Figure 2.17 Comparison of membrane translocation kinetics of Cry2-mCh- Rac1 and Cry2-mCh-RhoA. A) Membrane translocation was measured by assessing mCherry fluorescence loss in the cytoplasm relative to nuclear fluorescence, which remained roughly constant. Difference between cytoplasmic intensity and nuclear intensity was normalized by the difference at t = 0. This normalized value was measured for 100 seconds of 0.5 Hz pulses of a 488 nm laser. Traces depict mean +/- 1 s.e.m. for n = 4 or 5 cells. Cry2-RhoA exhibits a smaller fraction of membrane translocation compared to the Cry2-Rac1 fusion. B) Representative images of HEK 293T cells expressing activated and unactivated constructs. Yellow circles represent regions where intensity was measured. Scale bars = 20 µm.

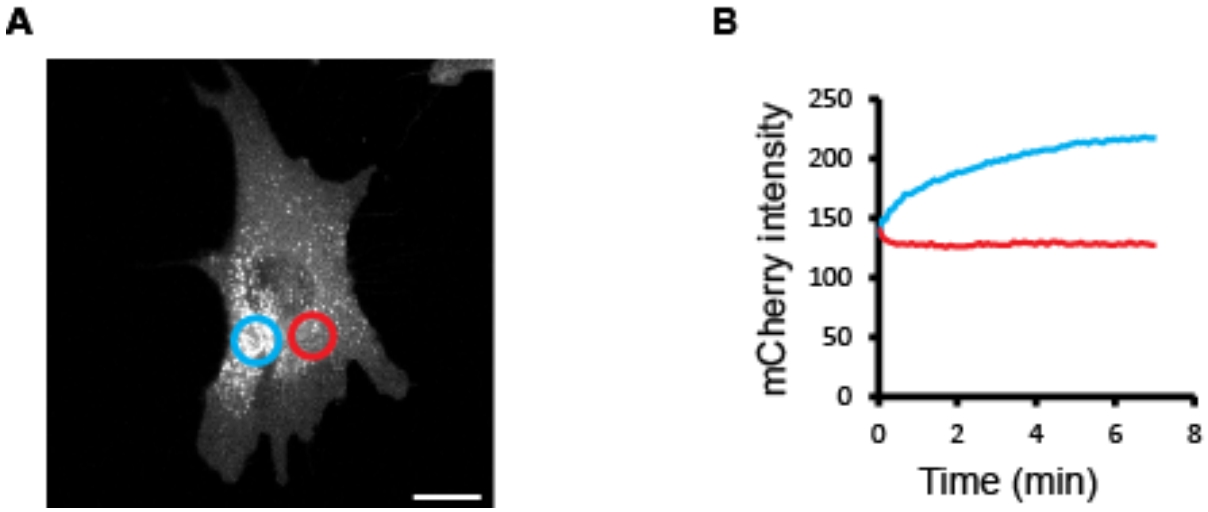

Figure 2.18 Focal illumination of 3T3 cells expressing Cry2-RhoA induces fluorescence accumulation and patterned cluster formation. A) Illumination with activating light (blue circle) recruits rapid fluorescence accumulation at the membrane and large clusters at and around the illumination spot, perhaps due to scatter from intense laser illumination or from diffusion of activated Cry2-RhoA. Cluster arrangement is non-random and appears localized to fibrillar structures. Scale bar = 20 µm. B) Fluorescence accumulation at the illumination region compared to an adjacent region is quantified. Trace shows mean fluorescence in blue and red regions in (A) over time.

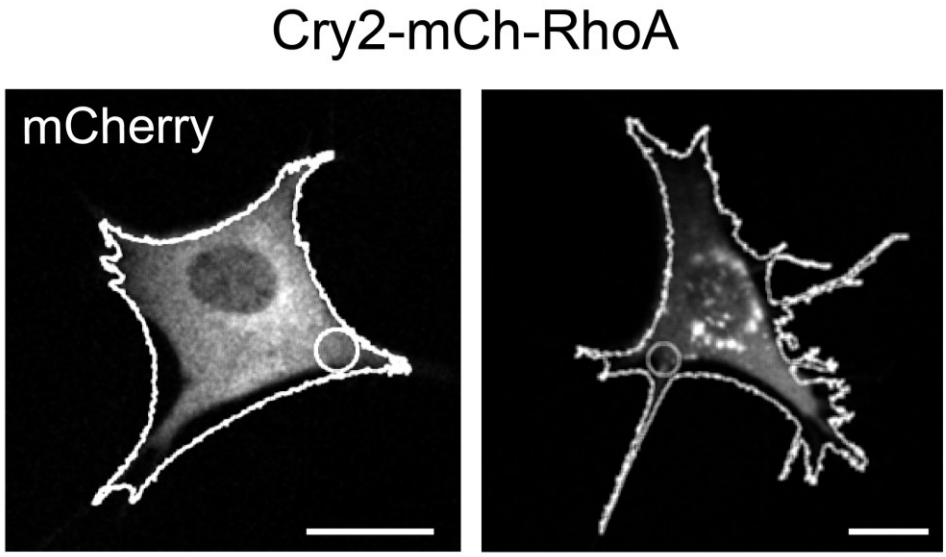

Figure 2.19 Single cell illumination of fibroblasts expressing Cry2-mCh-RhoA induces visible membrane retraction within minutes. Image shown at 8.5 minutes of activation, cell outline represents starting cell morphology, and circle depicts illumination region. Scale bar, 20 μm.

To biochemically verify that Cry2-mediated clustering was inducing RhoA activation, we used an ELISA assay (Figure 2.20) to probe for changes in levels of activated (GTP-bound) RhoA protein upon illumination of fibroblasts expressing Cry2-mCherry-RhoA. Light illumination induced a significant increase in RhoA-GTP levels compared to unilluminated controls ($p = 0.0495$, Mann-Whitney-Wilcoxon test, $n = 3$ replicates, representative of 5 experiments), though the observed activation may have been moderated since the pool of Cry2-mCherry-RhoA was only a fraction of the total RhoA content in the cells (Figure 2.21). To further characterize activity, we also examined the induction of stress fibers – bundles of filamentous actin that mediate cytoskeletal contractility and that are formed downstream of RhoA activation (*22*). Illumination of fibroblasts expressing Cry2-mCherry-RhoA showed a strong increase in both the number and intensity of stress fibers over unilluminated controls (Figure 2.22). Interestingly, in highly-expressing cells, visible light-induced Cry2-mCherry-RhoA clusters orient along – and in many cases colocalize with – the stress fibers. To further investigate the functional specificity of the photo-clustered RhoA response, fibroblast contractility was observed under wide field microscopy by assessing cell membrane retraction in the presence of pathway inhibitors. Illuminated cells expressing Cry2-mCherry-RhoA contracted at a higher frequency than cells expressing Cry2-mCh ($p < 0.001$, Tukey-Kramer test, $n = 6$ and 8 fields of view, Figure 2.23). Furthermore, inhibition of the RhoA downstream effector Rho-associated protein kinase (ROCK) with the small molecule Y-27632 reduced the percentage of contractile cells ($p < 0.001$, Tukey-Kramer test , $n = 8$ and 8), but inhibition of myosin light chain kinase – which mediates cytoskeletal contractility independently of RhoA and ROCK – did not ($p = 0.3$, Tukey-Kramer test, $n = 8$ and 10), indicating that the light-induced contractile response is in large part specific to RhoA activity. Taken together, these data strongly suggest that Cry2-mediated, light-inducible clustering of RhoA activates the RhoA pathway and induces cytoskeletal remodeling.

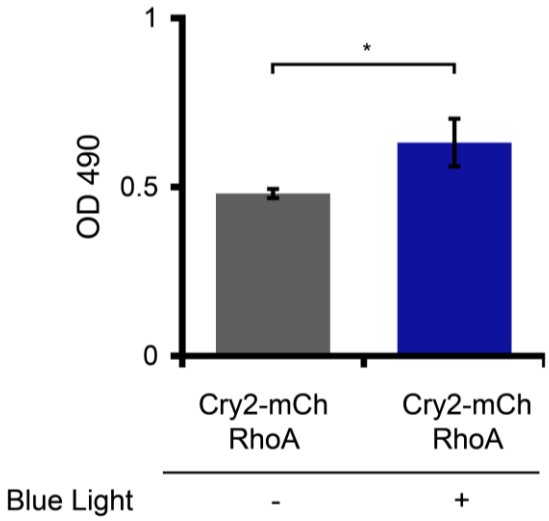

Figure 2.20 Biochemical validation of light-induced Cry2-mCh-RhoA activation. ELISA analysis shows cells expressing Cry2-mCh-RhoA have increased levels of GTP-bound (active) RhoA under blue light compared to unilluminated controls (mean +/- 1 s.d., n = 3 replicates, *p = 0.0495).

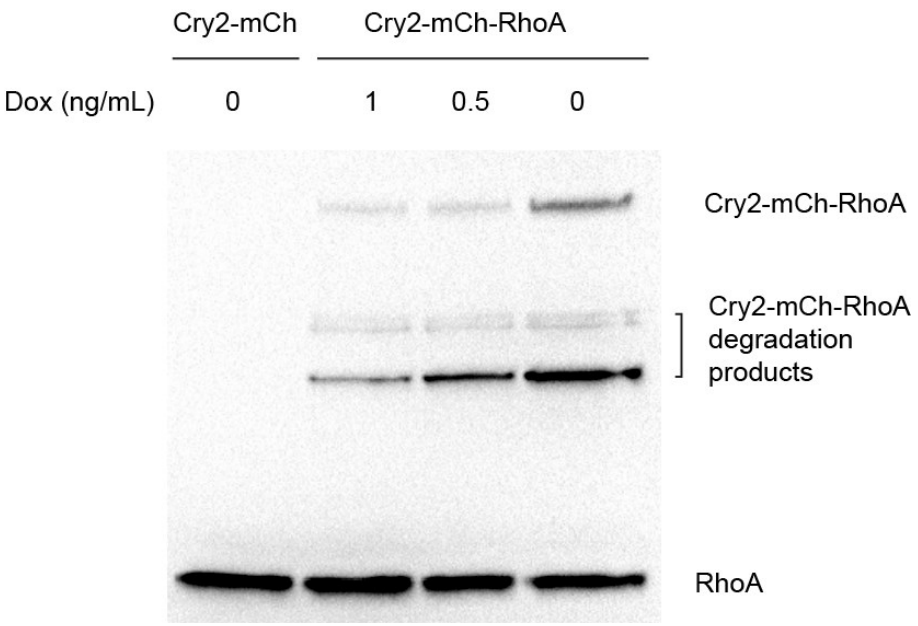

Figure 2.21 RhoA levels from Cry2-RhoA expression represent a fraction of endogenous RhoA levels. Western blotting shows RhoA expression levels in 3T3 fibroblasts transduced with Tet-Off controlled Cry2-mCh (lane 1) or Cry2-RhoA (lanes 2-4). 16 hours before lysing, cells were seeded and transferred from fully repressed conditions (100 ng/mL tetracycline) to moderately- or non-repressive conditions (various doxycycline concentrations). Most experiments were conducted under the 1 ng/mL condition, suggesting that Cry2-RhoA is sufficiently sensitive to modulate cell behavior at sub-physiological protein levels.

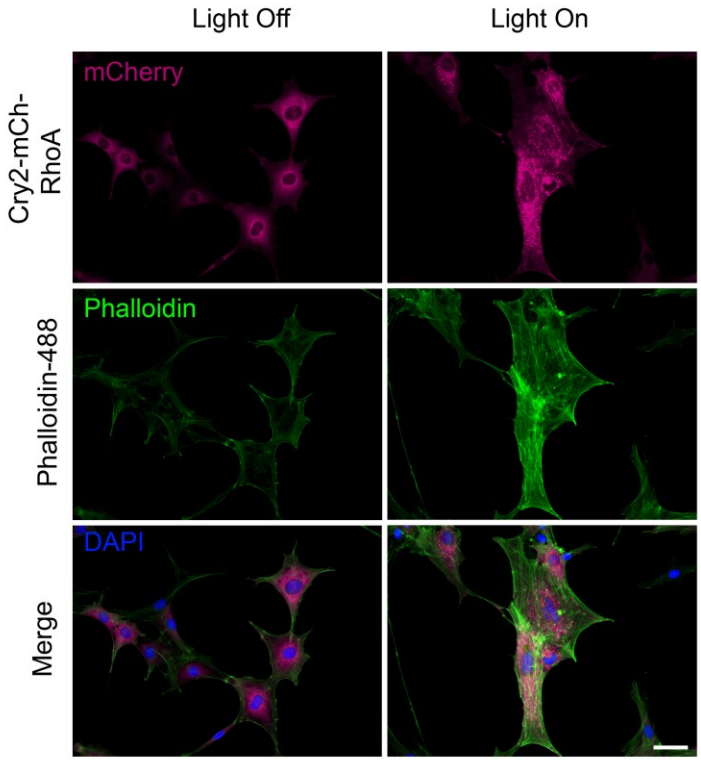

Figure 2.22 Cry2-mCh-RhoA photoactivation induces enhanced stress fiber formation in fibroblasts. Scale bar = 50 μm.

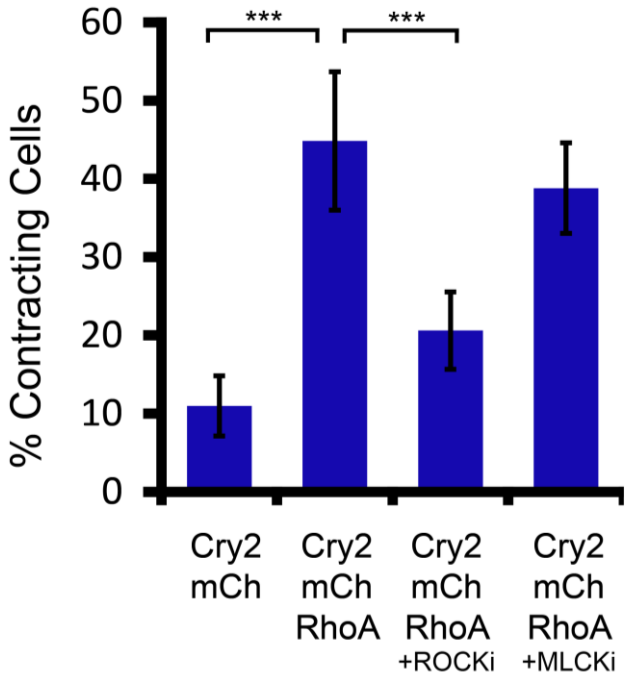

Figure 2.23 Whole-field light activation induces contractility in fibroblasts expressing Cry2-mCh-RhoA. Inhibition with a Rho associated kinase inhibitor Y-27632 (ROCKi), but not myosin light chain kinase inhibitor ML-7 (MLCKi), attenuates this effect, demonstrating dependence of light induced membrane retraction on RhoA pathway activation and independence from MLCK activity. Graph shows means +/- 1 s.d., n = 6-10 fields. ***p < 0.001.

2.3 Discussion

There is great anticipation that new tools allowing precise manipulation of cellular signaling may yield a more complete understanding of how protein signals modulate cell function and fate. Though similar approaches have been widely accepted in to study electrophysiological signaling in neuroscience and have transformed the field, optical perturbation of cell signaling is still not widely used as a common cell biology technique, in part because of the lack of appropriate or ideal tools to regulate signaling processes of interest. In this chapter, we have expanded on the modest existing optogenetic toolbox by demonstrating that the propensity of *Arabidopsis* Cry2 to cluster in response to light in mammalian cells can be harnessed to regulate diverse signaling cascades in a modular fashion.

The ability for Cry2 to homo-oligomerize was initially unexpected, though a review of the literature of within plant biology does reveal reports of nuclear and cytoplasmic formation of Cry2 "photobodies" (*11, 23*). Regardless, photobody formation had not been described in mammalian cells, and our published results, along with more recent results (*24*), demonstrate that no other plant-specific components are necessary for photobody formation. In plants, Cry2 forms clusters that also contain the proteins SPA1 and COP1. Though human cells possess no homologue to SPA1, they do contain a COP1 homolog, and it has recently been shown that *Arabidopsis* Cry2 can interact with human COP1 in a blue-light promoted manner (*24*). It is unclear whether COP1 is necessary for clustering, or whether the Cry2:COP1 interaction can affect native COP1 function within mammalian cells. Future protein engineering may yield truly orthogonal variants that do not interact with endogenous mammalian signaling proteins.

Heterodimeric association of Cry2 with CIB1 within mammalian cells had been reported with no mention of homomeric Cry2 association (*5*). Although we show that Cry2 clustering can be compatible with Cry2:CIB1 interaction (Figure 2.5), we have not performed rigorous studies on the effects of CIB1 presence on Cry2 clustering kinetics. As very little is known about the Cry2 structure or the binding interfaces employed in either Cry2 clustering or Cry2:CIB1 dimerization, it remains possible that these two processes are competitive or antagonistic. Though Cry2 clustering did not interfere with the heterodimerization demonstrations in the initial publication, the authors do mention a loss of function of Cry2 tethered to the membrane, which may be caused for instance by enhanced Cry2-Cry2 interactions due to enhanced local concentration upon membrane tethering. This dual nature of Cry2 is a key factor to consider when planning experiments based on Cry2:CIB1 association.

Our ability to regulate Rho GTPase localization and signaling by clustering represents an interesting finding and an unappreciated mode of regulation for this widely studied class of proteins. Although *in vitro* (i.e. test tube) Rac1 oligomerization was examined in one report (*19*), further investigations on this subject were not performed. To our knowledge, there have been no studies on the effects of RhoA multimerization. The finding that Rac1 and RhoA both can be regulated in this same manner suggests that a commonality in their shared activation cycle is responsible for their sensitivity to clustering. Indeed, family member Cdc42 also exhibits membrane translocation upon clustering (Chapter 4). We further examined the mechanisms of Rho GTPase cluster-induced activation, with results described in Chapter 4.

In summary, Cryptochrome 2-mediated protein clustering can modulate diverse signaling pathway activities in a dynamic manner, offering an approach for both quantitative investigation of signal transduction dynamics and for analysis of oligomerization as a potentially important mechanism in cellular signaling. The modular, genetically encodable, and single-construct nature of Cry2 – which in the future can be adapted to additional signal transducers – thus represents a versatile protein clustering system with potential to extend the benefits of precise photoactivation to numerous signaling molecules and pathways.

2.4 Methods

Cloning and viral production

The LRP6 C-terminus (*16*) was amplified from the pCS2+ LRP6 and inserted into the Cry2PHR-mCherry plasmid between *Bsr* GI and *Xba* I sites, resulting in Cry2-mCherry-linker-LRP6c, with the linker GGGGSGGGGS. 1x and 3x DmrB-mCh-LRP6c constructs were created by first amplifying the DmrB domain from pMSCV-F-del-Casp9.IRES.GFP (www.addgene.org, plasmid #15567) and inserting them upstream of mCh-LRP6c through the CPEC method (*25*). Rac1 and RhoA were subcloned into Cry2PHR-mCherry between *Bsr* GI and *Not* I with the same linker as for LRP6c. Cry2 fusions were then subcloned into the MMLV retroviral vector CLPIT or CLGPIT, which provide tetracycline repressible transgene control. Virus was packaged as described (*26*), in the presence of 100 ng/mL doxycycline to repress transgene expression. CA-GSK3β was generated by point mutagenesis of sequence recovered from NSC cDNA via RT-PCR and was cloned into CLPIT. A lentiviral plasmid encoding the 7x TFP luciferase reporter was obtained from Addgene (www.addgene.org, plasmid # 24308) and was packaged in HEK 293T cells. Stable cell lines were created through infection and puromycin selection. A list of all DNA constructs generated is provided in Appendix A.

Cell culture

HEK 293Ts were cultured on polystyrene plates in Iscove's Modified Eagle Medium (Corning cellgro, Manassas, VA) with 10% fetal bovine serum (FBS) (Life Technologies) and 1% penicillin/streptomycin (P/S) (Life Technologies) at 37°C and 5% CO_2. Rat hippocampal adult neural stem cells (NSCs) (*27*), were cultured on polystyrene plates coated with poly-ornithine and 5 µg/mL laminin (Life Technologies, Grand Island, NY). NSCs were cultured in Dulbecco's Modified Eagle Medium (DMEM)/F12 (1:1) high-glucose medium containing N-2 supplement (both from Life Technologies) and 20 ng/mL recombinant human FGF-2 (Peprotech, Rocky Hill, NJ). Illumination experiments were conducted in the presence of 0.5% FBS to act as a carrier molecule for the controls containing Wnt3a (R&D Systems). NIH 3T3 fibroblasts were cultured in DMEM (Corning cellgro) supplemented with 10% bovine calf serum (BCS) and 1% P/S. Stable cell lines expressing the Cry2-RhoA construct were maintained in 100 ng/mL tetracycline to repress expression, as high levels of sustained Cry2-RhoA expression impaired cell growth. Tetracycline was withdrawn 24 h before contractility experiments and replaced with 1ng/mL doxycycline, and serum was reduced to 2%.

Luciferase assay

For chemically induced oligomerization experiments, 293T cells harboring the 7x TCF luciferase reporter were seeded in 48-well plates. When ~70% confluent, cells were transfected with 300 ng of the expression vectors and 150 ng pBluescript by the calcium phosphate method. 24 hours after transfection, 500 nM of B/B Homodimerizer (Clontech, Mountain View, CA) was added to designated wells. After 16 hours of treatment, cells were lysed, and luciferase was measured with the Luc-screen Firefly Luciferase Gene Reporter System (Life Technologies).

Experiments testing Cry2-mCh-LRP6c function were carried out in a similar manner, but cells were seeded in black walled 96-well plates, and only 5 ng of expression vector diluted in 150 ng pBluescript was transfected. 24 hours after transfection, cells were subjected to a light illumination protocol from a custom LED illumination device. Briefly, an LED array was constructed based on the open source electronics Arduino platform (www.arduino.cc). 5 mm blue LEDs (470 nm, 6000 mCandella, 20° illumination, www.electron.com) with a 3 mW measured output (Coherent, Santa Clara, CA) were placed underneath wells of a 96 well plate and were driven through independent channels by the Arduino. Custom software was written to allow illumination with definable light pulse width, frequency, and intensity. The code can be found in Appendix B. The illumination device is pictured in Figure 2.13. The plate with cells was placed on top of the LED device so that the LEDs illuminated directly underneath individual wells. 500 ms blue light pulses were admnistered every 10 s. After 16 hours of illumination, cells were lysed ,and luciferase was measured as above. For NSC experiments, cells carying the 7x TCF reporter were seeded in a 35 mm dish and infected with retrovirus encoding Cry2-mCh-LRP6c at a multiplicity of infection of 3. After 2 days, cells were seeded at 80,000 cells per well in a black walled, 96-well, laminin coated plate, and after 1 hour were illuminated with the custom LED array for 16 hours. Luciferase readout from NSCs was measured as above.

Immunobloting

Cells were lysed with RIPA buffer containing protease inhibitors, and cell lysates were electrophoretically separated on an SDS-PAGE gel. Proteins were then transferred onto a nitrocellulose membrane and probed for active β-catenin (Millipore, cat. # 05-665), RhoA (Cell Signaling, cat. #2117) and GAPDH (Abcam, cat. # ab9485) as a loading control.

Stress Fiber Visualization

Cry2-mCh-RhoA expressing NIH 3T3s were serum starved by seeding at 2500 cells/cm^2 on glass-bottom 6-well plates (MatTek Corporation, Ashland, MA) in DMEM/F12 (Life Technologies) supplemented with 1% P/S, 10% FBS, and 100 ng/mL tetracycline. After 24 hr, cells were gently washed twice with PBS and the same medium was added but with 0.1% FBS. 24 hrs later, the process was repeated, but serum free medium was added and tetracycline withdrawn. Cells were repeatedly pulsed (3s on, 12s off) with light from a blue 19-LED array (ledlight.com, cat. # 28345) for 10 minutes and then immediately fixed in 4% paraformaldehyde. Cells were incubated in Alexa 488-conjugated phalloidin (Life Technologies) and DAPI diluted in phosphate buffered saline containing 0.3% Triton-X for 30 minutes. Images were obtained through epifluorescence microscopy using a TE2000-E2 microscope (Nikon Corporation, Tokyo, Japan).

ELISA

Cry2-mCh-RhoA expressing NIH 3T3 cells were seeded in 6 well plates at 70,000 cells per well and serum starved over 3 days, as above. After 24 hrs in serum free medium

supplemented with 1 ng/mL doxycycline, cells were exposed to 2 minutes of blue LED light. The samples were processed, and the levels of GTP-loaded (active) RhoA were determined using the G-LISA RhoA Activation Assay Biochem Kit (Cytoskeleton, Inc., Denver, CO) according to manufacturer instructions. This ELISA-based assay uses the differential binding of GDP- vs GTP-loaded RhoA to the binding domain of Rhotekin to determine the relative levels of only active RhoA in a sample.

Live Cell Imaging

Time lapse microscopy of activated Cry2 fusions in HEK 293Ts was performed using a BX51WI microscope (Olympus Corporation, Center Valley, PA) equipped with Swept Field Confocal technology (Prairie Technologies, Inc., Middleton, WI). Clustering visualization in 293Ts was carried out at room temperature. Simultaneous blue light exposure and mCherry imaging was accomplished by imaging in both 488 nm and 561 nm laser channels, 1 exposure per 2-5 seconds, with 488 nm laser varied between 0.1 and 100% power. Given the minute-timescale of the dissociation kinetics of Cry2 clustering, this intermittent pulsing was considered a sufficient approximation of continuous exposure and was necessary to avoid extensive photobleaching of the mCherry fluorophore. Focal illumination of NIH 3T3 cells expressing Cry2-mCh-RhoA was performed on a Zeiss LSM 710 AxioObserver confocal microscope with full incubation chamber in conjunction with the Zeiss ZEN software. All experiments were carried out at 37°C and in 5% CO_2. mCherry was visualized with 561 nm laser excitation through a 63x oil immersion objective, and blue light focal illumination was carried out through the FRAP application with the 458 nm laser light between 0.1%-10% power for 6-100 μs dwell time per pixel in a 10 μm diameter region. FRAP, z-stacks, and timelapse microscopy observing cluster formation were also acquired with the Zeiss LSM 710. For wide field contractility measurements, cells were imaged under bright field using a Nikon Eclipse Ti inverted microscope and exposed to 200 us pulses of blue light from a xenon arc lamp passed through a GFP filter cube. Pulses were delivered every 20 seconds for 10 minutes, and images were assembled in ImageJ. Contraction was determined by membrane retraction, which was assessed through visual inspection, and the number of contracting cells was divided by total number of cells in the field to obtain percentage of contracting cells.

Image Analysis

Stacks of single-cell clustering timelapse images were assembled in ImageJ (http://rsbweb.nih.gov/ij/). Clusters were then counted in each frame of the timelapse in CellProfiler (www.cellprofiler.com) by first thresholding the fluorescence image so that the software recognized clusters in the right intensity range. This appropriate threshold was determined manually for each cell due to cell-to-cell fluorescence intensity variation. Plotting cluster number vs. time yielded a sigmoidal relationship, which was fit to the Hill function for the purposes of extracting $T_{1/2}$, the time the cluster number reached half of its final value:

$$C = \frac{t^n}{t^n + T_{\frac{1}{2}}^{\ n}}$$

where C represents cluster number, t is time, n is the hill coefficient. $T_{1/2}$ provides a metric by which to compare clustering conditions. To demonstrate the dependence of clustering on laser power, $T_{1/2}$ was plotted vs. 488 nm laser power after normalization by mean cell fluorescence to correct for protein expression level differences. To determine the relationship between mean cell fluorescence and $T_{1/2}$, $T_{1/2}$ was measured for cells at 4 different laser intensities, and for each laser intensity setting, linear relationships were observed between mean cell fluorescence and $T_{1/2}$. The mean of the slopes of the linear fit for each laser setting were averaged, and this value represented the estimated $T_{1/2}$ change per change in mean cell fluorescence. Individual $T_{1/2}$ values were then adjusted by this factor to effectively normalize protein concentration among all cells.

Quantitation of fluorescence relocalization in HEK 293T cells expressing Cry2-mCh-Rac1 and Cry2-mCh-RhoA was accomplished by the following algorithm:

$$\frac{I_{Cyto,t} - I_{Nuclear,t}}{I_{Cyto,initial} - I_{Nuclear,initial}}$$

where $I_{Cyto,t}$ and $I_{Nuclear,t}$ are cytoplasmic and nuclear fluorescence intensity at time t, respectively, and $I_{Cyto,\ initial}$ and $I_{Nuclear,\ initial}$ are the initial values of cytoplasmic and nuclear fluorescence.

Statistical Analysis

All statistical analysis was performed using the JMP 10 software. Jonckheere-Terpstra trend analysis is a nonparametric method used to ascertain whether population medians have an *a priori* ordering. The Mann-Whitney-Wilcoxon test is a nonparametric method for comparing two sample sets. For details on both, see Hollander and Wolfe (1999).

2.5 Acknowledgements

We thank Dr. Sanjay Kumar for technical discussions and use of equipment and reagents, and Joanna McKay and Dr. Sebastian Rammensee for experimental advice and assistance. We received the Cry2PHR-mCherry construct as a gift from Dr. Chandra Tucker, constitutively active variants of Rac1, RhoA, and Cdc42 as gifts from Dr. G. Steven Martin, the full length LRP6 construct as a gift from Dr. Xi He, and CA-β-catenin as a gift from Dr. Anand Asthagiri. We would also like to thank Dr. Magdalena Niewiadomska-Bugaj for statistical analysis, Dr. Albert Keung for retroviral constructs encoding the Rho GTPases, and Ashley Fritz for retroviral constructs encoding CA-β-catenin and CA-GSK-3β. This work was supported by the Department of Energy Award DE-SC0001216 and DE-SC0001874.

2.6 Appendices

2.6.1 Appendix A

List of DNA constructs generated for Chapter 2.

Construct Name	***Backbone***	***Description***
Cry2-mCh	pmCherry-N1	PHR domain of *At* Cry2 (a.a.1-498) fused to mCherry
Cry2-mCh	CLPIT retroviral vector	PHR domain of *At* Cry2 (a.a.1-498) fused to mCherry
Cry2(D387A)-mCh	pmCherry-N1	PHR domain of *At* Cry2 (a.a.1-498) fused to mCherry
Cry2-LRP6c	pmCherry-N1	Endodomain of LRP6 receptor fused to the C-terminus of Cry2-mCh
Cry2-LRP6c	CLGPIT retroviral vector	Endodomain of LRP6 receptor fused to the C-terminus of Cry2-mCh
Cry2(D387A)-LRP6c	pmCherry-N1	Light insensitive mutant of Cry2-LRP6
Cry2-Rac1	pmCherry-N1	Full length wild-type Rac1 fused to the C-terminus of Cry2-mCh
Cry2-Rac1	CLPIT retroviral vector	Full length wild-type Rac1 fused to the C-terminus of Cry2-mCh
Cry2(D387A)-Rac1	pmCherry-N1	Light insensitive mutant of Cry2-Rac1
Cry2(D387A)-Rac1	CLPIT retroviral vector	Light insensitive mutant of Cry2-Rac1
Cry2-RhoA	pmCherry-N1	Full length wildtype RhoA fused to the C-terminus of Cry2-mCh
Cry2-RhoA	CLPIT retroviral vector	Full length wildtype RhoA fused to the C-terminus of Cry2-mCh
Cry2(D387A)-RhoA	pmCherry-N1	Light insensitive mutant of Cry2-RhoA
Cry2(D387A)-RhoA	CLPIT retroviral vector	Light insensitive mutant of Cry2-RhoA
DIX-mCh	CLPIT retroviral vector	DIX domain if Dishevelled2 (a.a 8-94) fused to the N-terminus of mCherry
DIX-mCh-RhoA	CLPIT retroviral vector	Full length wild-type RhoA fused to the C-terminus of DIX-mCh
mCh-RhoA	CLPIT retroviral vector	Full length wild-type RhoA fused to the C-terminus of mCherry
1xDmrB-mCh-LRP6c	pmCherry-N1	One DmrB domainfused to mCh and the endodomain of LRP6 receptor
2xDmrB-mCh-LRP6c	pmCherry-N1	Two DmrB domains fused to mCh and the endodomain of LRP6 receptor
3xDmrB-mCh-LRP6c	pmCherry-N1	Three DmrB domains fused to mCh and the endodomain of LRP6 receptor

2.6.2 Appendix B

Code used for controlling Arduino Uno for defined LED illumination programs

/*

Multiple_Channel_LED_Control:

This code was written in the Arduino programming language to drive an Arduino Uno microcontroller. To download a free copy of the software environment, please visit http://arduino.cc/en/main/software.

This program allows independent control of LED illumination pulse length, pulse interval, and illumination intensity for up to 6 independent LED channels, though it can readily be expanded for up to as many channels as pins in an Arduino board.

To use, first define each channel *pin1, pin2, etc.* by assigning a physical pin number from the Arduino board. To change the length of time between LED pulses within a channel, assign the corresponding *interval* variable (e.g. *interval1* defines the pulse interval for *pin1*) the desired time interval between pulses, in milliseconds. Similarly, to change the pulsewidth of a channel, assign to corresponding *pulse* variable a pulsewidth time, given in milliseconds. For example, as given below, channel 1 is transmitted through pin 2 on the Arduino board and will give a 500 ms pulse of light every 10 seconds.

Each pin of an Arduino Uno board puts out 5V. To adjust intensity of illumination, define the *intensity* variable with a value from 0-255, with 0 being no illumination and 255 being full illumination. Alternatively, choose the appropriate resistor or circuit architecture to regulate current flow through the LED, being careful not to exceed the current limits of your individual LED.

This program was developed and published by Lukasz Bugaj in the following publication:

Bugaj, L. J., Choksi, A. T., Mesuda, C. K., Kane, R. S., & Schaffer, D. V., *Nat Methods* (2013). *Advanced Online Publication*
http://www.nature.com/nmeth/journal/vaop/ncurrent/full/nmeth.2360.html

The hardware used in this study is depicted in Supplementary Figure 5.

For help or further clarification, consult the above publication or email lukasz at berkeley.edu.

Good luck!

*/

```
/*assigns physical arduino pins to variables.   */
/*for analog control, must use pins 3,5,6,9,10,11 */
const int pin1 = 3;
const int pin2 = 5;
const int pin3 = 6;
const int pin4 = 9;
const int pin5 = 10;
const int pin6 = 11;

/*defines initial state of pins (0 = OFF)*/
int ledState1 = 0;
int ledState2 = 0;
int ledState3 = 0;
int ledState4 = 0;
int ledState5 = 0;
int ledState6 = 0;

/* defines variable determining % duty cycle of "ON" pulse. */
/*Simulates analog intensity modulation" */
/* intensity on scale from 0-255*/
/*255 = full intensity, 128 = half intensity, etc*/
int intensity1 = 255;
int intensity2 = 128;
int intensity3 = 64;
int intensity4 = 32;
```

```
int intensity5 = 16;
int intensity6 = 8;

/*defines variable for storing run time (ms)*/
long prevMillis1 = 0;
long prevMillis2 = 0;
long prevMillis3 = 0;
long prevMillis4 = 0;
long prevMillis5 = 0;
long prevMillis6 = 0;

/*defines variable for intervals between pulses (ms)*/
long interval1 = 1000;
long interval2 = 1000;
long interval3 = 1000;
long interval4 = 1000;
long interval5 = 1000;
long interval6 = 1000;

/*defines pulse width (ms)*/
long pulse1 = 500;
long pulse2 = 500;
long pulse3 = 500;
long pulse4 = 500;
long pulse5 = 500;
long pulse6 = 500;

void setup(){
  pinMode(pin1,OUTPUT);
  pinMode(pin2,OUTPUT);
  pinMode(pin3,OUTPUT);
  pinMode(pin4,OUTPUT);
  pinMode(pin5,OUTPUT);
  pinMode(pin6,OUTPUT);

}

void loop(){
 /*defines variable for storing run time (ms)*/
 unsigned long currentMillis1 = millis();
 unsigned long currentMillis2 = millis();
 unsigned long currentMillis3 = millis();
 unsigned long currentMillis4 = millis();
 unsigned long currentMillis5 = millis();
 unsigned long currentMillis6 = millis();
```

```
/*
 Code to determine on or off state of each channel. There are 6 parallel independent  loops (1 for
each channel)

 loop logic:
   if defined "interval" has elapsed
     if light is off, turn it on
     else if light is on and defined "pulse" has lapsed, turn it off

   else do nothing
 */



 /*Channel 1*/
 if (currentMillis1-prevMillis1 >= interval1)
   {

    if (ledState1 == 0){
      ledState1 = intensity1;
      prevMillis1 = currentMillis1;
    }
   }
    else {
      if (currentMillis1-prevMillis1 >= pulse1)
      ledState1 = 0;
    }

/*Channel 2*/
   if (currentMillis2-prevMillis2 >= interval2)
   {

    if (ledState2 == 0){
      ledState2 = intensity2;
      prevMillis2 = currentMillis2;
    }
   }
    else {
      if (currentMillis2-prevMillis2 >= pulse2)
      ledState2 = 0;
    }

 /*channel 3*/
   if (currentMillis3-prevMillis3 >= interval3)
   {
```

```
    if (ledState3 == 0){
      ledState3 = intensity3;
      prevMillis3 = currentMillis3;
    }
   }
    else {
      if (currentMillis3-prevMillis3 >= pulse3)
      ledState3 = 0;
    }

 /*Channel 4*/
   if (currentMillis4-prevMillis4 >= interval4)
   {

    if (ledState4 == 0){
      ledState4 = intensity4;
      prevMillis4 = currentMillis4;
    }
   }
    else {
      if (currentMillis4-prevMillis4 >= pulse4)
      ledState4 = 0;
    }

/*Channel 5*/
    if (currentMillis5-prevMillis5 >= interval5)
   {

    if (ledState5 == 0){
      ledState5 = intensity5;
      prevMillis5 = currentMillis5;
    }
   }
    else {
      if (currentMillis5-prevMillis5 >= pulse5)
      ledState5 = 0;
    }

/*Channel 6*/
    if (currentMillis6-prevMillis6 >= interval6)
   {

    if (ledState6 == 0){
      ledState6 = intensity6;
      prevMillis6 = currentMillis6;
```

```
    }
   }
    else {
      if (currentMillis6-prevMillis6 >= pulse6)
      ledState6 = 0;
    }


  /*outputs result of loops to LEDs*/
  analogWrite(pin1,ledState1);
  analogWrite(pin2,ledState2);
  analogWrite(pin3,ledState3);
  analogWrite(pin4,ledState4);
  analogWrite(pin5,ledState5);
  analogWrite(pin6,ledState6);



}
```

2.7 References

1. L. Dehmelt, P. I. H. Bastiaens, Spatial organization of intracellular communication: insights from imaging. *Nat. Rev. Mol. Cell Biol.* **11**, 440 (2010).
2. M. Mammen, S.-K. Choi, G. M. Whitesides, Polyvalent Interactions in Biological Systems: Implications for Design and Use of Multivalent Ligands and Inhibitors. *Angew. Chem. Int. Ed. Engl.* **37**, 2754 (1998).
3. D. Spencer, T. Wandless, S. Schreiber, G. Crabtree, Controlling signal transduction with synthetic ligands. *Science* **262**, 1019 (1993).
4. A. Moglich, K. Moffat, Engineered photoreceptors as novel optogenetic tools. *Photochem. Photobiol. Sci.* **9**, 1286 (2010).
5. M. J. Kennedy *et al.*, Rapid blue-light-mediated induction of protein interactions in living cells. *Nat. Meth.* **7**, 973 (2010).
6. A. Levskaya, O. D. Weiner, W. A. Lim, C. A. Voigt, Spatiotemporal control of cell signalling using a light-switchable protein interaction. *Nature* **461**, 997 (2009).
7. D. Strickland *et al.*, TULIPs: tunable, light-controlled interacting protein tags for cell biology. *Nat. Meth.* **9**, 379 (2012).
8. M. Yazawa, A. M. Sadaghiani, B. Hsueh, R. E. Dolmetsch, Induction of protein-protein interactions in live cells using light. *Nat. Biotech.* **27**, 941 (2009).
9. S. Shimizu-Sato, E. Huq, J. M. Tepperman, P. H. Quail, A light-switchable gene promoter system. *Nat. Biotech.* **20**, 1041 (2002).
10. X. Wang, X. Chen, Y. Yang, Spatiotemporal control of gene expression by a light-switchable transgene system. *Nat. Meth.* **9**, 266 (2012).
11. P. Mas, P. F. Devlin, S. Panda, S. A. Kay, Functional interaction of phytochrome B and cryptochrome 2. *Nature* **408**, 207 (2000).
12. H. Liu *et al.*, Photoexcited CRY2 Interacts with CIB1 to Regulate Transcription and Floral Initiation in Arabidopsis. *Science* **322**, 1535 (2008).
13. M. Hollander, D. A. Wolfe, *Nonparametric statistical methods*. Wiley series in probability and statistics Text and references section (Wiley, New York, ed. 2nd, 1999), pp. xiv, 787 p.
14. J. Bilić *et al.*, Wnt Induces LRP6 Signalosomes and Promotes Dishevelled-Dependent LRP6 Phosphorylation. *Science* **316**, 1619 (2007).
15. F. Cong, L. Schweizer, H. Varmus, Wnt signals across the plasma membrane to activate the β-catenin pathway by forming oligomers containing its receptors, Frizzled and LRP. *Development* **131**, 5103 (2004).
16. C. Metcalfe, C. Mendoza-Topaz, J. Mieszczanek, M. Bienz, Stability elements in the LRP6 cytoplasmic tail confer efficient signalling upon DIX-dependent polymerization. *J. Cell Sci.* **123**, 1588 (2010).
17. C. Fuerer, R. Nusse, Lentiviral Vectors to Probe and Manipulate the Wnt Signaling Pathway. *PLoS ONE* **5**, e9370 (2010).

18. A. B. Jaffe, A. Hall, Rho GTPases: biochemistry and biology. *Annu. Rev. Cell Dev. Biol.* **21**, 247 (2005).
19. B. Zhang, Y. Gao, S. Y. Moon, Y. Zhang, Y. Zheng, Oligomerization of Rac1 gtpase mediated by the carboxyl-terminal polybasic domain. *J Biol Chem* **276**, 8958 (2001).
20. J. T. Parsons, A. R. Horwitz, M. A. Schwartz, Cell adhesion: integrating cytoskeletal dynamics and cellular tension. *Nat. Rev. Mol. Cell Biol.* **11**, 633 (2010).
21. Y. I. Wu *et al.*, A genetically encoded photoactivatable Rac controls the motility of living cells. *Nature* **461**, 104 (2009).
22. A. J. Ridley, A. Hall, The small GTP-binding protein rho regulates the assembly of focal adhesions and actin stress fibers in response to growth factors. *Cell* **70**, 389 (1992).
23. X. Yu *et al.*, Formation of Nuclear Bodies of Arabidopsis CRY2 in Response to Blue Light Is Associated with Its Blue Light–Dependent Degradation. *Plant Cell* **21**, 118 (2009).
24. I. Ozkan-Dagliyan *et al.*, Formation of Arabidopsis Cryptochrome 2 Photobodies in Mammalian Nuclei: APPLICATION AS AN OPTOGENETIC DNA DAMAGE CHECKPOINT SWITCH. *Journal of Biological Chemistry* **288**, 23244 (2013).
25. J. Quan, J. Tian, Circular Polymerase Extension Cloning of Complex Gene Libraries and Pathways. *PLoS ONE* **4**, e6441 (2009).
26. J. H. Yu, D. V. Schaffer, Selection of novel vesicular stomatitis virus glycoprotein variants from a peptide insertion library for enhanced purification of retroviral and lentiviral vectors. *Journal of virology* **80**, 3285 (2006).
27. F. H. Gage *et al.*, Survival and differentiation of adult neuronal progenitor cells transplanted to the adult brain. *Proc. Natl. Acad. Sci. U S A* **92**, 11879 (1995).

Chapter 3

Regulation of Endogenous Transmembrane Receptors through Optogenetic Cry2 Clustering

3.1 Introduction

Cells receive environmental information via transmembrane receptor transmission, and these "data" are integrated to regulate diverse biological processes including cell proliferation, motility, differentiation, and death. Often, these biological signals have rich temporal and spatial components. Cells can respond differentially to transient, sustained, or oscillatory presentation of the same signal (*1*), and behavior can be regulated within a cell (*3*) or population of cells (*4*) through polarization and spatially defined gradients of signaling molecules.

To study how information is translated through individual receptors, numerous methods have been developed to inducibly regulate receptor function. Since oligomerization is a common mechanism by which receptor activity is mediated (*5-11*), many of these tools have focused on inducing receptor clustering to modulate receptor activity. These methods include application of cross-linked antibodies specific to the receptor ectodomain, treatment with synthetic multivalent ligands (*12, 13*), or chemically-induced dimerization (CID) of tandem dimerization domains in exogenously expressed protein fusions (*14*). Another strategy has been the engineering of novel G-protein coupled receptors that respond only to orthogonal small molecules, termed RASSL (Receptors activated solely by a synthetic ligand) (*15*). However, due to the reliance of these methods on addition of exogenous molecules, they are unable to recapitulate signaling with the spatiotemporal resolution observed in biological systems.

In addition to the above strategies, exogenous receptor overexpression is also commonly used to study receptor function. However, artifacts associated with the introduction of high copy number receptor expression often result in hypersensitive or constitutive signal generation, which can fundamentally alter how cells respond to a particular stimulus. For example, overexpression of insulin-like growth factor receptor (IGF-R) or epidermal growth factor receptor (EGFR) in PC12 cells changes the IGF- or EGF-induced response from proliferation to differentiation (*16, 17*), and overexpression of the tumor necrosis factor receptor 1 (TNF-R) receptor induces constitutive signaling and cell death (*18*). Methods allowing manipulation of endogenous receptors may avoid these concerns and avoid experimental misinterpretation due to artifactual data.

In recent years, the emerging field of optogenetics has offered a handful of methods to optically control and study numerous biological phenomena with spatiotemporal precision, including protein-protein interactions (*2, 19-23*), protein secretion (*24*), gene transcription (*25-27*), gene translation (*28*), cell motility (*29*), and temporally dynamic protein signal transduction (*30*). These efforts have allowed targeted activation of intracellular signaling proteins, including Rho GTPases, Raf-1, PI3-kinase β-catenin, and caspases. However, the environment communicates through receptors to activate numerous pathways simultaneously, and thus activation of a single pathway offers limited ability to study receptor-ligand regulation of cell behavior.

A general method for photoregulation of endogenous transmembrane receptors would thus be a powerful tool for studying how cells interpret and respond to signals resulting from intrinsic and extrinsic receptor dynamics as these proteins sense the time-varying extracellular environment. We recently co-opted the inherent blue-light-dependent oligomerization of *Arabidopsis* Cry2 to regulate clustering of fusion proteins in mammalian cells, which enabled the robust cytoplasmic activation of the Wnt/β-catenin and RhoA pathways (*2*)**.** However, Cry2 clustering of cell membrane proteins was not achieved in this previous study.

In this report, we re-designed and implemented the Cry2 clustering module in a methodology called Clustering Indirectly using Cryptochrome 2, or CLICR. The CLICR approach enabled clustering and activation of binding partners, which allowed us to successfully target and activate both cytoplasmic and cell surface receptors with blue light. We further demonstrate that this strategy provides sufficient potency to modulate receptor activity of several endogenous receptors including FGFR, PDGFRβ, and β-integrins, and we exhibit its capability for defined spatiotemporal regulation of endogenous receptors through Cry2-mediated, PDGFRβ-dependent phototaxis in mammalian cells.

3.2 Results

In designing CLICR (Figure 3.1), we hypothesized that Cry2 fused to a binding domain (Cry2-BD) possessing limited affinity for a target receptor would remain largely in the cytoplasm in the absence of light. Upon blue light illumination, clusters of Cry2-BD would assemble and thereby effectively create high local concentrations of the BD that may enable simultaneous binding to multiple receptor endodomains, resulting in receptor clustering and signal activation.

As optogenetic clustering using Cry2 had been characterized only with cytoplasmic proteins (*2*), we first assessed the feasibility of CLICR by investigating whether we could optically cluster a Cry2 binding target in the cytoplasm and whether indirect clustering could induce signal activation (Figure 3.2). Using a heterodimeric pair of leucine zippers (*31*), we grafted one of the LZ helices (LZa) onto the Cry2 module and its partner helix (LZb) onto a GFP-LRP6c fusion, whose clustering has been shown to robustly stimulate β-catenin pathway signaling (*2, 32*). A list of fusion architectures examined can be found in Table 3.1, and a complete list of constructs generated for this work can be found in Appendix A. Upon co-transfection of the LZ-appended Cry2 and LRP6c fusions into HEK 293T cells, we observed

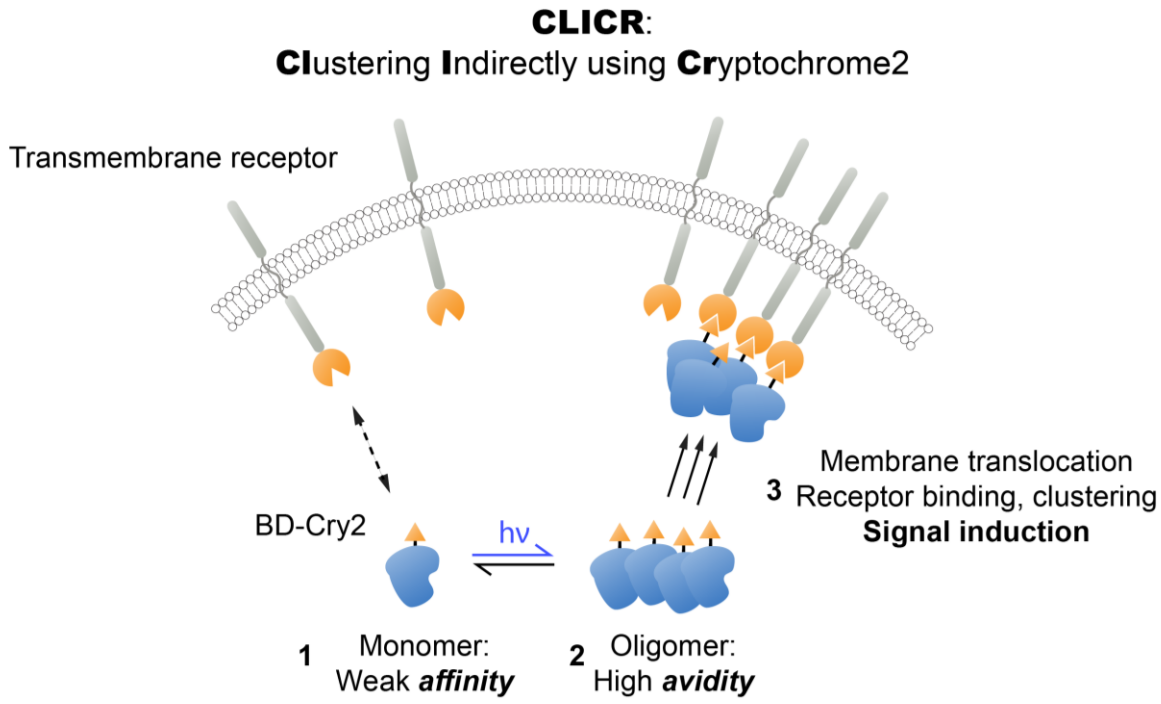

Figure 3.1 The CLICR strategy enables Cry2 activation of transmembrane receptors. CLICR allows modular Cry2 clustering and activation of membrane receptors via non-covalent interactions, avoiding complications associated with overexpression of receptor fusions. With CLICR, Cry2 fused to a receptor-targeting binding domain (BD) is expressed in the cytoplasm. In the dark, unclustered state, BD affinity for the receptor is insufficient to impart membrane localization. Upon light induced clustering, BD-Cry2 oligomers increase local BD concentration, enabling membrane translocation, binding, and nucleation of a receptor cluster.

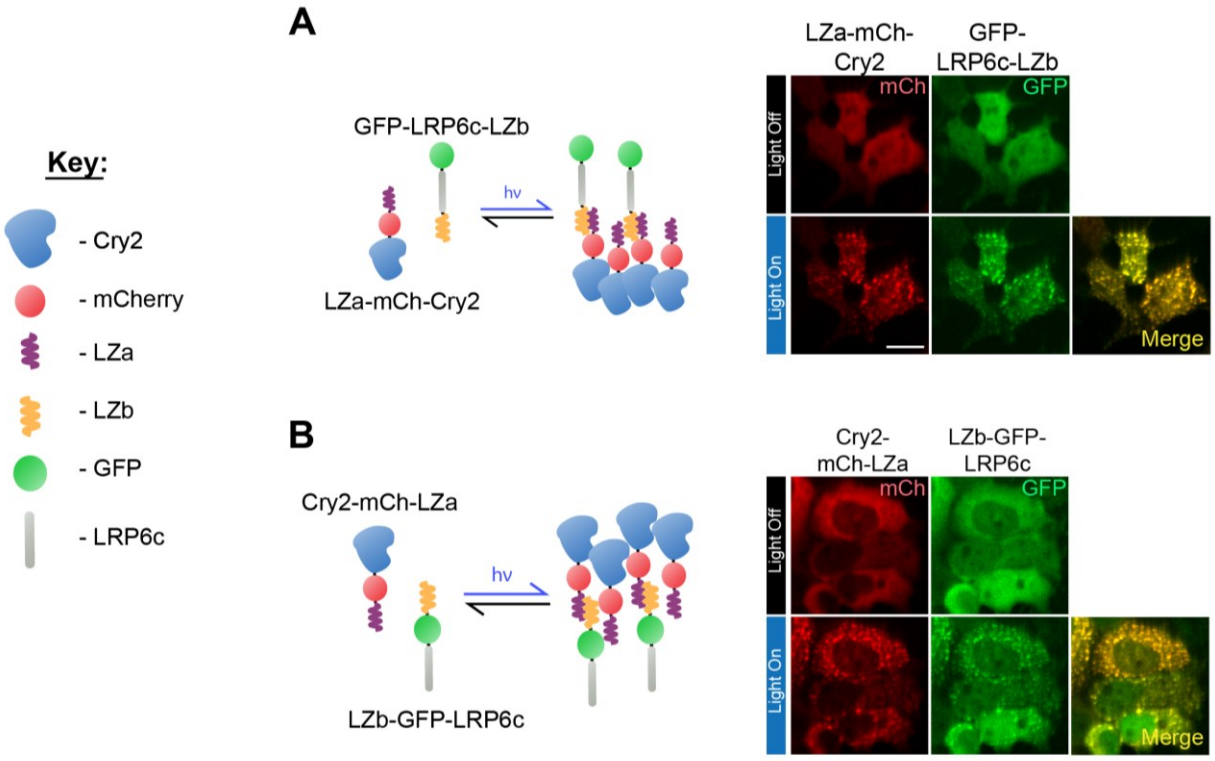

Figure 3.2 CLICR allows clustering of cytoplasmic protein targets. (A,B) Upon light activation, the Cry2 (red) and LRP6c (green) components co-cluster due to the heterodimeric interaction between the LZa and LZb adapters in conjunction with Cry2 clustering. Panels (A) and (B) demonstrate the same concept but with different fusion architectures (N- and C- terminal LZa, C- and N-terminal LZb).

Construct	Expression	Visible Light-induced Clusters?
Cry2-mCh-LZa	+++	YES
LZa-mCh-Cry2	+++	YES
LZa-Cry2-mCh	+++	NO

Construct	Expression	Co-clusters?
LZb-LRP6c-GFP	+	YES
LZb-GFP-LRP6c	++	YES
GFP-LRP6c-LZ	++	YES

Table 3.1 Above are listed the initial constructs tested for cytoplasmic CLICR, how well they expressed in HEK 293T cells, and whether or not they clustered (for Cry2-LZa fusions) or co-clustered, via CLICR, with Cry2 (for GFP-LZb fusions)

light-induced cluster formation in both the mCherry and GFP channels, and these clusters colocalized, suggesting that Cry2 clusters were successfully recruiting GFP-LRP6c fusions via the LZa-LZb interaction (Figure 3.2). To determine whether the induced LRP6c clusters were sufficient to induce β-catenin signaling, we transfected combinations of Cry2- and LRP6c-containing fusion pairs into 293T cells harboring a β-catenin responsive luciferase reporter (*33*)

(Figure 3.3A). Significant increases in β-catenin signaling in illuminated vs. unilluminated samples were observed with all Cry2/LRP6c fusion pairs tested, though this signal was markedly diminished compared to that obtained with a single-chain Cry2-mCh-LRP6c fusion (Figure 3.3B) (*2*), potentially due to LRP6c cluster geometries, expression level differences, or differences in efficiencies of 2-component vs. 1-component clustering. We further demonstrated the feasibility and modularity of the CLICR approach by indirectly clustering the Rac1 GTPase with the same LZ binding adapters (Figure 3.4A**)**. Consistent with previous reports of clustering the Rac1 protein (*2*), indirect Rac1 clustering induced rapid membrane translocation of the Rac1 (and associated Cry2) fusion (Figure 3.4B). Together, the LRP6c and Rac1 results demonstrate that CLICR can serve as a modular strategy for clustering binding partners via non-covalent interactions.

We next investigated whether a CLICR-induced avidity increase was sufficient to induce translocation of a cytoplasmic Cry2 fusion to the plasma membrane, which would be necessary for CLICR activation of membrane receptors (Figure 3.1). We co-transfected cells with a membrane-localized LZb-GFP-CaaX construct, which is lipid-modified at the C-terminal CaaX box, and Cry2 fused to mCherry with the LZa helix at either the C- or N-terminus (Figure 3.5). Upon light illumination, both Cry2 fusions exhibited translocation to the cell periphery and to immobilized puncta within the cell body, suggesting binding to cell membranes (Figure 3.5). To analyze whether CLICR-induced membrane translocation could induce signaling upon binding and clustering of a transmembrane receptor, we replaced the LZb-GFP-CaaX fusion with a GFP-LZb fused to the C-terminus of the full-length LRP6 receptor (Figure 3.6A), whose clustering induces β-catenin signaling (*32, 34*). LRP6-GFP-LZb was localized to multiple cellular compartments (Figure 3.6A**)**, and illumination of Cry2 with N- or C-terminally fused LZa (Figure 3.6B,D), but not with Cry2 lacking the LZa (Figure 3.6C,E), successfully induced Cry2 translocation and colocalization with LRP6-GFP-LZ as well as activation of the β-catenin luciferase reporter, though high background signal was observed in the dark due to receptor overexpression (Figure 3.7B). By comparison, a direct LRP6-Cry2 fusion resulted in a constitutive signal that could not be further enhanced by light, representative of artifact that can accompany overexpression of transmembrane receptor constructs (Figure 3.8**)**. These results both provided support for the CLICR approach and motivated adapting it to activate endogenous receptors and thus overcome overexpression artifact.

The receptor tyrosine kinase (RTK) class of receptors is broadly important in regulating proliferation, growth, differentiation, survival, and motility, and activation of many RTKs involves lateral interactions including clustering (*10*). To target native RTKs with CLICR, we used the N-terminal src-homology 2 (SH2) domain from PLC-γ as our binding domain adapter (Figure 3.9A). Since the SH2 domain typically does not bind unphosphorylated peptide sequences, we hypothesized that SH2 domain clustering may enhance its avidity for unactivated or weakly activated receptors (*35*) and subsequently cluster and activate the RTKs. To test RTK-targeting ability, we expressed mCherry-Cry2 with an N-terminal SH2 domain (SH2-N) in

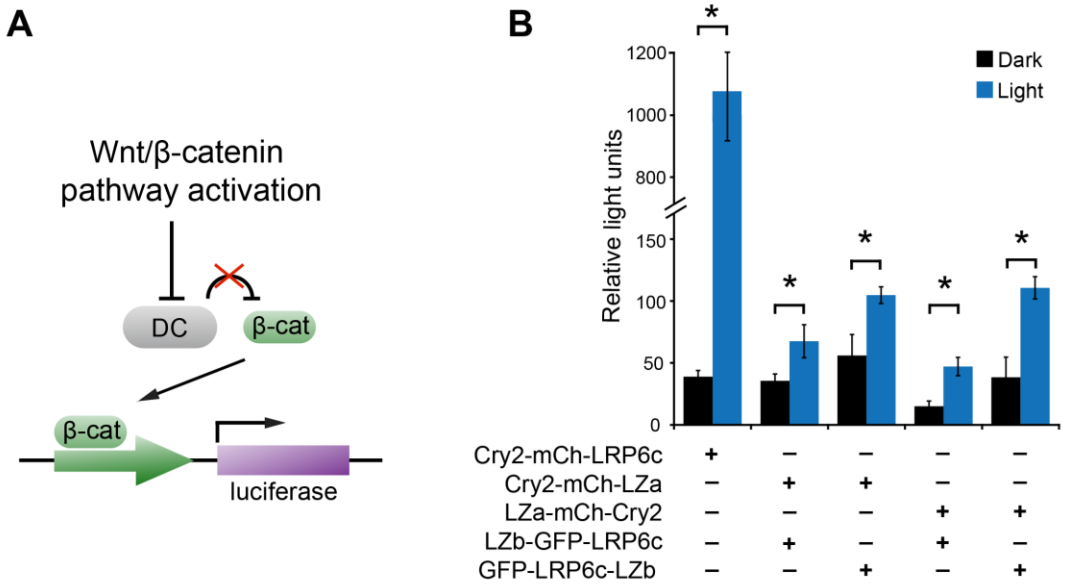

Figure 3.3 CLICR allows clustering and activation of cytoplasmic protein targets. A luciferase reporter of β-catenin (β-cat) activity, which is induced when destruction complex (DC)-mediated inhibition of β-catenin is released, allows readout of the β-catenin pathway activation. (D) CLICR clustering of cytoplasmic LRP6c activates β-catenin signaling (means ± 1 s.d, *p = 0.0495, Mann-Whitney Wilcoxon test, n = 3 biological replicates).

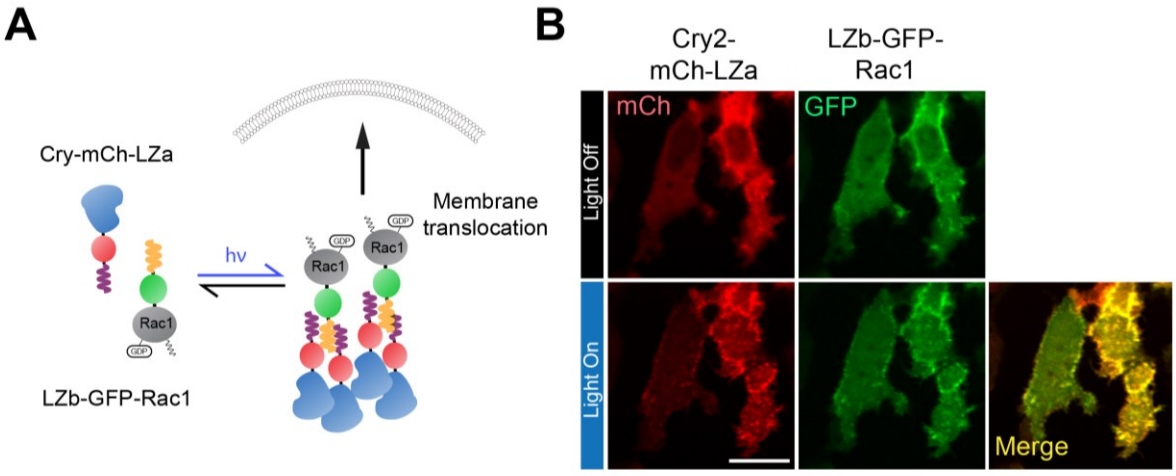

Figure 3.4 CLICR allows clustering and activation of cytoplasmic protein targets. CLICR clustering of cytoplasmic Rac1 induces membrane translocation of both CLICR components, consistent with previous reports of Rac1 clustering (*2*) and demonstrating CLICR modularity in regulating a different cytoplasmic protein through indirect clustering. Scale bars = 20 μm.

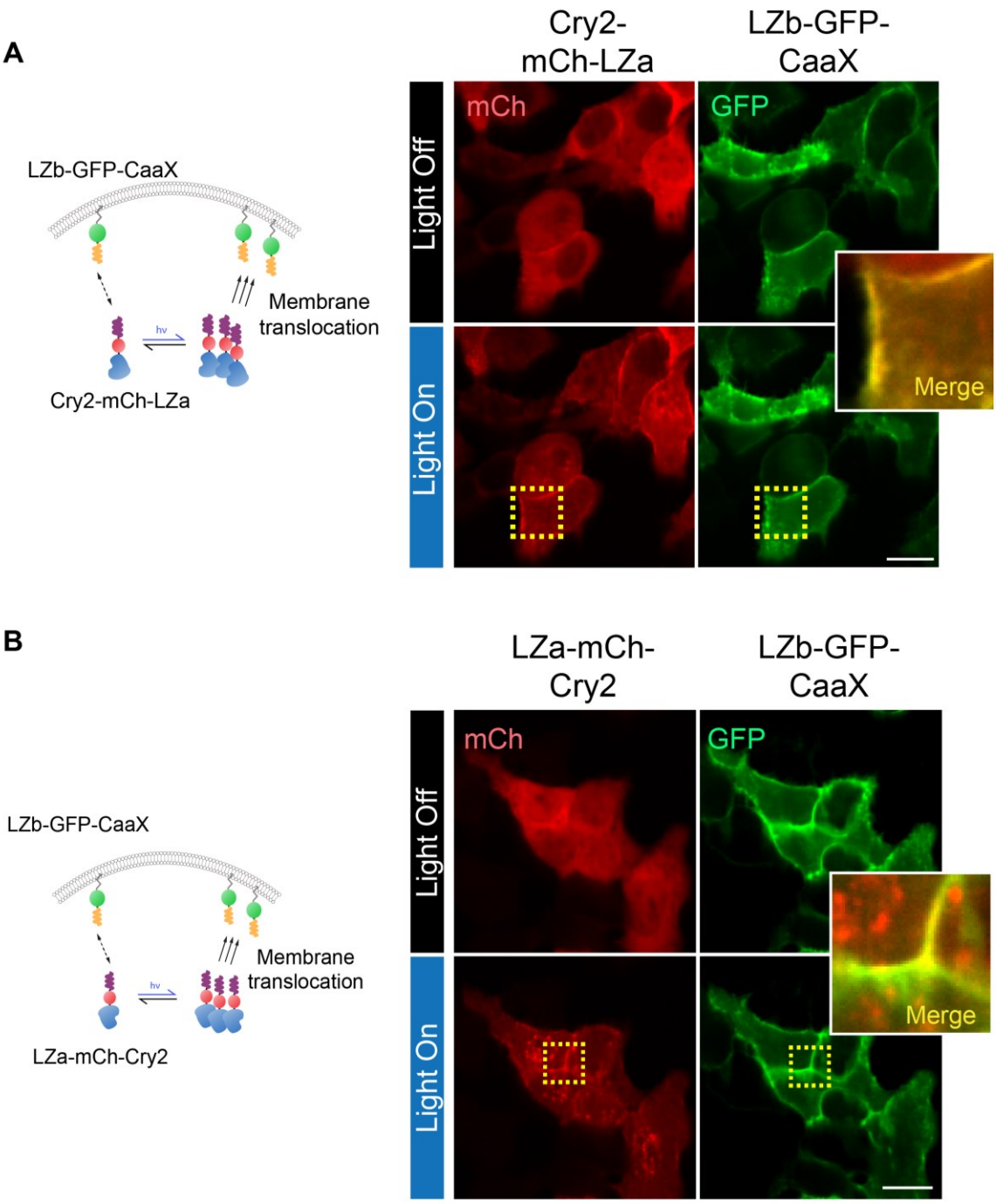

Figure 3.5 Cry2 membrane translocation through CLICR clustering. A C-terminal (A) and N-terminal (B) LZa fusion on the Cry2 module exhibits translocation from the cytoplasm to membrane-tethered GFP-LZb upon CLICR induced avidity increase. Scale bar = 20 μm.

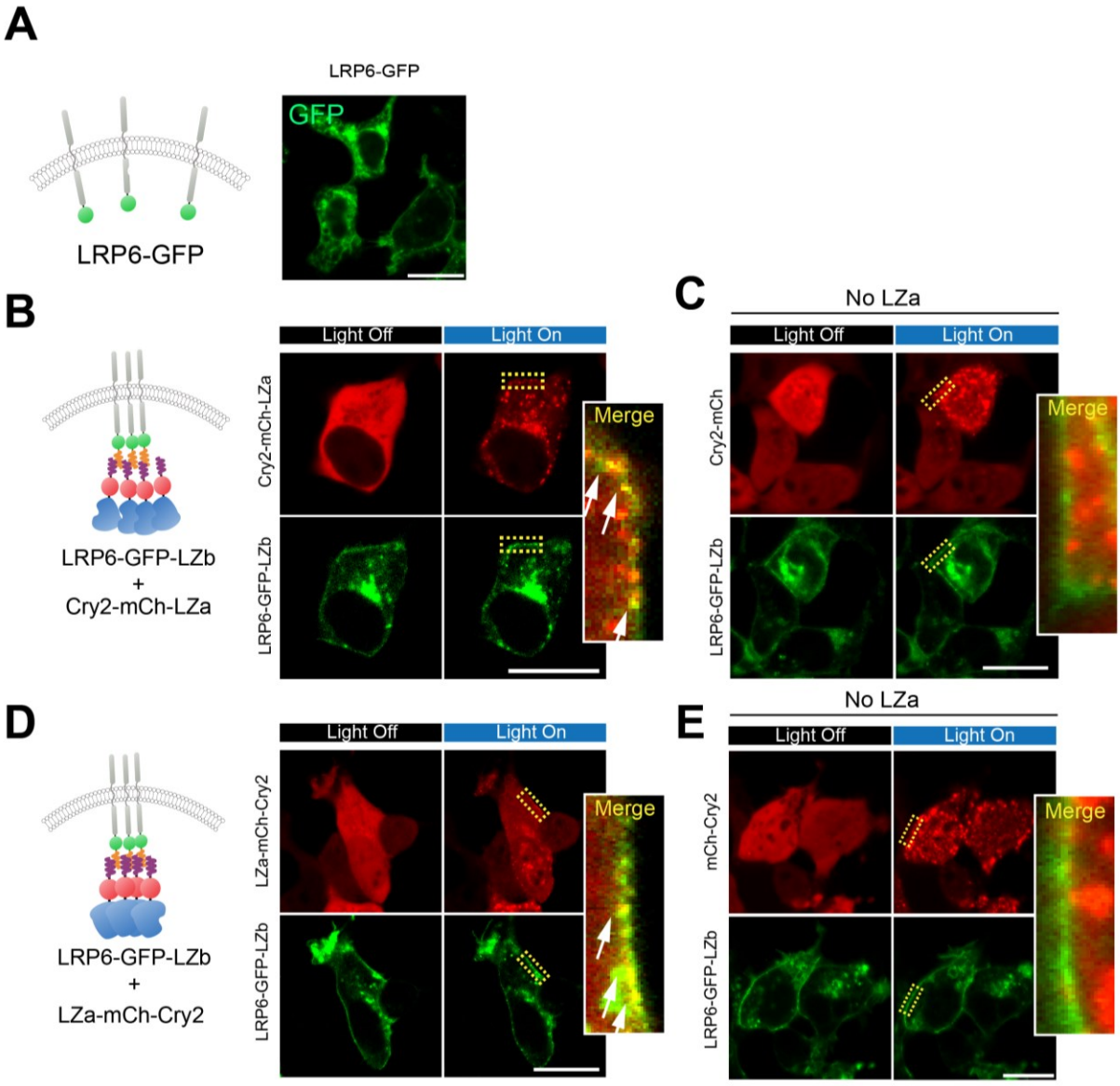

Figure 3.6 CLICR enables targeting of full-length transmembrane LRP6 co-receptor. (A) The CLICR method was applied to cluster and activate exogenously expressed LRP6-GFP-LZb. (B) Expression of LRP6-GFP alone exhibits receptor localization to both plasma membrane and non-plasma membrane compartments. Both C-terminal (C) and N-terminal (D) LZa fusions of Cry2 exhibit light-dependent membrane translocation and colocalization with LRP6-GFP-LZb. By comparison, Cry2 constructs lacking LZa exhibit clustering but no membrane localization or co-localization with LRP6-GFP-LZb (E,F). Scale bars = 20 μm.

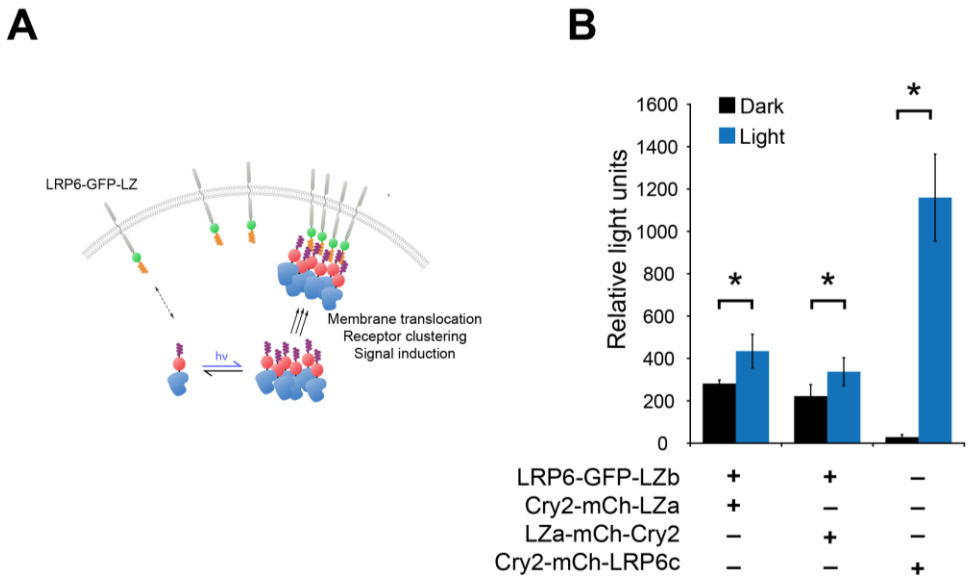

Figure 3.7 CLICR enables activation of full-length transmembrane LRP6 co-receptor. β-catenin pathway activation was induced via CLICR using either N- or C-terminal LZa fusion to Cry2, albeit with high background in the dark and with lower signal induction compared to cytoplasmic Cry2-mCh-LRP6c activation. Graph shows means ± 1 s.d., *p = 0.0495, Mann-Whitney Wilcoxon test, n = 3 biological replicates.

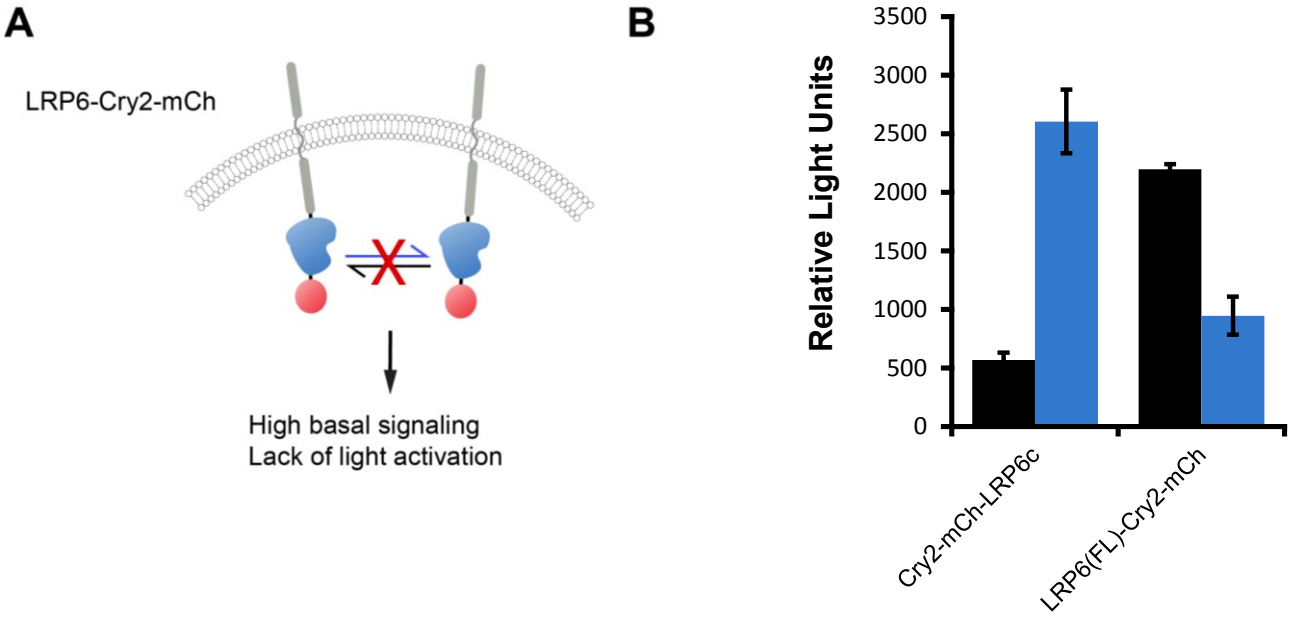

Figure 3.8 Expression of full-length LRP6 fused to Cry2-mCh is not suitable for optical induction of β-catenin activity. Full length transmembrane receptor LRP6 was fused at the C-terminus to Cry2-mCherry to investigate whether a receptor-Cry2 direct fusion could be used to optically regulate receptor clustering and activation (A), as had previously been demonstrated for cytoplasmic proteins (2). B) Cytoplasmic clustering of a Cry2-mCh fused to the endodomain of LRP6 (Cry2-mCh-LRP6c) allows photoactivation of a luciferase reporter for β-catenin in 293T cells. In contrast, LRP6(FL)-Cry2-mCh exhibits high basal signaling in the dark, and blue light exposure induces an unexpected decrease in β-catenin signal. Graphs shows mean ± 1 s.d., n = 3 biological replicates.

several cell types, including HEK 293Ts, 3T3 fibroblasts, and adult neural stem cells (NSCs). In 293Ts, illumination of SH2-N yielded membrane-anchored puncta (Figure 3.10A, top row). Analogously, 3T3 fibroblasts exhibited rapid localization of SH2-N to membrane anchored puncta as well as to focal adhesion structures (Figure 3.10B, top row), and NSCs exhibited light-induced punctate formation in neurite extensions as well as in the cell body, collectively suggesting that SH2-N may target endogenous membrane proteins. (Figure 3.10C, top row). A C-terminal fusion of SH2 to Cry2-mCh (SH2-C) was also tested and yielded similar phenotypes, though with slower kinetics, and the SH2-N construct was thus used for all further experiments. Treatment with the RTK inhibitor PD-089828 (RTKi) – which inhibits the RTKs FGFR1, PDGFRβ, and EGFR – markedly reduced SH2-N focal enrichment at the membrane in all three cell types (Figure 3.10A,B,C, bottom rows). These data indicate that strong SH2-N localization is dependent on RTK phosphorylation, and thus that SH2-N clusters are indeed targeting endogenous RTK receptors.

To further validate SH2-N was binding RTKs, we transfected the SH2-N construct into 293Ts stably expressing GFP-tagged, full-length FGFR1 or PDGFRβ receptors, representing two RTKs that bind the PLCγ SH2 domain (*36, 37*) . In cells expressing ectopic FGFR1-GFP, the SH2-N construct exhibited light-dependent membrane translocation and formation of punctae that colocalized with GFP (Figure 3.11A). Addition of 50 μM FGFR1-4 inhibitor (PD-166866, FGFRi) abrogated this colocalization (Figure 3.11B). Similar behavior was obtained in cells expressing PDGFRβ-GFP, where light-induced SH2-N colocalization with PDGFRβ-GFP (Figure 3.12 A) was abrogated in the presence of 50 μM PDGFR-α and -β inhibitor (CAS 205254-94-0, PDGFRi) (Figure 3.12B). Light-promoted SH2-N binding to FGFR1 and PDGFRβ was further established through co-immunoprecipitation of SH2-N with either the FGFR1 or PDGFRβ receptors (Figure 3.11C, Figure 3.12C). Together, these results indicate that the cytoplasmic SH2-N construct can successfully target native transmembrane RTKs via CLICR in response to light.

We next investigated whether SH2-based CLICR targeting of endogenous RTKs is capable of signal activation. Illumination of 3T3 fibroblasts expressing SH2-N yielded a broad increase in tyrosine phosphorylation, compared to unilluminated and RTKi-inhibited controls (Figure 3.13). Furthermore, analysis of canonical RTK signaling pathways showed an increase in levels of phospho-Akt and phospho-Erk1/2 upon 15 minutes of blue light illumination, a difference abrogated in the presence of the RTKi inhibitor. We further investigated whether CLICR clustering of the PLCγ SH2 domain demonstrated specificity towards individual receptors. Since activated PDGFRβ has been shown to colocalize with focal adhesions through interaction with focal adhesion kinase (FAK) (*38*), we hypothesized that endogenous PDGFRβ activation was largely responsible for the CLICR induced signal activation and focal adhesion translocation of SH2-N (Figure 3.10B). To address this possibility, we examined the light-induced translocation of SH2-N in the presence of pathway specific inhibitors. In 3T3 fibroblasts, SH2-N exhibited a rapid, light-induced localization to the plasma membrane and focal adhesion structures. Moreover, 10 μM PDGFRi treatment largely inhibited focal adhesion translocation of SH2-N (Figure 3.14), whereas 10 μM FGFRi had minimal observed effect on focal SH2-N localization, suggesting that translocation was indeed PDGFRβ dependent and that CLICR clustering was modulating PDGFRβ activity.

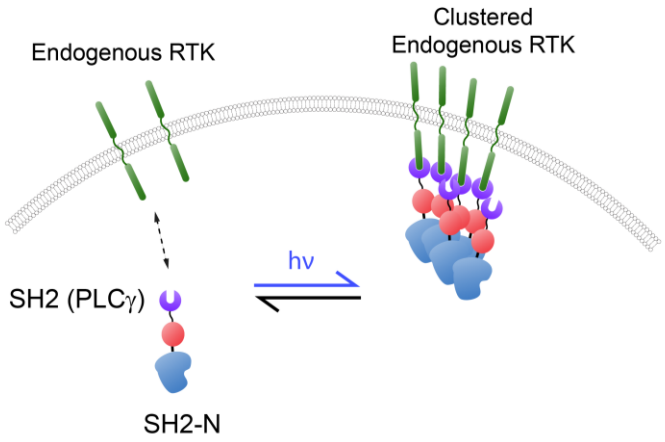

Figure 3.9 CLICR targeting of endogenous receptors. To target endogenous receptors with CLICR, an adapter domain with affinity for native receptors was used in place of the engineered LZa-LZb interaction used previously. The SH2 domain from PLCγ was used as a binding domain fused to the N-terminus of mCh-Cry2 (SH2-N) to target endogenous receptor tyrosine kinases.

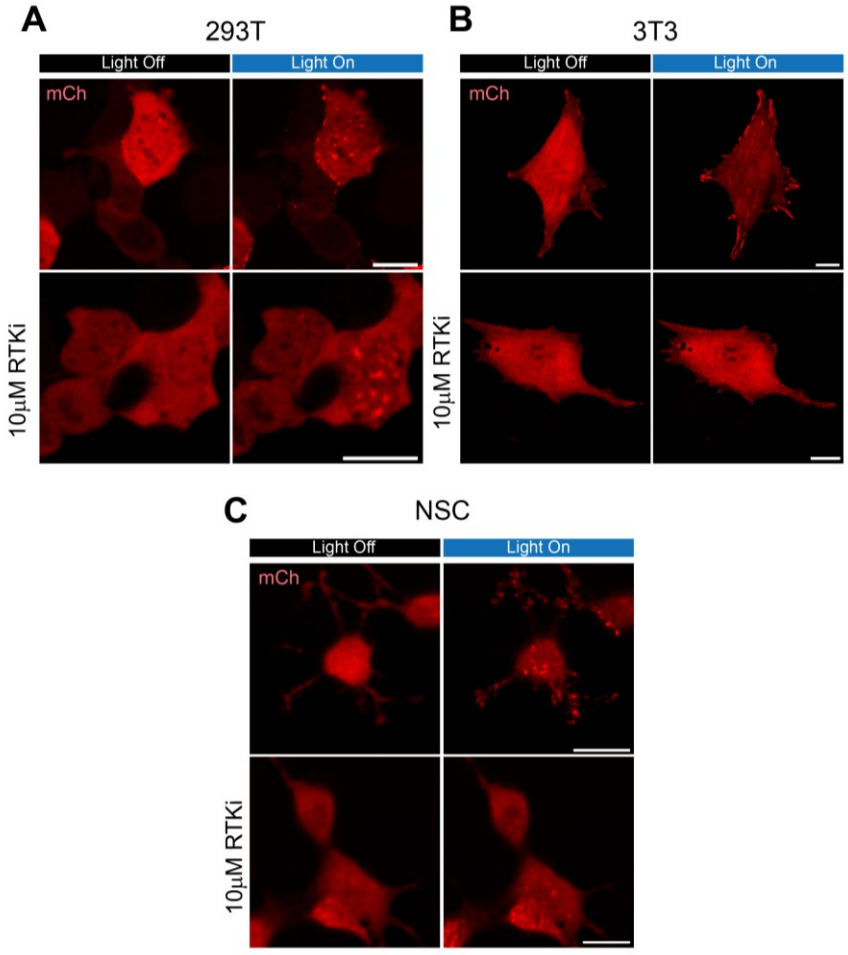

Figure 3.10 CLICR targeting of endogenous receptors. Illuminated SH2-N expressed in 293Ts (A, top panels) localized to membrane-anchored foci. In 3T3 fibroblasts (B, top panels), illumination of SH2-N induced translocation to the membrane periphery and to structures resembling focal adhesions. In neural stem cells (NSC) (C, top panels), illuminated SH2-N localized to immobilized membrane clusters both in the cell body and in neurites. In all 3 cell types, inhibition with an FGFR1/PDGFRβ/EGFR-specific inhibitor (RTKi) largely abrogated visible SH2-N translocation. (A,B,C, lower panels). Scale bars = 20 μM.

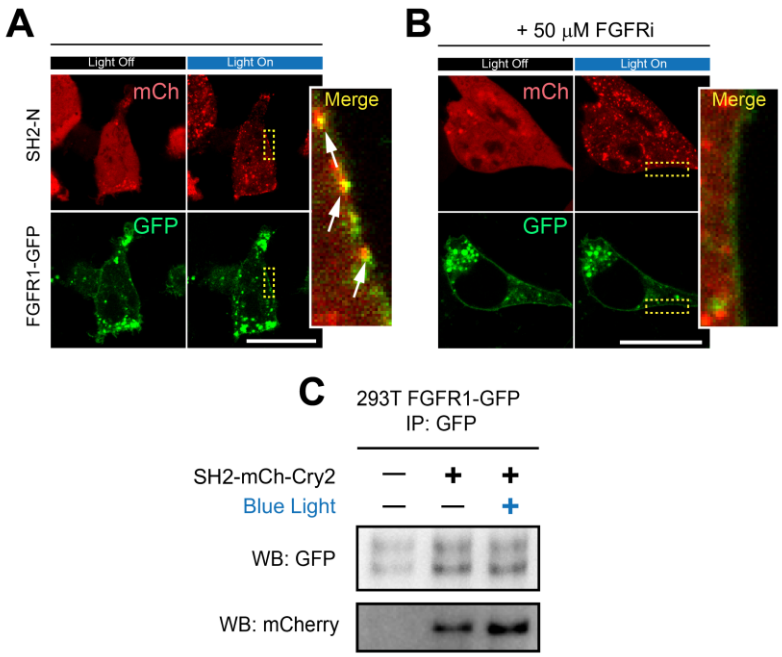

Figure 3.11 SH2-N localizes to FGFR1 under blue light. In 293Ts, upon blue light illumination SH2-N colocalized (arrows) to exogenously expressed, full-length FGFR1 fused to GFP (A), and this colocalization was abrogated in the presence of an FGFR-specific inhibitor (FGFRi) (B). Scale bars = 20 μm. Light-stimulated association of SH2-N with either FGFR1-GFP was confirmed through co-immunoprecipitation of SH2-N with the receptor (C).

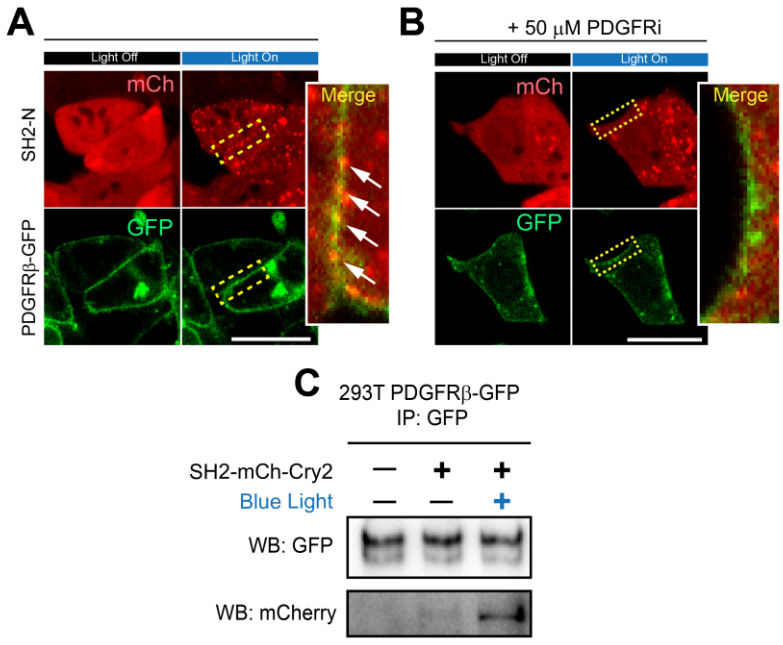

Figure 3.12 SH2-N localizes to PDGFRβ under blue light. In 293Ts, upon blue light illumination SH2-N colocalized (arrows) to exogenously expressed, full-length PDGFRβ fused to GFP (A), and this colocalization was abrogated in the presence of an PDGFRβ-specific inhibitor (PDGFRi) (B). Scale bars = 20 μm. Light-stimulated association of SH2-N with either PDGFRβ-GFP was confirmed through co-immunoprecipitation of SH2-N with the receptor (C).

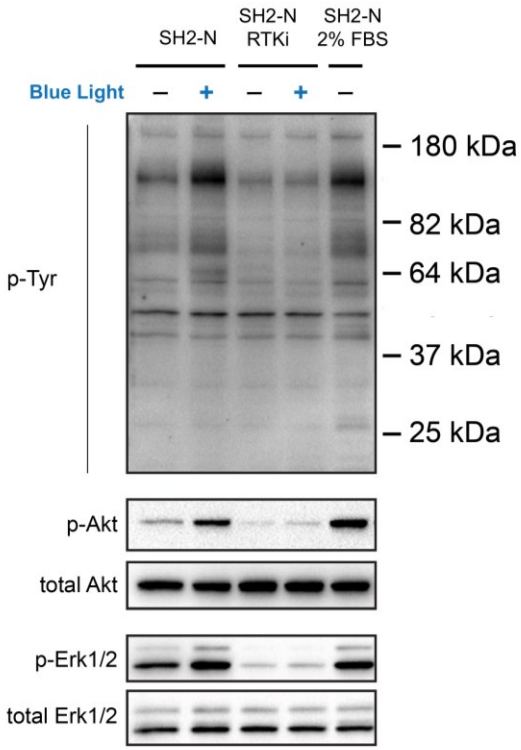

Figure 3.13 CLICR clustering allows photoactivation of endogenous RTKs in fibroblasts. Western blot analysis of serum-starved fibroblasts treated for 10 minutes with blue light shows broad upregulation of tyrosine phosphorylation in illuminated vs unilluminated samples, and this difference is abrogated upon 10 μm RTK inhibition. Samples grown in 2% serum were used as a positive control. In particular, light-treated samples demonstrated an RTK-dependent increase in Akt and Erk1/2 phosphorylation.

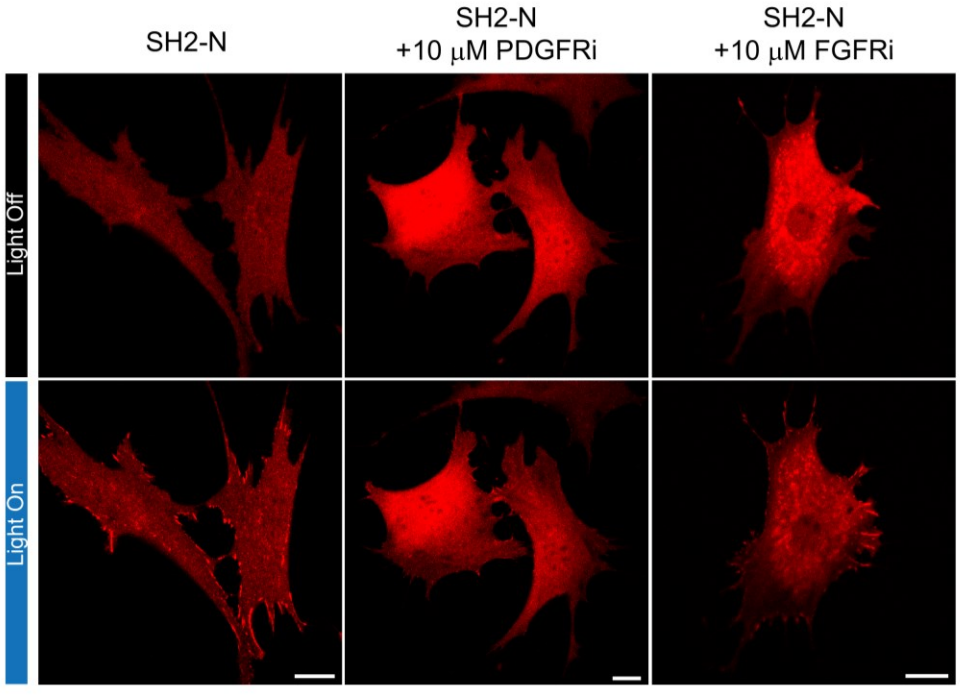

Figure 3.14 SH2-N translocation to focal adhesions is dependent on PDGFR, but not FGFR1, activity. Whole cell light activation stimulates SH2-N translocation to focal adhesion structures (top row). This translocation is largely abrogated in the presence of PDGFR inhibitor (middle row), but not in the presence of FGFR1 inhibitor (bottom row), suggesting that PDGFR activity must remain intact to observe this phenotype and that CLICR clustering is modulating PDGFR activity. All illuminated images were taken after 6.5 minutes of illumination. Scale bar = 20 μm.

Activated PDGFR colocalization with FAK within focal adhesions has been shown to modulate FAK activation, focal adhesion turnover, and cell migration (*39*). Additionally, PDGFRβ induced membrane recruitment of phosphatidylinositol-3-kinase (PI3K) leads to conversion of phosphatidylinositol-4,5-bisphosphate (PIP2) to phosphatidylinositol-3,4,5-trisphosphate (PIP3) (*40*), whose localization at the leading edge of cells is a key factor in cellular polarity establishment and PDGFR-dependent fibroblast migration. We found that in fibroblasts, SH2-N translocation was accompanied by filopodial and lamellipodial extension, often followed by cellular polarization and movement (Figure 3.15). This polarization was dependent on PI3K activity, since addition of the PI3K inhibitor wortmannin led to only transient lamellipodial extensions (Figure 3.16), which then rapidly stopped protruding or collapsed. PI3K activity was thus required to sustain membrane extensions and establish morphological polarity, consistent with CLICR-mediated activation of PDGFRβ and PI3K.

We next quantified these PDGFR and PI3K dependent effects. Lamellipodial extension induced by whole field illumination was observed in 78% of cells expressing SH2-N, and RTKi inhibition significantly reduced this response to 17% of cells (Figure 3.17, with significance determined through non-overlapping 95% confidence intervals). Likewise, PDGFRi significantly decreased the number of cells extending light-induced lamellipodia from 78%to 37%. In contrast, FGFRi had no effect on cell morphological responses. In cells that did exhibit lamellipodial response, we quantified the time interval from the start of blue light exposure to the first apparent lamellipodial extension. Untreated cells extended initial lamellipodia with an average interval of 123 s, while RTKi or PDGFRi significantly delayed such lamellipodial extension in responding cells to 481 s and 300 s, respectively (Figure 3.18, ANOVA with Tukey post-hoc analysis, $p < 0.0001$). In contrast, FGFRi treatment had no apparent effect on lamellipodial extension timing. We then examined the fraction of cells that established polarity and initiated migration upon light treatment, as observed by inspecting lamellipodial extension coupled with trailing edge retraction and morphological reorientation. 65% of uninhibited fibroblasts exhibited polarity establishment, and this response was significantly suppressed to 17% and 12% of cells treated with RTKi and PDGFRi, respectively (Figure 3.19**,** significance determined through non-overlapping 95% confidence intervals). By comparison, FGFRi treatment only moderately reduced light-dependent polarity induction (47% of cells). These results were further corroborated through Western blotting, as light-induced Akt activity was observed in uninhibited and FGFRi inhibited cells, but absent in RTKi and PDGFRi inhibited cells (Figure 3.20). Collectively, these data demonstrate selectivity of SH2-N for PDGFRβ activation and suggest that SH2-N CLICR may be used as a tool to study PDGFRβ activity in living cells.

Since PDGFRβ is a key mediator of fibroblast chemotaxis (*41*), we next sought to exploit the spatiotemporal precision of CLICR and rewire a cell's chemotactic circuitry to regulate migration in response to a light signal instead of a chemical one. We hypothesized that focal blue light illumination would re-establish and define a local PIP3 gradient, and that this would allow directed polarization, actin polymerization, and motility of the cell. In fibroblasts co-expressing SH2-N and PH-Venus, which comprises Venus fused to the pleckstrin homology (PH) domain of Akt and is an established biosensor of (PIP3) production (*42*), the PH-Venus was initially inhomogeneously distributed, indicating initial polarization of PIP3 within the cell. Illuminating the cell in a region not exhibiting initially high levels of PIP3 induced membrane

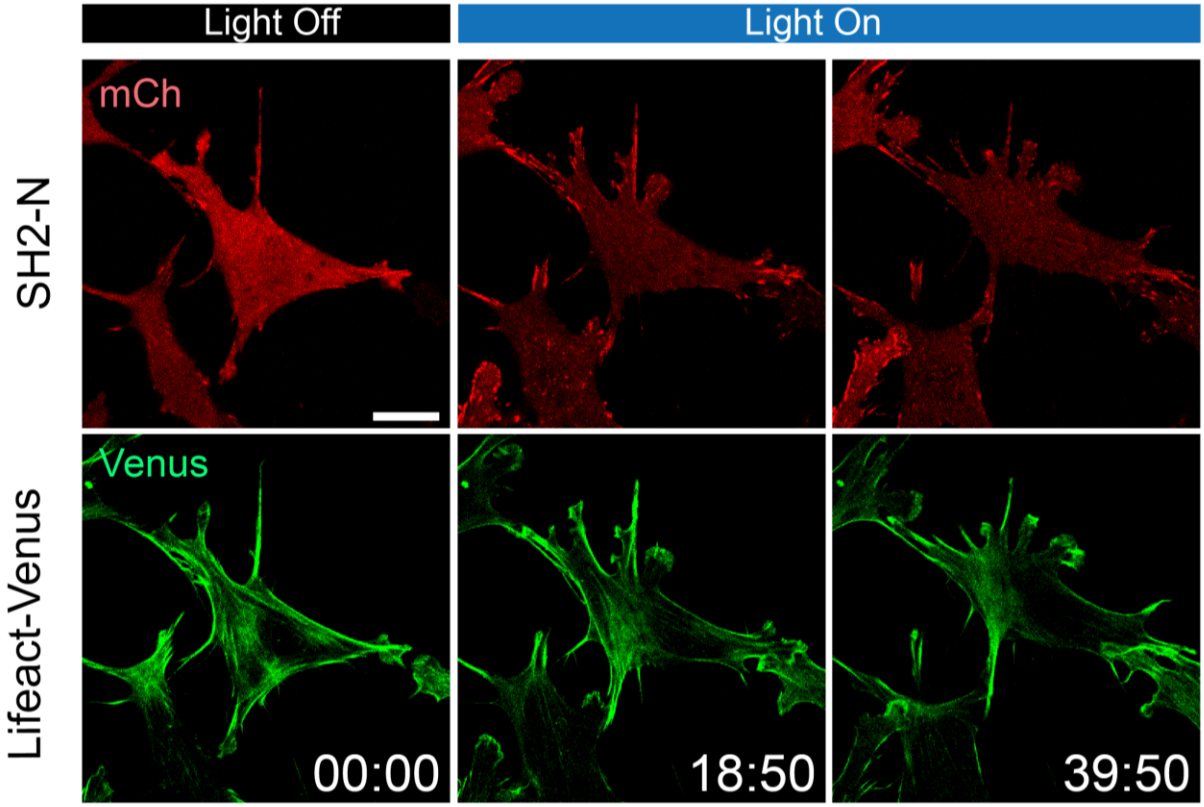

Figure 3.15 CLICR clustering allows photoactivation of endogenous RTKs in fibroblasts and induces changes in polarity and motility. Time lapse imaging of SH2-N expressing fibroblasts shows lamellipodial extension and cell repolarization upon whole field blue light exposure. Scale bar = 20 μm

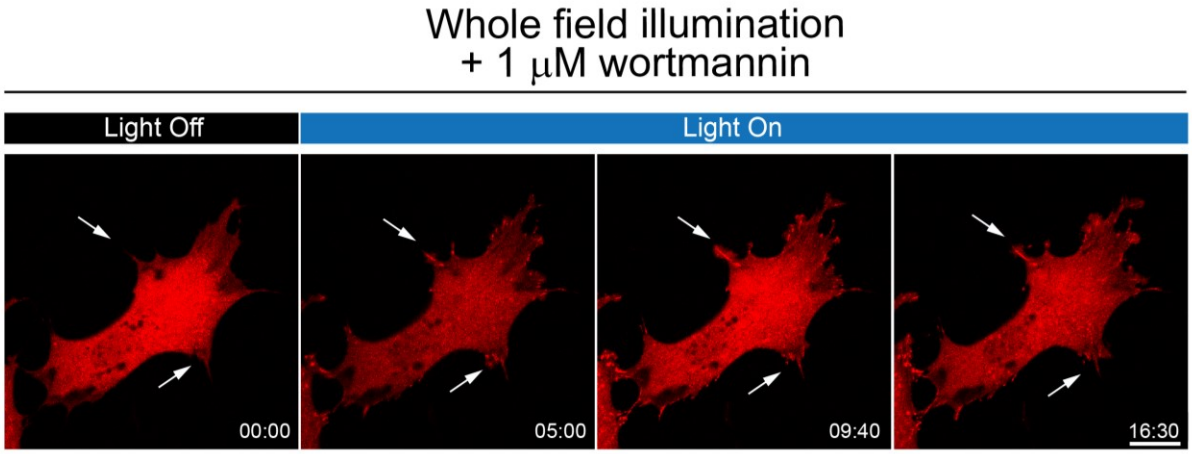

Figure 3.16 Wortmanin prevents SH2-N dependent polarity establishment. Whole field illumination of SH2-N expressing fibroblasts in the presence of PI3K inhibitor wortmannin reveals that light-dependent polarity establishment is PI3K dependent. Cells exhibit transient lamellipodial protrusions in all directions that collapse within minutes (arrows).

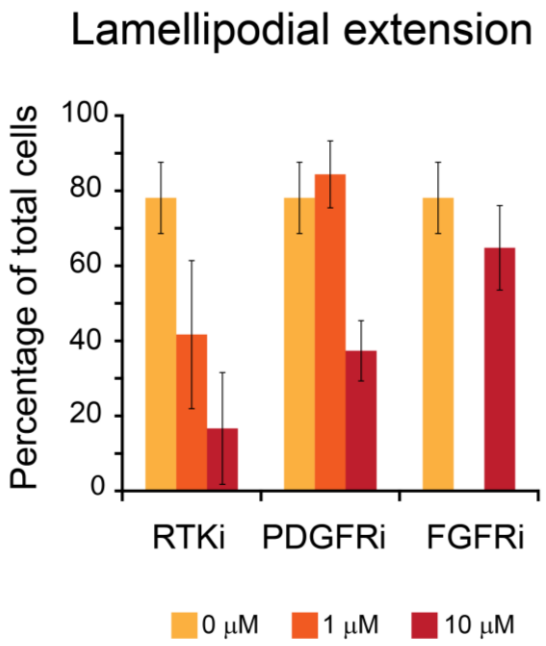

Figure 3.17 RTK specificity in SH2-N-induced lamellipodial extension. The proportion of cells extending lamellipodia in response to whole field illumination was reduced by broad RTK or PDGFR inhibition, but not FGFR inhibition. Error bars represent 95% confidence intervals, n = 24-83 cells per condition.

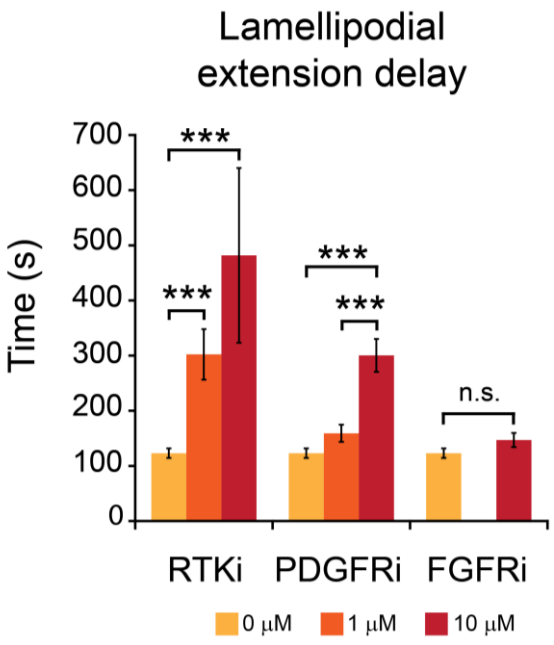

Figure 3.18 RTK dependence in SH2-N lamellipodial extension timing. Among cells extending light-induced lamellipodia (from Figure 3.17) under broad RTK inhibition or PDGFR inhibition, a longer delay before initial lamellipodial extension was evident, while FGFR inhibition did not induce a delay in extension. Graph shows means $\pm$ 1 s.d, n = 4-58 cells per condition. ***p < 0.001 by one way ANOVA with Tukey pairwise analysis.

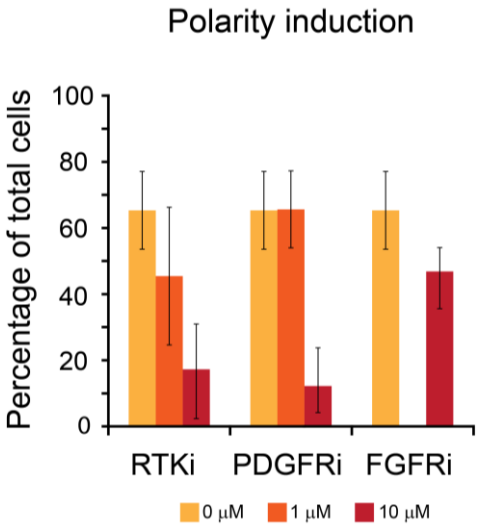

Figure 3.19 RTK specificity in SH2-N-induced re-polarization. The proportion of cells exhibiting light-induced polarization was reduced by RTKi or PDGFRi treatment, and slightly reduced by FGFRi treatment. Error bars represent 95% confidence intervals, n = 24-83 cells per condition.

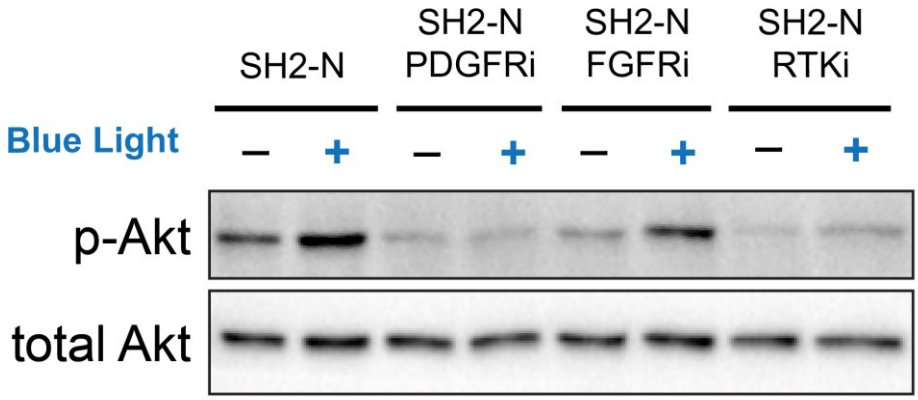

Figure 3.20 RTK specificity in SH2-N-induced AKT activation. Fibroblasts expressing SH2-N show a light-induced increase in p-Akt levels. Treatment with PDGFR or broad RTK inhibitor abrogates this increase, while FGFR inhibition has little effect.

ruffling and lamellipodial extension toward the illumination region, coupled with a redistribution of PH-Venus **(**Figure 3.21**)**. In particular, the extending lamellipodium exhibited high levels of PH-Venus recruitment, and within minutes the cell began moving towards the light, establishing a PIP3 gradient and a new leading edge as defined by the illumination region (Figure 3.21). In the presence of PI3K inhibitor wortmannin, however, focal illumination was unable to induce the sustained extension of the illuminated region and establishment of a PIP3 gradient, confirming that local PIP3 production, polarization, and motility were PI3K dependent (Figure 3.22). Additionally, focal blue light illumination of SH2-N cells coexpressing a Lifeact-Venus probe for F-actin stimulated initial lamellipodial actin polymerization, membrane ruffling, and extension within 30s along with a coordinated initiation of trailing edge retraction (Figure 3.23). The cell proceeded to phototax in the direction of the initial illumination region until the light stimulus was reoriented, at which point the established lamellipodium collapsed, and the cells repolarized to migrate in the newly defined direction (Figure 3.23).

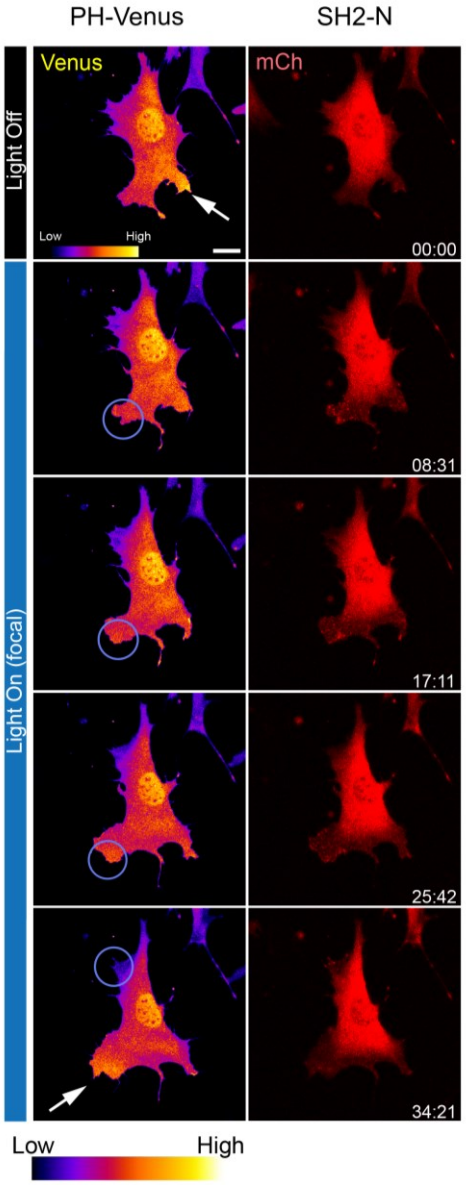

Figure 3.21 SH2-N allows spatial activation of PI3K/PIP3. Focal illumination enabled the spatial definition of the lamellipodial extension region coupled with re-establishment of a PIP3 gradient at the site of illumination (arrows), as observed through a PH(Akt)-Venus biosensor. Scale bar = 20 μm.

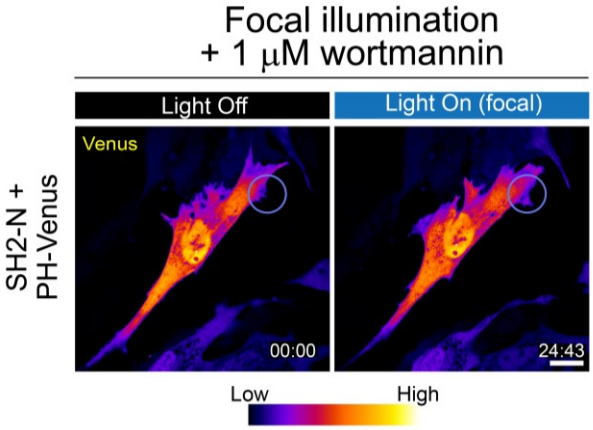

Figure 3.22 SH2-N-induced PIP3 gradient and lamellipodial extension require PI3K for activation. Focal illumination of these cells again reveals an inability to extend sustained lamellipodia and establish a PIP3 gradient. Time given in minutes:seconds, scale bars = 20 μm.

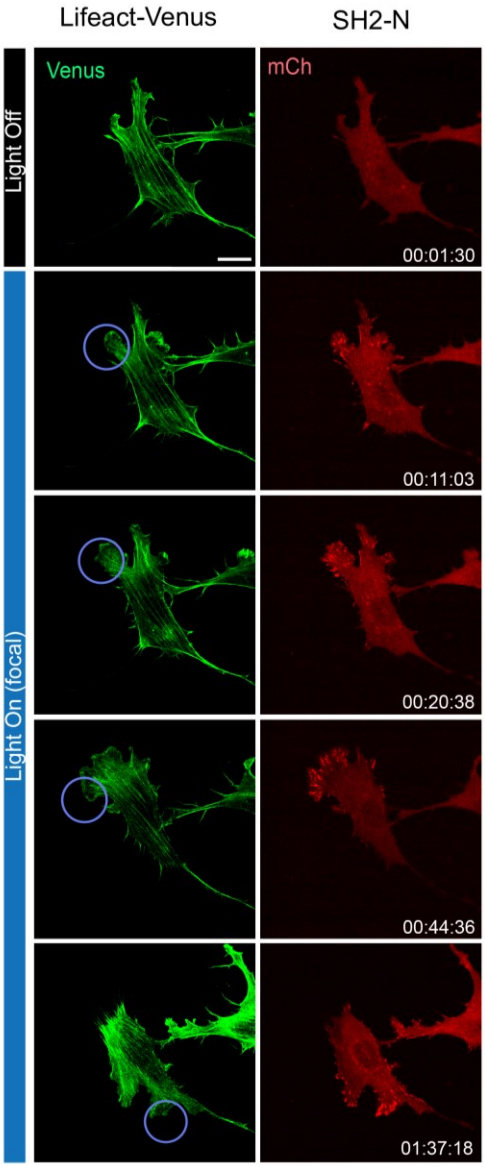

Figure 3.23 CLICR-enabled focal activation of lamellipodial extension and polarity establishment allows rewiring of PDGFR-dependent chemotaxis to respond to light. Fibroblasts co-expressing SH2-N and Lifeact-Venus were illuminated focally, and actin polymerization, lamellipodial extension, and cell motility were induced in the direction of the illuminated region. Illuminating the trailing edge induced re-polarization and a reversal of migration direction. Scale bars = 20 μm.

Finally, to demonstrate that CLICR may be a highly modular method for regulating diverse endogenous pathways, we devised a method to target β-integrin receptors, which participate in cellular adhesion complexes in their active state and can diffuse freely in the membrane in an inactive state. The important role of clustering in integrin affinity and activation (*43*) renders endogenous integrins an attractive CLICR target. For the binding adapter, we used the DOK1 phosphotyrosine binding (PTB) domain, which binds a phosphotyrosine residue in an NPXY motif on β-integrin cytoplasmic tails (*44*). Adapter protein binding to this motif, in turn, has previously been shown to modulate the talin:integrin association and importantly to stimulate endocytosis of integrins from the dorsal membrane with radially inward trafficking of the integrin containing vesicles (*45, 46*). Thus, we anticipated that CLICR clustering might influence cellular mechanics and regulate integrin endocytosis. Illumination of the Dok1(PTB)-mCh-Cry2 (Dok1-N) fusion in fibroblasts yielded rapid punctate formation, visible cellular membrane retraction, and notable dynamic fusion and inward motion of the induced vesicles along defined trajectories (Figure 3.24A). Removal of light yielded only partial redistribution of Dok1-N, suggesting that light activation of Dok1-N can sequester the fusion within an intracellular membranous compartment. In addition, the PH-GFP biosensor indicated enhanced PIP3 generation in lamellipodial extensions (arrows) originating at ~10-15 minutes of illumination. Cellular extensions extended further under light withdrawal (Figure 3.24A). PI3K pathway activation was further verified through Western blot for active Akt (Figure 3.25). The phenotypes observed upon Dok1-N clustering were distinct from those described for SH2-N and were absent in cells expressing mCherry-Cry2 without the Dok1 PTB domain (Figure 3.26B), demonstrating dependence on the Dok1 PTB binding adapter and, moreover, demonstrating the generality of the CLICR approach for targeting diverse endogenous membrane targets (*47*).

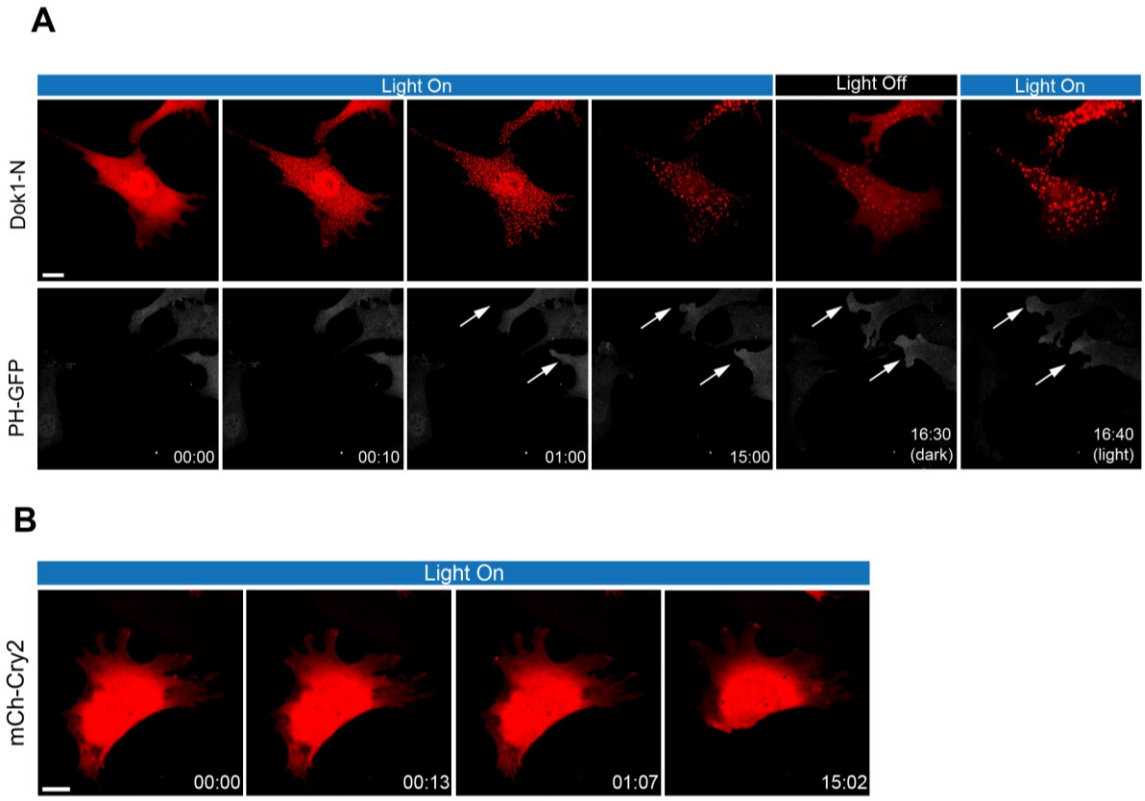

Figure 3.24 CLICR targeting of β-integrins via clustering of the Dok1 PTB induces endocytosis. A) Fibroblasts expressing Dok1-N show rapid light-dependent formation of uniform puncta from the dorsal cell membrane. The dynamic puncta fuse and move radially inward, consistent with induction of intracellular trafficking. Punctate localization was only moderately reversible in the dark, suggesting both reversibility but also light-dependent compartmentalization of Dok1-N within intracellular membranous compartments. In addition, the PH-GFP biosensor indicated enhanced PIP3 generation in lamellipodial extensions (arrows) originating at ~10-15 minutes of illumination. Cellular extensions extended further under light withdrawal. The phenotypes in (A) are not observed in the absence of the integrin-targeting Dok1 PTB domain (B). The final panel in (A) was brightened for clarity. Scale bars = 20 μm.

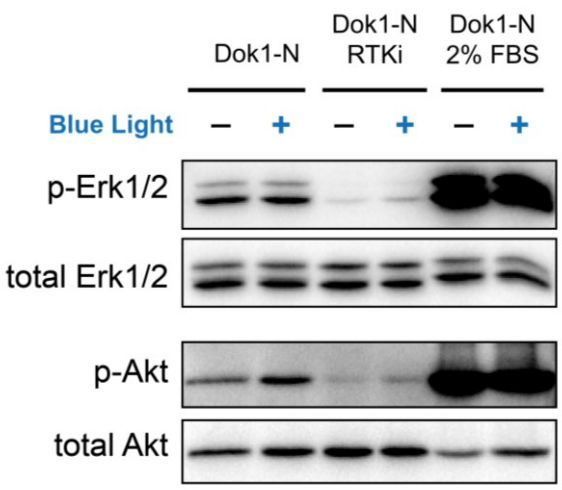

Figure 3.25 CLICR using DOK1-N enhances pAkt activation. Serum starved fibroblasts expressing Dok1-N were illuminated for 15 minutes before lysis. Western blot revealed an increase in pAkt levels which was largely abrogated upon RTK inhibition.

3.3 Discussion

Spatially defined and rapidly time-varying signal modulation has been observed as a key factor in diverse biological processes including cell migration (*48*), asymmetric cell division (*49*), differentiation (*17*), and apoptosis (*50*). The difficulty of perturbing biological systems with such precise definition, however, precludes our understanding of how dynamic signals regulate cellular function. Optogenetic tools address this need. Although methods for optical protein homodimerization (*23, 25*), heterodimerization (*19-22*), and homo-oligomerization (*2*) of ectopically expressed proteins have been developed, a genetically encoded method to optically activate endogenous transmembrane protein receptors has remained unrealized. We devised the CLICR method to address this need.

The CLICR method provides a modular, single construct system to optically cluster and activate transmembrane receptors from within the cytoplasmic compartment. With CLICR, Cry2 fused to a binding domain (BD) with low affinity for a target receptor is expressed and maintained within the cytoplasm. Blue-light induced Cry2-BD clusters exhibit enhanced BD avidity, allowing these clusters to target and cluster endogenous transmembrane receptors. CLICR may also be employed to activate exogenously expressed receptors (Figure 3.6), though increased cell-to-cell heterogeneity of two-component expression and increased basal signaling from overexpressed receptors must be accounted for in such experiments.

To demonstrate that CLICR can target endogenous receptor tyrosine kinases (RTKs), we showed that Cry2 fused to the N-terminal SH2 domain from PLCγ (SH2-N) could bind FGFR1 and PDGFRβ receptors in a light-dependent manner (Figure 3.11**,** Figure 3.12). Since SH2 domains bind a phosphorylated peptide sequence, the SH2-N construct has low affinity for the inactivated, unphosphorylated RTK in the dark state. Upon light induced clustering, SH2-N successfully bound and activated RTKs. Although SH2-binding suggests a prerequisite of receptor activation/phosphorylation, we found that SH2-based CLICR bound its target receptor even in both low-serum and serum free conditions, which are expected to exhibit minimal levels of basally phosphorylated receptor. We believe this paradox may be explained by the fact that RTKs undergo constant rapid cycles of activating autophosphorylation counterbalanced by inactivating dephosphorylation (*35, 51*). High SH2 avidity via CLICR clustering may allow trapping of the phosphorylated RTK and protection from dephosphorylation, thus permitting SH2-N binding and allowing clustering of the endogenous receptors. As a caution, we note that we also attempted to target the FGFR1 receptor with a phosphotyrosine binding (PTB) domain from the FRS2 protein, which binds FGFR1 (*52*). Although it, too, localized to focal cellular structures, these structures did not co-localize with the FGFR1-GFP fusion (Figure 3.26**)**, highlighting the need to empirically determine the suitability of the CLICR adapter domain

In fibroblasts, SH2-N visibly localized to endogenous membrane focal structures upon light activation, inducing rapid lamellipodial extensions and polarization (Figure 3.15). RTKi and PDGFRi-specific inhibition significantly reduced the mean number of cells that extended lamellipodia and repolarized in response to light, and the remaining inhibited cells that did extend lamellipodia did so with significant delay. (Figure 3.17**,** Figure 3.18). FGFR inhibition did not have these effects, suggesting that the observed light induced phenotypes were due largely to CLICR targeting of endogenous PDGFRβ. The ability of some PDGFR-inhibited cells to still extend lamellipodia but only after significant delay may be due to an extended time of

formation of: 1) a critical number of PDGFR receptors within a cluster or sufficient accumulation of downstream signal, both of which would be impaired under PDGFR blockade, and/or 2) weak CLICR clustering/activation of another RTK implicated in cell motility, such as EGFR. Cell-to-cell response heterogeneity may be due to copy number variation of critical endogenous proteins necessary to respond to the activated RTKs.

Our demonstration of CLICR-based, PDGFR-dependent phototaxis highlights the utility of optical methods to study cellular information processing and to regulate cell fates with high spatial and temporal resolution. Similarly, Wu *et al (29)* developed light-induced directed motility with a photoactivatible Rac1 protein, which has since been used to study applications including collective cell migration in drosophila ovaries (*53*), neutrophil motility in zebrafish (*54*), and mouse neuronal response in cocaine addiction (*55*) with spatiotemporal precision. As we show, the CLICR method may also be used to precisely study cell motility from a different node of the signaling network, but its modularity may further empower photoactivation of numerous other receptor-mediated signaling pathways, expanding our ability to regulate diverse signaling pathways with optical precision.

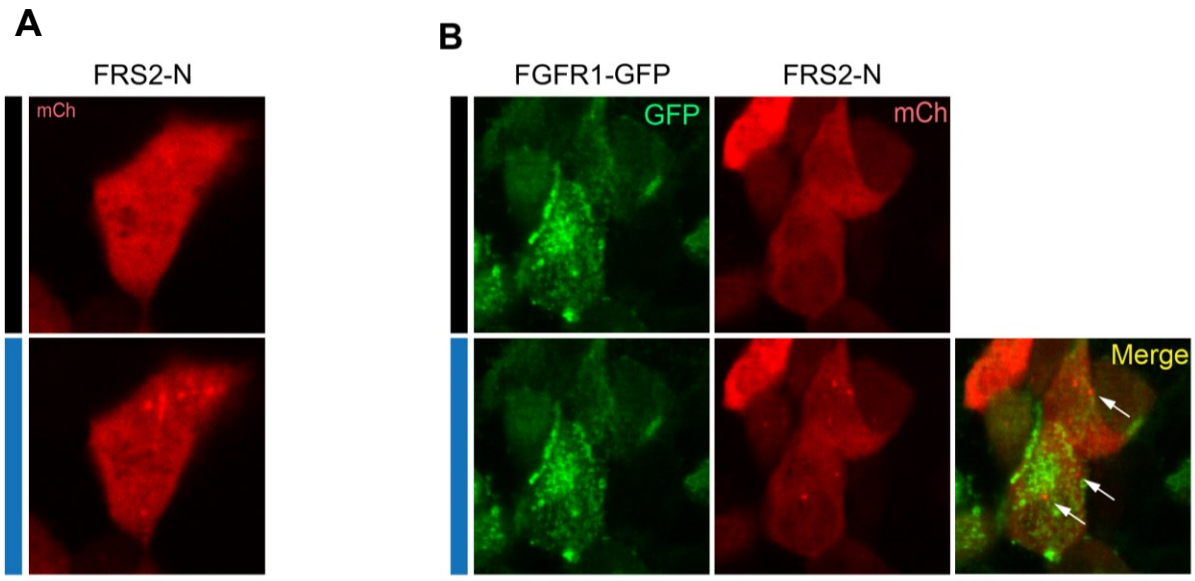

Figure 3.26 FRS2(PTB)-mCh-Cry2 (FRS2-N) localizes to immobilized structures but not to the target FGFR1 receptor. An N-terminal fusion of PTB to mCh-Cry2 (PTB-N) was hypothesized to enable light induced FGFR1 targeting. FRS2-N expressing 293T cells exhibited light-dependent formation of immobilized FRS2-N clusters (A). However, cells co-expressing FRS2-N and FGFR1-GFP reveal that the light induced clusters do not co-localize with FGFR1 (arrows) (B). These results emphasize the importance of empirically validating the CLICR adapter domain to activate a desired target. Scale bars = 20 μm.

This report serves as a proof of principle that the CLICR strategy is a useful and feasible method of optically clustering and activating endogenous transmembrane receptors. For our study in fibroblasts, the motility phenotype was mostly dependent on PDGFRβ signaling, but it remains possible that other endogenous RTKs were being clustered as well, as the PLCγ SH2 domain may bind many receptors, including including FGFR 1-4, PDGFRα and β, VEGFR1, Ret, TrkA, and TrkB. One may envision the ideal CLICR adapter would be an entirely receptor-specific domain that would be orthogonal to endogenous signaling, for example an intracellular antibody evolved to target the receptor endodomain without interfering with signaling (*56*). However, in many instances a naturally evolved domain may suffice, provided the appropriate tests and controls for undesired effects are performed.

The ability to optically regulate endogenous receptors represents an attractive alternative to studies employing receptor overexpression, which often elevates pathway signaling above the physiologically basal state. Since we also showed clustering and activation of overexpressed cytoplasmic proteins (Figure 3.3**,** Figure 3.4), we believe this method may be applicable to cluster endogenous cytoplasmic signaling proteins as well. Effectively having remote control over endogenous protein association and activation may allow more sensitive studies of cellular information transfer with fewer artifacts due to introduction of abundant exogenous signaling molecules.

In conclusion, we present an optogenetic methodology called Clustering Indirectly using Cryptochrome2*,* or CLICR, a Cry2 based strategy allowing oligomerization and activation of binding partners with a single protein construct at sensitivities allowing manipulation of endogenously expressed proteins. This strategy is particularly useful for targeting endogenous cell surface receptors, a class of molecules heretofore refractory to regulation through other optogenetic methods. The demonstrated expression and activity of CLICR across numerous cell types and the ease of engineering new tropism for the Cry2 clustering module make CLICR an attractive optogenetic tool for the manipulation of endogenous protein activity across biological systems.

3.4 Methods

DNA Vector Assembly

All vectors were constructed using the CPEC method (*57*) and as described previously (*2*). Full descriptions of all constructs used are provided in Appendix A. The LZa and LZb heterodimeric leucine zipper pair corresponds to leucine zipper pair (vii), as described (*31*), and was synthesized through primer overlap extension. We received the full length LRP6 construct from Dr. Xi He, the Rac1 construct from Dr. G. Steven Martin, the Akt construct from Dr. S. Ferguson, the PDGFRβ, and 7x TCF constructs from Addgene (#23893 and #24308, respectively), and the PLCγ-1 and FRS2 constructs from the DNASU plasmid repository (clone IDs HsCD00321979 and HsCD00435250, respectively).The FGFR1 construct was cloned from a rat NSC cDNA library by Dr. M. Varedi.

Cell culture, reagents, plasmid transfection and viral transduction

HEK 293Ts were cultured in Dulbecco's Modified Eagle Medium (Corning Cellgro) with 10% fetal bovine serum (FBS) (Life Technologies) and 1% penicillin/streptomycin (P/S) (Life Technologies) at 37°C and 5% CO_2. NIH 3T3 fibroblasts were cultured in DMEM supplemented with 10% bovine calf serum (BCS) and 1% P/S. Rat hippocampal adult neural stem cells (NSCs) (*58*) were cultured on polystyrene plates coated with poly-ornithine and 5 μg/mL laminin (Life Technologies), with Dulbecco's Modified Eagle Medium (DMEM)/F12 (1:1) high-glucose medium containing N-2 supplement (both from Life Technologies) and 20 ng/mL recombinant human FGF-2 (Peprotech). Transient plasmid transfection was performed using the calcium phosphate method. Retroviral and lentiviral packaging and transduction were performed as described (*59*). All retroviral constructs were based on the CLPIT retroviral vector and were packaged in the presence of 3 μg doxycycline to repress transgene expression in order to maximize viral titer.

Luciferase Assay

HEK 293T cells stably transduced with a 7x Tcf luciferase reporter were seeded in black-walled 96 well plates. When ~50% confluent, the cells were transfected with 5 ng of each expression vector diluted in 150 ng pBluescript. Cells were given 24 hrs to express protein and were then illuminated overnight for 16 hours with one 500 ms pulse of LED light every 10s as administered by a custom LED illumination device, as described (*2*). After illumination, cells were lysed, and luciferase was measured with the Luc-screen Firefly Luciferase Gene Reporter System (Life Technologies).

Confocal Microscopy

Time-lapse microscopy of activated Cry2 fusions was performed on a Zeiss LSM 710 AxioObserver confocal microscope with full incubation chamber in conjunction with the Zeiss ZEN software. Cry2 translocation experiments were carried out at 25°C, while experiments examining cell motility and polarity were carried out at 37°C and in 5% CO_2. EGFP, Venus, and mCherry were visualized with 488, 514, and 561 nm laser excitation, respectively, through either a 40x or 63x oil immersion objective. Whole field Cry2 activation was achieved using 450 or 488 nm illumination. Spatially defined activation was carried out under whole cell imaging of Venus with a 514 nm laser in conjuction with focal illumination using the FRAP application with 458 or 488 nm laser light at 1-5% power and 10 μs dwell time per pixel in a 10 μm diameter region. For whole field observation of lamellipodial induction and polarity establishment, cells were excited every 13 seconds with 488 nm light and mCherry was imaged simultaneously.

Image Analysis

Time-lapse image stacks were assembled in ImageJ, and each cell was examined for the appearance of new lamellipodia and the time elapsed from the start of blue light excitation to initial lamellipodial appearance. To assess polarity establishment, cells were scored for the presence of lamellipodial formation coupled with visible trailing edge retraction and morphological reorientation.

Western Blotting

3T3s expressing SH2-N were seeded in 35 mm plates at 50% confluence and 2% FBS. After 24 hrs, medium was exchanged and cells were serum starved for 16 hours. Positive control cells remained in 2% serum. 10 μM RTKi was added 30 minutes before illumination. Light-treated plates were illuminated with a 19 LED array (ledlight.com, cat. # 28345) at 37°C in a standard cell culture incubator with a 500 ms pulse every 2 seconds for 15 minutes. Cells were immediately lysed in cold RIPA buffer containing protease and phosphatase inhibitors, and were separated electrophoretically on a 8% or 10% SDS-PAGE gel. Proteins were then blotted onto a nitrocellulose membrane and probed for phospho-Tyrosine (Cell Signaling #9411), phospho-Akt (Cell Signaling #4060), total Akt (Cell Signaling #9272), phospho-Erk1/2 (Cell Signaling #4370), and total Erk1/2 (Cell Signaling #4695).

Immunoprecipitation

293Ts stably expressing full-length PDFGRβ-GFP or FGFR1-GFP were seeded in 10 cm plates. When ~70% confluent, each plate was transfected with 1 μg 6xHis-SH2-mCh-Cry plasmid DNA diluted in 9 μg pBluescript by the calcium phosphate method. 24 h after transfection, cells were serum starved overnight. Light-treated plates were illuminated with a 19-LED array for 10 minutes at 25°C, after which cells were lysed in 1 mL RIPA buffer. After incubation on ice for

30 minutes, the cell lysate was spun at 4°C for 10 minutes, and the supernatant from each sample was incubated with 5 μg of anti-GFP antibody (Life Technologies, A-11122). Antibody-lysate solutions were incubated overnight at 4°C with gentle shaking and were then incubated in 12.5 μL immobilized protein A/G agarose beads (Thermo Scientific #20421) for 1 hour as per manufacturer instructions. Beads were spun down and washed with lysis buffer three times, followed by one final wash with water. Beads were then incubated in 2X SDS sample buffer, boiled for 10 minutes, spun down one final time, separated via SDS-PAGE, and blotted onto a nitrocellulose membrane. Blots were then probed for GFP or mCherry (Clontech # 632543).

Statistical methodology

Statistical power in luciferase assays was determined through the non-parametric Mann-Whitney Wilcoxon test. For comparing lamellipodial extension delays, varying dosages for RTKi and PDGFRi treatment were compared using one-way ANOVA followed by Tukey post-hoc pairwise analysis, with a significance threshold adjusted using the Bonferroni correction. All statistical analysis was performed using the JMP statistical software suite

3.5 Acknowledgements

We would like to thank Dr. M. Niewiadomska-Bugaj (Western Michigan University) for assistance with statistical analysis, and A. Choksi and S. Pandit for experimental assistance. This work was supported by the Department of Energy Award DE-SC0001216, NIH R01 NS087253, and funding from the Siebel Scholars Foundation (L.J.B). L.J.B conceived and directed the study, designed and performed experiments, and analyzed data. C.K.M. and M.V. provided experimental assistance and performed experiments. D.V.S provided conceptual and technical guidance and support. L.J.B wrote the manuscript, with revision and editing from D.V.S and R.S.K.

3.6 Appendices

3.6.1 Appendix A

List of DNA constructs generated for Chapter 3.

Construct Name	*Backbone*	*Description*
Cry2-mCh	pmCherry-N1	PHR domain of AtCry2 (a.a.1-498) with C-terminal mCherry fusion
mCh-Cry2	pmCherry-N1	PHR domain of AtCry2 (a.a.1-498) with N-terminal mCherry fusion
Cry2-mCh-LRP6c	pmCherry-N1	Endodomain of LRP6 receptor fused to the C-terminus of Cry2-mCh
Cry2-mCh-LZa	pmCherry-N1	Leucine zipper helix (a) fused to the C-terminus of Cry2-mCh
LZa-mCh-Cry2	pmCherry-N1	Leucine zipper helix (a) fused to the N-terminus of mCh-Cry2
LZa-Cry2-mCh	pmCherry-N1	Leucine zipper helix (a) fused to the N-terminus of Cry2-mCh
LZb-GFP-LRP6c	pEGFP-N1	Leucine zipper helix (b) fused to the N-terminus of GFP-LRP6c
GFP-LRP6c-LZb	pEGFP-N1	Leucine zipper helix (b) fused to the C-terminus of GFP-LRP6c
LZb-LRP6c-GFP	pEGFP-N1	Leucine zipper helix (b) fused to the N-terminus of LRP6c-GFP
LRP6c-GFP-LZb	pEGFP-N1	Leucine zipper helix (b) fused to the C-terminus of LRP6c-GFP
LZb-GFP-Rac1	pEGFP-N1	Leucine zipper helix (b) fused to the N-terminus of GFP-Rac1
LZb-GFP-CaaX	pEGFP-N1	Leucine zipper helix (b) fused to the N-terminus of GFP-CaaX
LRP6-GFP	pEGFP-N1	Full length LRP6 with C-terminal GFP fusion
LRP6-GFP-LZb	pEGFP-N1	Leucine zipper helix (b) fused to the C-terminus of full length LRP6-GFP
FGFR1-GFP	CLPIT retroviral vector	Full length FGFR1 with C-terminal GFP fusion
PDGFRβ-GFP	CLPIT retroviral vector	Full length PDGFR1β with C-terminal GFP fusion
SH2-mCh-Cry2	pmCherry-N1	N-terminal SH2 domain from PLCγ-1 fused to N-terminus of mCherry-Cry2
SH2-mCh-Cry2	CLPIT retroviral vector	N-terminal SH2 domain from PLCγ-1 fused to N-terminus of mCherry-Cry2
Cry2-mCh-SH2	pmCherry-N1	N-terminal SH2 domain from PLCγ-1 fused to C-terminus of Cry2-mCherry
Cry2-mCh-SH2	CLPIT retroviral vector	N-terminal SH2 domain from PLCγ-1 fused to C-terminus of Cry2-mCherry
PTB-mCh-Cry2	pmCherry-N1	PTB domain of human FRS2 protein fused to N-terminus of mCherry-Cry2
PTB-mCh-Cry2	CLPIT retroviral vector	PTB domain of human FRS2 protein fused to N-terminus of mCherry-Cry2
Cry2-mCh-PTB	pmCherry-N1	PTB domain of human FRS2 protein fused to C-terminus of Cry2-mCherry
Cry2-mCh-PTB	CLPIT retroviral vector	PTB domain of human FRS2 protein fused to C-terminus of Cry2-mCherry
Lifeact-Venus	pFU lentiviral vector	F-actin-targeting Lifeact peptide fused to the N-terminus of Venus
Venus-PH(Akt)	CLPIT retroviral vector	PH domain (a.a. 1-150) from human Akt fused to the C-terminus of Venus
Dok1-mCh-Cry2	CLPIT retroviral vector	PTB domain of mouse Dok1 protein fused to N-terminus of mCh-Cry2

3.7 References

1. J. E. Purvis, G. Lahav, Encoding and Decoding Cellular Information through Signaling Dynamics. *Cell* **152**, 945 (2013).
2. L. J. Bugaj, A. T. Choksi, C. K. Mesuda, R. S. Kane, D. V. Schaffer, Optogenetic protein clustering and signaling activation in mammalian cells. *Nature methods* **10**, 249 (2013).
3. B. N. Kholodenko, J. F. Hancock, W. Kolch, Signalling ballet in space and time. *Nat Rev Mol Cell Biol* **11**, 414 (2010).
4. A. D. Lander, Morpheus Unbound: Reimagining the Morphogen Gradient. *Cell* **128**, 245 (2007).
5. S. Davis *et al.*, Ligands for EPH-related receptor tyrosine kinases that require membrane attachment or clustering for activity. *Science* **266**, 816 (1994).
6. C.-H. Heldin, Dimerization of cell surface receptors in signal transduction. *Cell* **80**, 213 (1995).
7. F. Letourneur, R. D. Klausner, T-cell and basophil activation through the cytoplasmic tail of T-cell-receptor zeta family proteins. *Proceedings of the National Academy of Sciences* **88**, 8905 (1991).
8. C. Margadant, H. N. Monsuur, J. C. Norman, A. Sonnenberg, Mechanisms of integrin activation and trafficking. *Current Opinion in Cell Biology* **23**, 607 (2011).
9. C. Romeo, B. Seed, Cellular immunity to HIV activated by CD4 fused to T cell or Fc receptor polypeptides. *Cell* **64**, 1037 (1991).
10. J. Schlessinger, Cell Signaling by Receptor Tyrosine Kinases. *Cell* **103**, 211 (2000).
11. Y. Zhao, C. Tong, J. Jiang, Hedgehog regulates smoothened activity by inducing a conformational switch. *Nature* **450**, 252 (2007).
12. L. L. Kiessling, J. E. Gestwicki, L. E. Strong, Synthetic multivalent ligands in the exploration of cell-surface interactions. *Current Opinion in Chemical Biology* **4**, 696 (2000).
13. A. Conway *et al.*, Multivalent ligands control stem cell behaviour in vitro and in vivo. *Nat Nano* **8**, 831 (2013).
14. D. Spencer, T. Wandless, S. Schreiber, G. Crabtree, Controlling signal transduction with synthetic ligands. *Science* **262**, 1019 (1993).
15. P. Coward *et al.*, Controlling signaling with a specifically designed Gi-coupled receptor. *Proceedings of the National Academy of Sciences* **95**, 352 (1998).
16. I. Dikic, J. Schlessinger, I. Lax, PC12 cells overexpressing the insulin receptor undergo insulin-dependent neuronal differentiation. *Current Biology* **4**, 702 (1994).
17. S. Traverse *et al.*, EGF triggers neuronal differentiation of PC12 cells that overexpress the EGF receptor. *Current Biology* **4**, 694 (1994).
18. Y. Jiang, J. D. Woronicz, W. Liu, D. V. Goeddel, Prevention of Constitutive TNF Receptor 1 Signaling by Silencer of Death Domains. *Science* **283**, 543 (1999).
19. A. Levskaya, O. D. Weiner, W. A. Lim, C. A. Voigt, Spatiotemporal control of cell signalling using a light-switchable protein interaction. *Nature* **461**, 997 (2009).
20. M. J. Kennedy *et al.*, Rapid blue-light-mediated induction of protein interactions in living cells. *Nat. Meth.* **7**, 973 (2010).
21. M. Yazawa, A. M. Sadaghiani, B. Hsueh, R. E. Dolmetsch, Induction of protein-protein interactions in live cells using light. *Nat. Biotech.* **27**, 941 (2009).

22. D. Strickland *et al.*, TULIPs: tunable, light-controlled interacting protein tags for cell biology. *Nat. Meth.* **9**, 379 (2012).
23. X. X. Zhou, H. K. Chung, A. J. Lam, M. Z. Lin, Optical Control of Protein Activity by Fluorescent Protein Domains. *Science* **338**, 810 (2012).
24. D. Chen, E. S. Gibson, M. J. Kennedy, A light-triggered protein secretion system. *The Journal of Cell Biology* **201**, 631 (2013).
25. X. Wang, X. Chen, Y. Yang, Spatiotemporal control of gene expression by a light-switchable transgene system. *Nat. Meth.* **9**, 266 (2012).
26. S. Konermann *et al.*, Optical control of mammalian endogenous transcription and epigenetic states. *Nature* **500**, 472 (2013).
27. L. R. Polstein, C. A. Gersbach, Light-Inducible Spatiotemporal Control of Gene Activation by Customizable Zinc Finger Transcription Factors. *Journal of the American Chemical Society* **134**, 16480 (2012).
28. J. Cao *et al.*, Light-inducible activation of target mRNA translation in mammalian cells. *Chemical Communications* **49**, 8338 (2013).
29. Y. I. Wu *et al.*, A genetically encoded photoactivatable Rac controls the motility of living cells. *Nature* **461**, 104 (2009).
30. Jared E. Toettcher, Orion D. Weiner, Wendell A. Lim, Using Optogenetics to Interrogate the Dynamic Control of Signal Transmission by the Ras/Erk Module. *Cell* **155**, 1422 (2013).
31. J. J. Havranek, P. B. Harbury, Automated design of specificity in molecular recognition. *Nat Struct Mol Biol* **10**, 45 (2003).
32. C. Metcalfe, C. Mendoza-Topaz, J. Mieszczanek, M. Bienz, Stability elements in the LRP6 cytoplasmic tail confer efficient signalling upon DIX-dependent polymerization. *J. Cell Sci.* **123**, 1588 (2010).
33. C. Fuerer, R. Nusse, Lentiviral Vectors to Probe and Manipulate the Wnt Signaling Pathway. *PLoS ONE* **5**, e9370 (2010).
34. F. Cong, L. Schweizer, H. Varmus, Wnt signals across the plasma membrane to activate the β-catenin pathway by forming oligomers containing its receptors, Frizzled and LRP. *Development* **131**, 5103 (2004).
35. R. Zippel *et al.*, Inhibition of phosphotyrosine phosphatases reveals candidate substrates of the PDGF receptor kinase. *European journal of cell biology* **50**, 428 (1989).
36. M. Mohammadi *et al.*, A tyrosine-phosphorylated carboxy-terminal peptide of the fibroblast growth factor receptor (Flg) is a binding site for the SH2 domain of phospholipase C-gamma 1. *Molecular and Cellular Biology* **11**, 5068 (1991).
37. D. Anderson *et al.*, Binding of SH2 domains of phospholipase C gamma 1, GAP, and Src to activated growth factor receptors. *Science* **250**, 979 (1990).
38. D. J. Sieg *et al.*, FAK integrates growth-factor and integrin signals to promote cell migration. *Nat Cell Biol* **2**, 249 (2000).
39. H. M. ROSENFELDT *et al.*, EDG-1 links the PDGF receptor to Src and focal adhesion kinase activation leading to lamellipodia formation and cell migration. *The FASEB Journal* **15**, 2649 (2001).
40. V. Kundra *et al.*, Regulation of chemotaxis by the platelet-derived growth factor receptor-[beta]. *Nature* **367**, 474 (1994).
41. C.-H. Heldin, B. Westermark, Mechanism of Action and In Vivo Role of Platelet-Derived Growth Factor. *Physiological Reviews* **79**, 1283 (1999).

42. S. J. Watton, J. Downward, Akt/PKB localisation and 3′ phosphoinositide generation at sites of epithelial cell–matrix and cell–cell interaction. *Current Biology* **9**, 433 (1999).
43. G. Maheshwari, G. Brown, D. A. Lauffenburger, A. Wells, L. G. Griffith, Cell adhesion and motility depend on nanoscale RGD clustering. *Journal of Cell Science* **113**, 1677 (2000).
44. N. J. Anthis *et al.*, β Integrin Tyrosine Phosphorylation Is a Conserved Mechanism for Regulating Talin-induced Integrin Activation. *Journal of Biological Chemistry* **284**, 36700 (2009).
45. A. Teckchandani *et al.*, Quantitative proteomics identifies a Dab2/integrin module regulating cell migration. *The Journal of Cell Biology* **186**, 99 (2009).
46. T. Nishimura, K. Kaibuchi, Numb Controls Integrin Endocytosis for Directional Cell Migration with aPKC and PAR-3. *Developmental Cell* **13**, 15 (2007).
47. D. Bouvard, J. Pouwels, N. De Franceschi, J. Ivaska, Integrin inactivators: balancing cellular functions in vitro and in vivo. *Nat Rev Mol Cell Biol* **14**, 430 (2013).
48. V. S. Kraynov *et al.*, Localized Rac Activation Dynamics Visualized in Living Cells. *Science* **290**, 333 (2000).
49. S. J. Habib *et al.*, A Localized Wnt Signal Orients Asymmetric Stem Cell Division in Vitro. *Science* **339**, 1445 (2013).
50. J. E. Purvis *et al.*, p53 Dynamics Control Cell Fate. *Science* **336**, 1440 (2012).
51. B. Jallal, J. Schlessinger, A. Ullrich, Tyrosine phosphatase inhibition permits analysis of signal transduction complexes in p185HER2/neu-overexpressing human tumor cells. *Journal of Biological Chemistry* **267**, 4357 (1992).
52. S. H. Ong *et al.*, FRS2 Proteins Recruit Intracellular Signaling Pathways by Binding to Diverse Targets on Fibroblast Growth Factor and Nerve Growth Factor Receptors. *Molecular and Cellular Biology* **20**, 979 (2000).
53. X. Wang, L. He, Y. I. Wu, K. M. Hahn, D. J. Montell, Light-mediated activation reveals a key role for Rac in collective guidance of cell movement in vivo. *Nat Cell Biol* **12**, 591 (2010).
54. S. K. Yoo *et al.*, Differential Regulation of Protrusion and Polarity by PI(3)K during Neutrophil Motility in Live Zebrafish. *Developmental Cell* **18**, 226 (2010).
55. D. M. Dietz *et al.*, Rac1 is essential in cocaine-induced structural plasticity of nucleus accumbens neurons. *Nat Neurosci* **15**, 891 (2012).
56. S. Hyland, R. R. Beerli, C. F. Barbas, III, N. E. Hynes, W. Wels, Generation and functional characterization of intracellular antibodies interacting with the kinase domain of human EGF receptor. *Oncogene* **22**, 1557 (2003).
57. J. Quan, J. Tian, Circular Polymerase Extension Cloning of Complex Gene Libraries and Pathways. *PLoS ONE* **4**, e6441 (2009).
58. F. H. Gage *et al.*, Survival and differentiation of adult neuronal progenitor cells transplanted to the adult brain. *Proceedings of the National Academy of Sciences of the United States of America* **92**, 11879 (1995).
59. J. H. Yu, D. V. Schaffer, Selection of novel vesicular stomatitis virus glycoprotein variants from a peptide insertion library for enhanced purification of retroviral and lentiviral vectors. *Journal of virology* **80**, 3285 (2006).

Chapter 4

Shedding Light on Oligomerization-induced Activation of the Rho GTPase Family

4.1 Introduction

Rho GTPases are small G-proteins regulating a wide range of processes within mammalian cells, most notably sensing and regulating biophysical cellular properties, including cytoskeletal mechanics, cellular tension, and cell motility (*1*). This class of GTPases has thus been a focus of intense study in the fields of cancer progression and metastasis, directed stem cell differentiation, and developmental morphogenesis, among many others.

Though the human genome encodes 22 known members of the Rho GTPase family, the three most extensively studied Rho GTPases are Rac1, RhoA, and Cdc42. Rac1 mediates membrane ruffling and lamellipodial extension within migrating cells (*2*). RhoA often acts antagonistically to Rac1 and mediates cellular tension via stress fiber formation and focal adhesion assembly (*3*). Cdc42 activity stimulates the formation of long protruding actin spikes termed filopodia that aid in cell movement and directional sensing (*4*). Though possessing different cellular functions, the Rho GTPases share a similar activation cycle (Figure 4.1). Rho GTPases cycle between a GTP-bound (active) state and a GDP-bound (inactive) state. When inactive, the GTPases are sequestered in the cytoplasm via binding to guanine nucleotide dissociation inhibitors (GDI), which bind and obstruct the prenylated C-terminus that is common to the Rho GTPase family. Guanine nucleotide exchange factors (GEFs) catalyze activation by promoting GDP-to GTP exchange and the dissociation of GDIs. Once dissociated, the GTPase C-terminal lipid tail is exposed, and the active GTPases are inserted into the membrane compartment, where they interact with and activate downstream effectors. To complete the activation cycle, the bound GTP is hydrolyzed either through intrinsic GTPase activity or through the help of a GTPase activating protein (GAP), and the GDI once again binds the GTPase, extracts it from the membrane, and sequesters it in the cytoplasm (*5*).

Cells take advantage of the rapid activation/inactivation cycles of the Rho GTPases and use these proteins to coordinate fast cellular programs and functions with high spatiotemporal precision. With a sensor of Rac1 activity, Kraynov and colleagues first observed that Rac1 activity was high at the leading edge protrusions of migrating cells (*6*). Later, this same group, using multiplexed reporters for Rac1, RhoA, and Cdc42, reported precise temporal and spatial orchestration between these three proteins within migrating cells, including the surprising finding that RhoA was not only mediating contractility at the trailing edge of cells, but also served a function in a thin, transient region at the very front of lamellipodial extensions just before the onset of Rac1 activation (*7*).

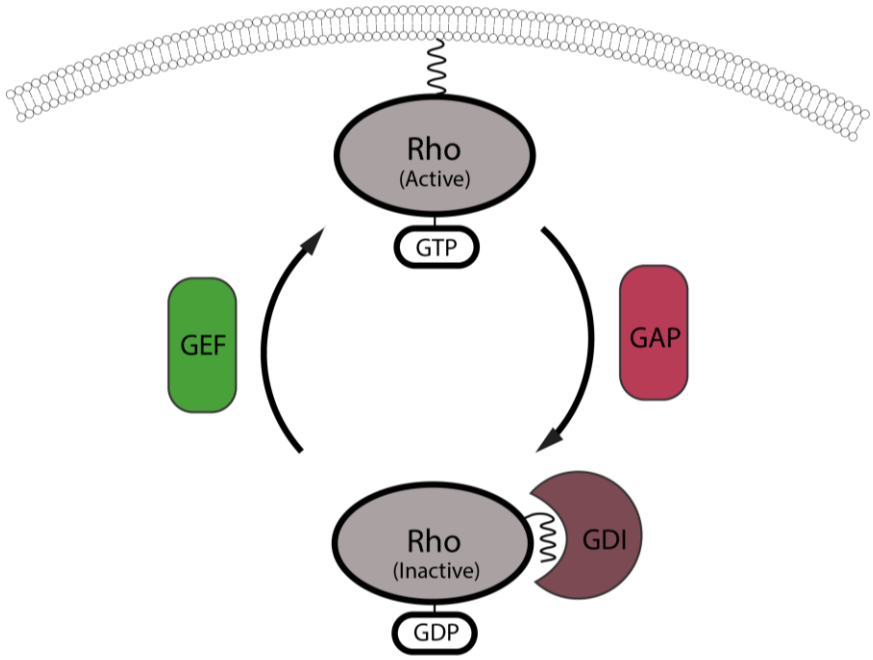

Figure 4.1 Rho GTPase activation cycle. Rho GTPases are sequestered in the cytoplasm in their inactive GDP-bound state by guanine dissociation inhibitors (GDIs), which bind the Rho GTPases and obstruct the prenylated C-terminus. Upon activation and GDP-to-GTP exchange catalyzed by guanine exchange factors (GEFs), GDIs dissociate, exposing the C-terminal lipid tail and allowing membrane translocation and insertion of the Rho proteins. The GTP-loaded membrane-bound form is the active form of the Rho GTPases. Upon hydrolyisis of GTP to GDP, which is stimulated by GTPases activating proteins (GAPs), Rho GTPases are inactivated and extracted from the membrane by GDIs.

Due to this interesting and rapid coordination of Rho GTPases to regulate cell motility and morphology, the earliest optogenetic tools for cell biology were designed towards regulating Rho GTPase activity, as light is the optimal inducer for signaling inputs that vary quickly in both space and time. The first such published tool in mammalian cells was an engineered end-to-end fusion of the *A. sativa* LOV2 domain to a constitutively active (ca) Rac1 protein (*8*). In the dark, the compact folding of the LOV2 sterically hindered effector activation by the ca-Rac1. Upon light activation, unfolding released steric inhibition and permitted ca-Rac1 activity. Wu, Hahn and colleagues impressively demonstrated how cells could be induced to follow a spatially defined activating light beam, and this technology was further used to study cell migration in zebrafish neutrophils and *Drosophila* ovaries, as well as to study temporal Rac1 activation in mouse brains in the context of cocaine addiction (*9-11*). Subsequent optogenetic tools also demonstrated light induced manipulation of Rho GTPases. The Phy/PIF system was used to recruit the Rac1 GEF Tiam to the membrane, inducing local Rac1 activation and lamellipodial extension (*12*). GEFs for RhoA and Cdc42 were also recruited, and measurable pathway induction was observed (*12*). The blue-light sensitive FKF1/GI heterodimerizing platform was used to recruit a constitutively active form of Rac1 lacking its C-terminal lipid tail to the membrane, thus inducing activation and lamellipodial extension (*13*). Dronpa145N/Dronpa145K heterodimerization was used to regulate Cdc42 activity *via* fusions of DronpaN and DronpaK to the Cdc42 GEF Intersectin (ITSN) dbl-homology-pleckstrin-homology (DH-PH) catalytic domain (*14*). When DronpaN and DronpaK were bound, the conformational strain or steric hindrance inhibited the DH-PH domain. Upon Dronpa dissociation, the inhibition was released,

and Cdc42 activity was induced, producing dramatic filopodial extensions within fibroblasts (*14*). Finally, as described in Chapter 2, Cry2 clustering was also used to regulate Rho GTPase function. Though clustering a Cry2-Rac1 fusion induced membrane translocation of the fusion, the strongest cluster-induced activation was achieved with a Cry2-RhoA fusion (*15*).

Clustering as a mode of Rho GTPase activation is a poorly understood phenomenon of the well-studied Rho GTPase protein family. Zhang and colleagues described that oligomerization of the Rac1 protein enhances effector PAK1 autophosphorylation, suggesting enhanced Rac1 activation, but also an increases self-stimulatory GTPase activity in the clustered vs. unclustered form (*16*). This enhanced activation followed by enhanced inactivation was hypothesized to be due to a C-terminal "arginine-finger" motif that structurally mimicked the same motif in several GTPase-enhancing GAP proteins, though this hypothesis was not tested (*16*).

In this chapter, we examine the effects of clustering on Rac1, RhoA, and Cdc42, and we explore the mechanisms behind clustering-mediated Rho GTPase activity enhancement. We investigate the necessities for GEF binding, GEF catalysis, and the C-terminal lipid tail, and we develop tools to allow real time dynamic observation of light-induced Rac1 activation. We further examine the function of the postulated C-terminal arginine finger in modulating cluster-induced Rho GTPase activity, and we propose a model for how clustering may enhance activation across this family of signaling proteins.

4.2 Results

Though they modulate different downstream signaling pathways, the three main Rho GTPases share a similar activation cycle (Figure 4.1). The Rho GTPases are maintained in an inactive cytoplasmic state by binding the GDI protein. Upon activation, the GEF enzyme mediates nucleotide exchange and dissociation of the GDI, exposing the C-terminal lipid tail and inducing translocation to the membrane where these proteins are active. Because of this shared cycle, we expected that each Rho GTPase might yield a similar response to clustering.

To test this, we made fusions of Cry2-mCh attached to the N-terminal end of Rac1, RhoA, and Cdc42. As mentioned in Chapter 2, both Cry2-mCh-Rac1 and Cry2-mCh-RhoA expressed in 293T cells translocate to the plasma membrane upon light activation. Similarly, the Cry2-mCh-Cdc42 fusion exhibits similar light dependent activity, suggesting that membrane translocation of Rho GTPases may be a function of their shared signaling architecture (Figure 4.2). Excitingly, this may also point to a straightforward modular method for regulating each of these (and other) Rho GTPases via clustering and optogenetic approaches.

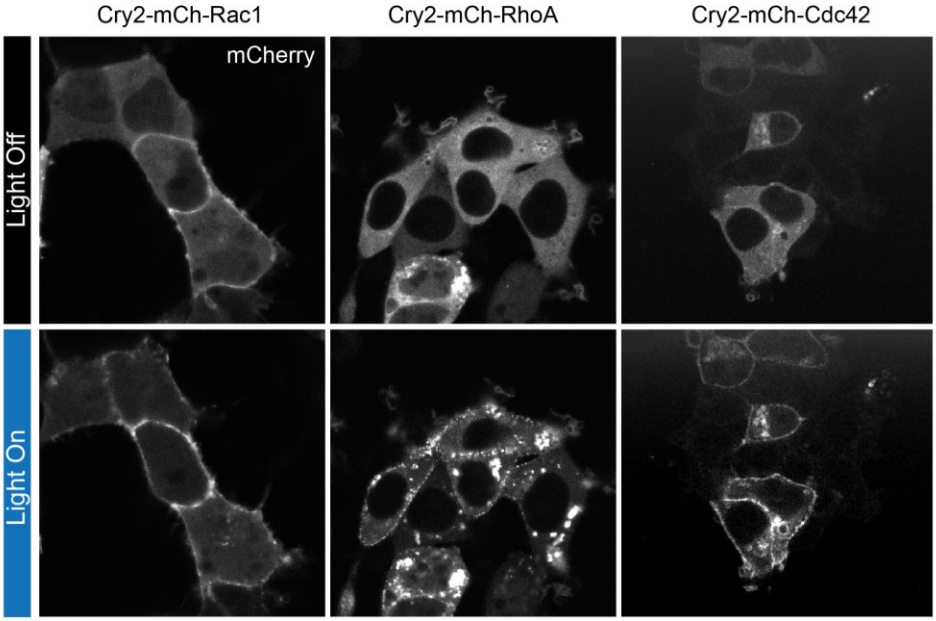

Figure 4.2 Rac1, RhoA, and Cdc42 translocate to the membrane upon clustering. 293T cells expressing fusions of Cry2-mCh to each of the GTPases exhibit light-induced mCherry translocation to the membrane, suggesting that clustering can bias GTPases activation across the Rho GTPase family.

As cluster-induced activation for Rho GTPases remains largely unexamined, we were interested to investigate why oligomerization might influence the Rho GTPase activation state. We identified two hypotheses (Figure 4.3): 1) Rho GTPase clustering induces a high avidity/local concentration between a GTPase cluster and the activating Rho GEF, inducing more efficient GDP/GTP exchange and thus promoting activation, and 2) perhaps the Cry2-mCh-Rho GTPase oligomers were physically dissociating the inhibitory GDIs, exposing the C-terminal lipid tails and promoting membrane translocation.

Since we anticipate a similar activation among the Rho GTPase family, we focused mechanistic characterization on Rac1, as the structure and characteristics of this protein have been determined in great detail. To examine our first hypothesis, we tested the GEF dependence of Cry2-mCh-Rac1 translocation. Tryptophan 56 of Rac1 has been shown to be crucial in mediating interaction between Rac1 three Rac1 GEFs: Tiam, Trio, And GEF-H1 (*17*). A W56F Rac1 mutant was shown incapable of interacting with these three important GEFs. By introducing this mutant into our Cry2-mCh-Rac1 fusion (Cry2-mCh-Rac1(W56F)), we largely abrogated the light-induced Rac1 translocation (Figure 4.4). Since GEF interaction appeared necessary for translocation, we looked further to determine whether GEF binding was sufficient for translocation, or whether GDP-GTP exchange was also required. We created Cry2-mCh-Rac1 constructs harboring either a Y32A or D65A mutation, both shown to permit GEF binding but abrogate GEF-mediated nucleotide exchange (*17*). These constructs exhibited near-wild-type light-induced translocation behavior (Figure 4.5), suggesting that GEF binding was sufficient and catalysis was dispensable, at least for the translocation phenotype.

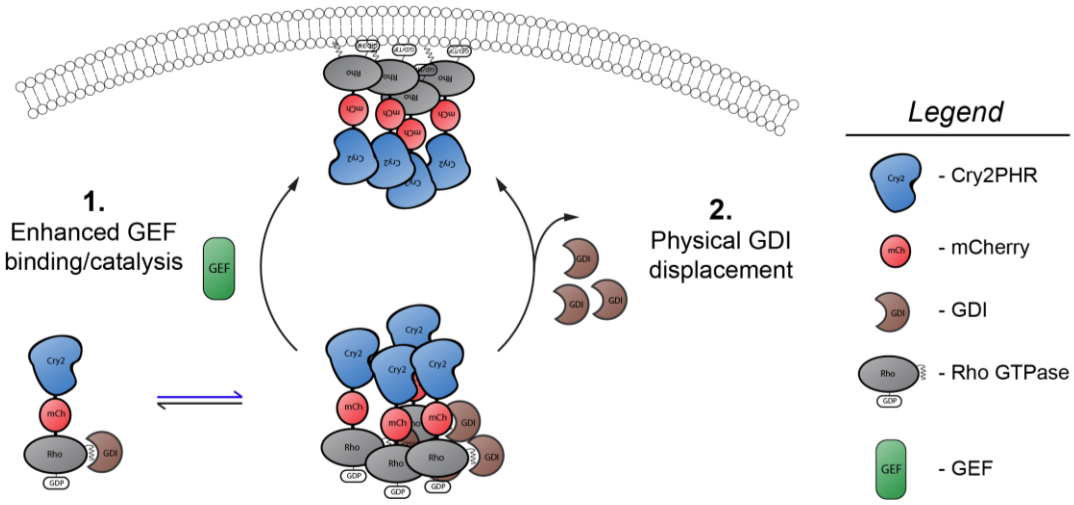

Figure 4.3 Potential mechanisms of cluster-induced activation of Rho GTPases. 1) GTPase clustering enhances avidity of the inactive GTPase for its GEF, enhancing GEF binding, catalysis, and activation. 2) GTPase clustering is sterically non-permissive for GDIs, inducing GDI displacement and exposing the prenylated GTPase C-termini, allowing for membrane insertion.

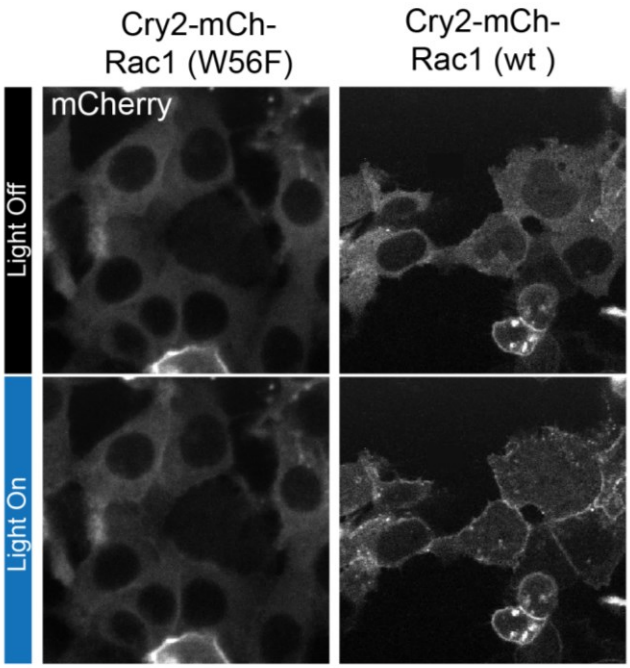

Figure 4.4 GEF interaction is necessary for cluster-induced Rac1 membrane translocation. Cry2-mCh-Rac1 (W56F), which harbors a mutation that abrogates Rac1 interaction with its main GEFs, loses its ability for robust membrane translocation upon illumination/clustering. Membrane translocation of Cry2-mCh-Rac1 (wt) is presented for comparison.

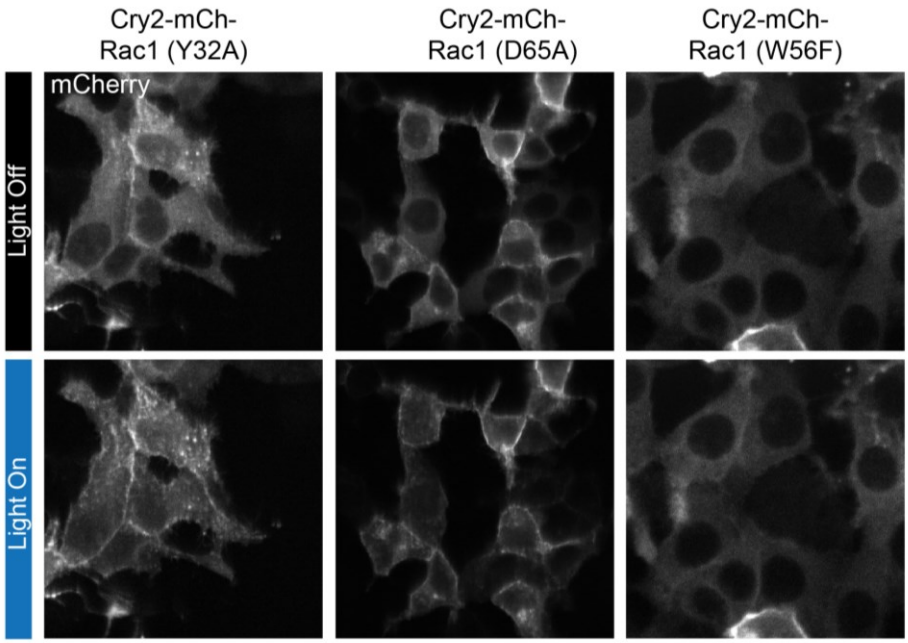

Figure 4.5 GEF catalysis is not necessary for cluster-induced Rac1 translocation. The Y32A and D65A mutations in Rac1 prevent GEF catalysis while leaving GEF binding unaffected. Introduction into either of these mutations within Rac1 in the Cry2-mCh-Rac1 fusion has no apparent effect on cluster-induced translocation, suggesting that GEF catalysis is dispensable for this process.

One potential mechanism consistent with the above results is a natural "CLICR" strategy (Chapter 3), whereby inactive Rac1 would have low affinity for an activating GEF, but upon clustering, the now high-avidity Rac1 cluster would translocate to wherever the Rac1 GEF was localized within the cell. We reasoned we could distinguish this possibility by "moving" the Rac1 GEF to a non-native localization and observing if clustered Rac1 would follow. To implement this, we overexpressed the DH-PH domain of the Rac1 GEF Tiam fused to GFP and a mitochondrial localization domain from the Tom20 protein. Co-expression of this fusion with Cry2-mCh-Rac1 within fibroblasts showed GFP fluorescence with distinctive mitochondrial morphology. mCherry distribution was initially diffuse, though surprisingly appeared somewhat excluded from the mitochondrial compartment (Figure 4.6). Light activation yielded the typical light-induced Cry2-mCh-Rac1 distribution and no recruitment or colocalization of mCh fluorescence with the mitochondria, suggesting that cluster-induced avidity increase is incapable of explaining clustered GTPase plasma membrane translocation.

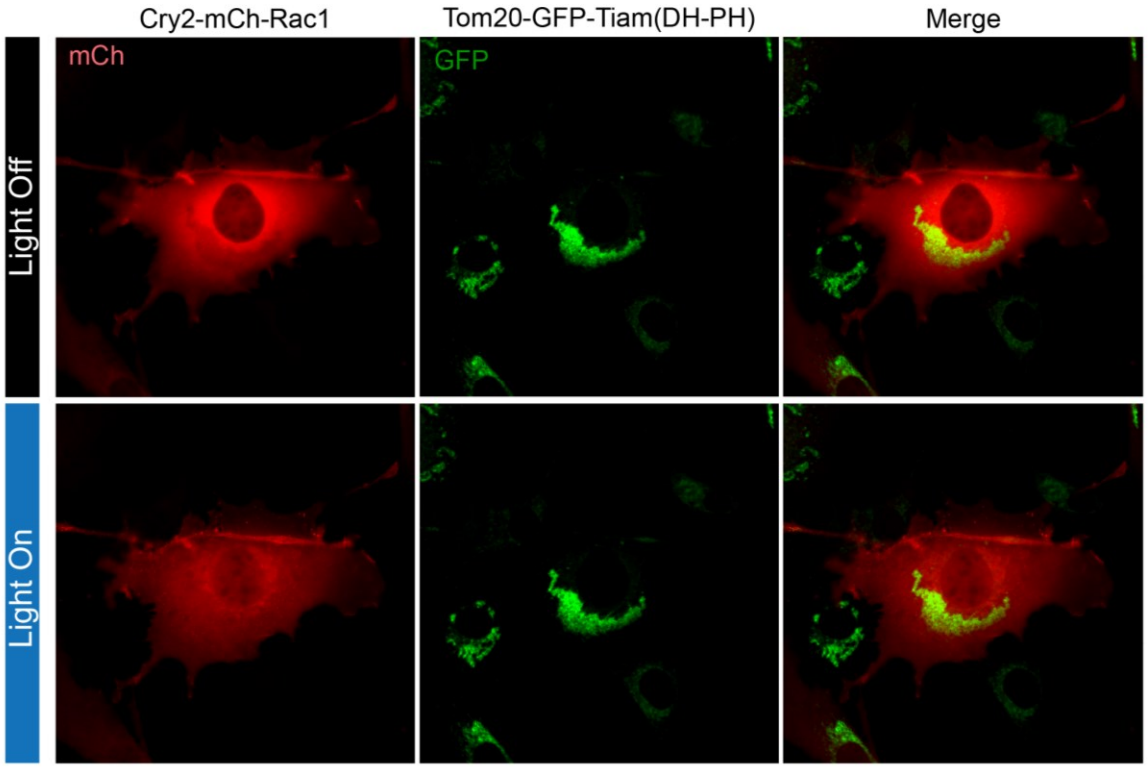

Figure 4.6 GEF interaction with Rac1 is not sufficient to mediate Rac1 translocation. 3T3 fibroblasts co-expressing Cry2-mCh-Rac1 and a mitochondrially localized Tom20-GFP-Tiam(DH-PH) were observed under light activation. Surprisingly, in the dark, mCherry fluorescence appeared excluded from areas of high GFP expression. Upon blue light activation, mCherry fluorescence was not recruited to the mitochondria, suggesting that the Rac1:GEF interaction is not sufficient for cluster-induced translocation.

As another test of the sufficiency of the GEF:GTPase interaction for membrane translocation, we observed translocation activity of a Cry2-mCh-Rac1 mutant lacking its C-terminal lipid tail (Cry2-mCh-Rac1 C189A). If the GEF:GTPase interaction were sufficient, we would expect little change in translocation kinetics of the C189A mutant. Unexpectedly, the

Cry2-mCh-Rac1(C189A) mutant is largely localized to the nucleus in the dark state and exhibits little change in the light, other than minor visible nuclear clustering (Figure 4.7). However, mutants of Cry2-mCh-RhoA and Cry2-mCh-Cdc42 without the prenylated C-terminal cysteines remain cytoplasmic and also fail to translocate to the membrane under light activation (Figure 4.7). Together, these data suggest that the GEF:GTPase interaction is insufficient to explain Rho GTPase translocation upon clustering, and that the C-terminal lipid tail plays an important role in Rac1 localization both in the clustered and unclustered form.

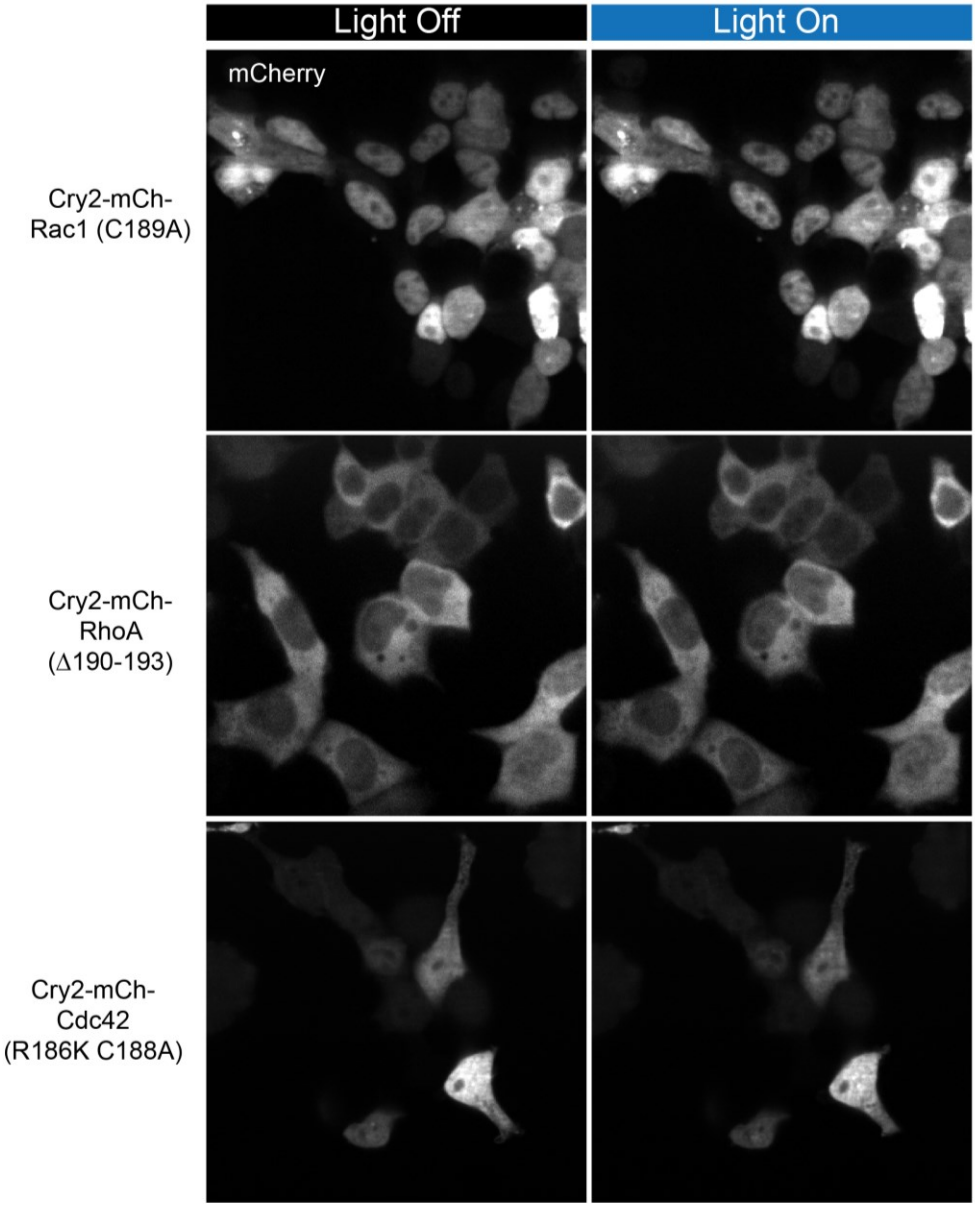

Figure 4.7 The C-terminal lipid tail is necessary for Rho GTPase membrane translocation. Cry2-mCh-Rac1 (C189A), which lacks the cysteine necessary for C-terminal prenylation, constitutively localizes to the nucleus upon expression in cells. Similar mutants of Cry2-mCh-RhoA and Cry2-mCh-Cdc42 remain cytoplasmic but also fail to localize to the plasma membrane upon light activation.

In light of these data, we anticipate cluster-induced activation of GTPases to be a combination of our proposed hypotheses (Figure 4.8). In the dark, monomeric Rac1 is sequestered in the cytoplasm. Upon clustering, GEF binding to the cytoplasmic GTPase is enhanced. This binding, which is mutually exclusive with GDI binding (*18*), displaces the GDI and exposes the lipid tails, allowing membrane translocation of the complex to the plasma membrane.

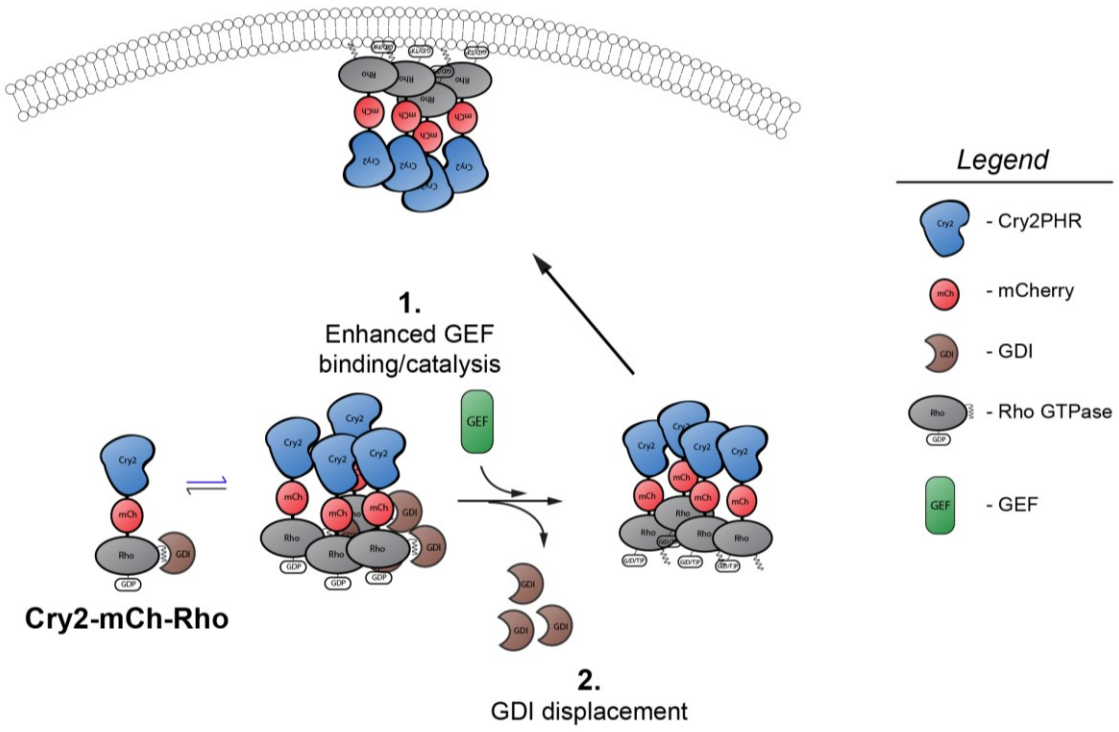

Figure 4.8 Model of cluster-induced Rho GTPase activation. In the unclustered dark state, Rho GTPases are held inactive in the cytoplasm by GDIs. Upon clustering, GEF binding is enhanced (1). As GEF and GDI binding are mutually exclusive, GEF binding induces displacement of GDIs (2), revealing the Rho GTPase C-terminal lipid tails that mediate plasma membrane translocation.

Importantly, this proposed mechanism for translocation is independent of GDP:GTP exchange. However, the necessity for GEF binding indicates that nucleotide exchange is occurring during this process, and indeed we demonstrate the ability to reliably bias RhoA GTP:GDP levels *via* ELISA upon light induced clustering (Figure 2.20). However, despite a similar activation cycle, ELISA for activated Cry2-mCh-Rac1 fusions failed to show a cluster-induced increase in activated Rac1 protein (Figure 4.9), and only modest morphological phenotypes such as cellular spreading were observed in cells upon light illumination. This suggested that Rho GTPase membrane localization may be decoupled from GTP loading and activation in the clustered form. Thus, we aimed to both investigate differences between GTPases that mediate these disparate responses, and develop more sensitive techniques to assay GTPase activation.

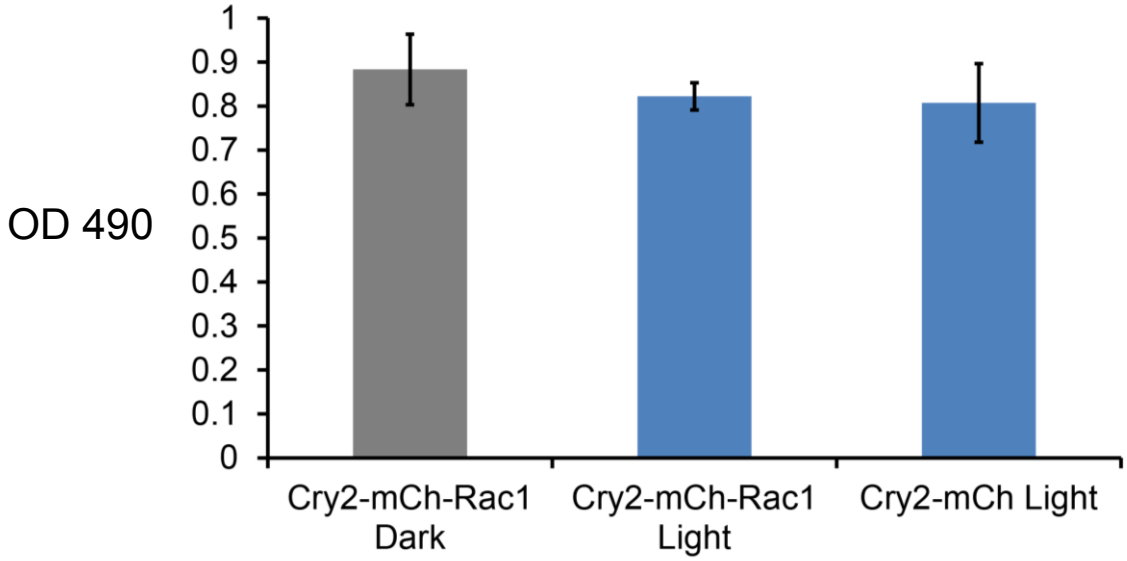

Figure 4.9 Cluster-induced Rac1 activation is undetectable via ELISA. No increase in Rac1-GTP levels is detected upon light activation of fibroblasts expressing Cry2-mCh-Rac1. Graph shows means ± 1 s.d. of biological triplicates. Experiment is representative of 9 independent experiments.

increased activation, but it was also reported to enhance the rate of GTP hydrolysis, indicating enhanced inactivation (*16*). Structural analysis led to the suggestion that an arginine in the 186 position was behaving like an "arginine finger," a motif commonly found in GAP proteins that reaches into the GTPase catalytic pocket and enhances GTP hydrolysis. Analysis of C-terminal sequences of Rac1, RhoA, and Cdc42 reveals that both Rac1 and Cdc42 have an arginine at this position, but RhoA does not (Figure 4.10)**.** The lack of this R186 in RhoA correlates with this protein being the most strongly activated of the three *via* clustering, supporting the inhibitory role of the C-terminal arginine and potentially pointing to a method to enhance Rac1 and Cdc42 activity using clustering.

Rac1 -PVKKRK**R**KCLLL
Cdc42 -PEPKKS**R**RCVLL
RhoA -RRGKKKSKCLVL

Figure 4.10 C-termini of Rac1 and Cdc42 contain putative GTPase-enhancing arginines. Rac1 and Cdc42 contain an arginine residue at the C-terminus that has been proposed to act as an arginine finger to enhance GTP hydrolysis. Such a mechanism may explain why cluster-induced GTP loading is difficult to observe in an ELISA assay, and why clustered Rac1 and Cdc42 yield moderate morphological phenotypes. In contrast, RhoA does not possess an arginine in this position, potentially explaining the ability to robustly activate RhoA through clustering.

We created Cry2-mCh-Rac1 and Cry2-mCh-Cdc42 mutants harboring an R186K mutation, which we expected to mediate stronger GTPase signaling responses upon clustering. Initial expression of Cry2-mCh-Rac1(R186K) in HEK 293T cells yielded striking lamellipodial extension and cell expansion within 293Ts upon light activation, with lamellipodial retraction and cell shrinkage upon light withdrawal (Figure 4.11**).** Further imaging and biochemical validation will be needed to confirm these initial results.

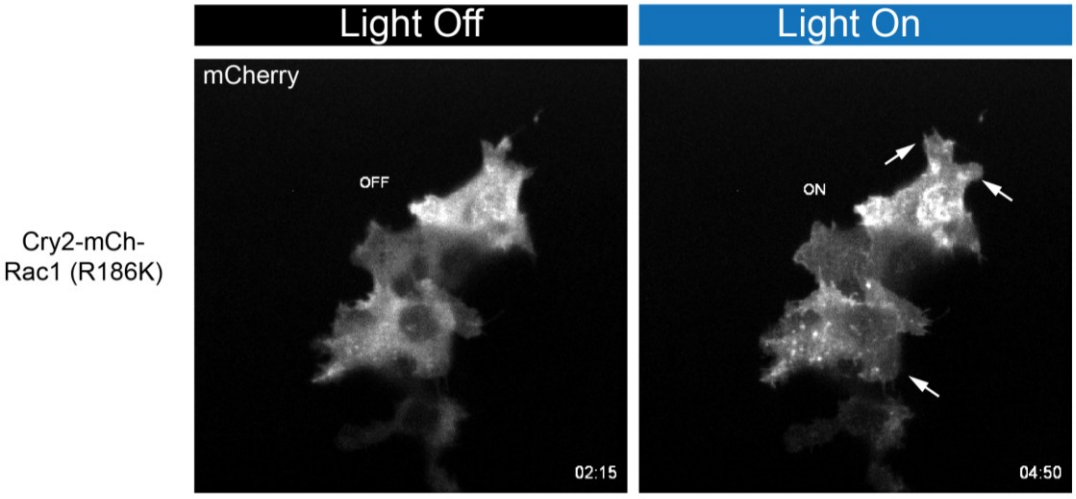

Figure 4.11 Removal of arginine finger may allow more prominent activity of Rac1 via clustering. 293Ts expressing Cry2-mCh-Rac1 (R186K) show striking lamellipodial extension and cellular expansion under light activation, and light withdrawal leads to cell shrinking. These morphological phenotypes are distinct and stronger than those observed by clustering wild-type Rac1.

Finally, as an additional and more sensitive method of assaying activation, we developed a FRET reporter of Cry2-induced Rac1 activity to measure activation in real-time within cells (Figure 4.12**)**. Based on the Rac1 FLAIR sensor (*6*), Cry2-Cypet-Rac1 was constructed as the FRET donor, and the acceptor was a Ypet fused to the Rac1 binding domain from effector PAK1 (Ypet-PBD), which only binds the activated form of Rac1. Coexpressing and imaging these two constructs within cells yielded a ratiometric FRET signal after raw image processing (see Methods). High FRET signal was initially localized at the cell periphery and in lamellipodial protrusions, as would be expected for Rac1, providing confidence that the FRET sensor is functioning properly (Figure 4.13). Further, analysis on cells coexpressing the Cry2-Cypet-Rac1 donor together with a Ypet lacking the PBD showed a noisy and very faint calculated FRET signal, suggesting that the specific Rac1-PBD interaction was necessary for the observed signal. Early data imaging this reporter using wild-type Rac1 containing the arginine finger motif yielded a blue-light dependent decrease in FRET signal (Figure 4.13). Further experimentation and characterization is needed to ensure that this is not an artifactual result, but this result is consistent with clustering inducing rapid hydrolysis and inactivation of active Rac1. Donor constructs encoding Rac1(R186K) have been constructed but not yet tested.

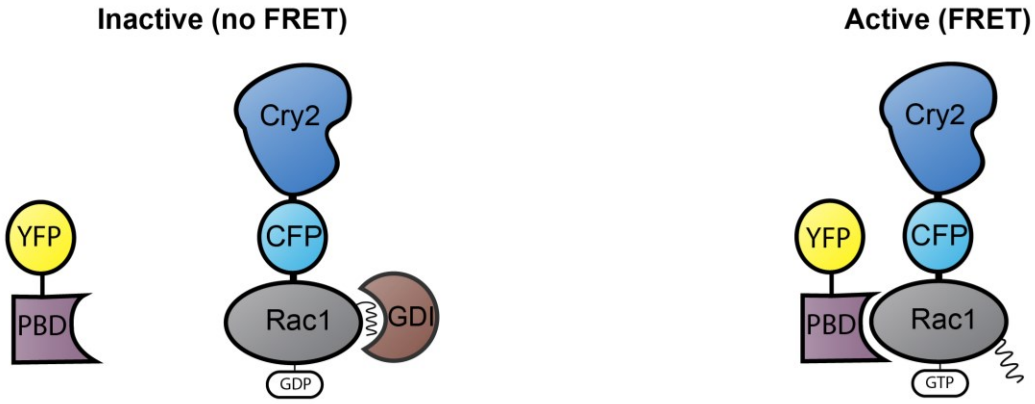

Figure 4.12 Design of FRET system to measure Rac1 activation. For FRET, Cry2 was fused to Cypet (CFP) and Rac1. Ypet (YFP) was fused to the Rac1 binding domain of PAK1 (PBD). In the inactive state, Rac1 will not bind PBD and FRET will not be observed. Upon Rac1 activation, binding of Rac1 to PBD will colocalize the CFP and YFP, allowing FRET to occur.

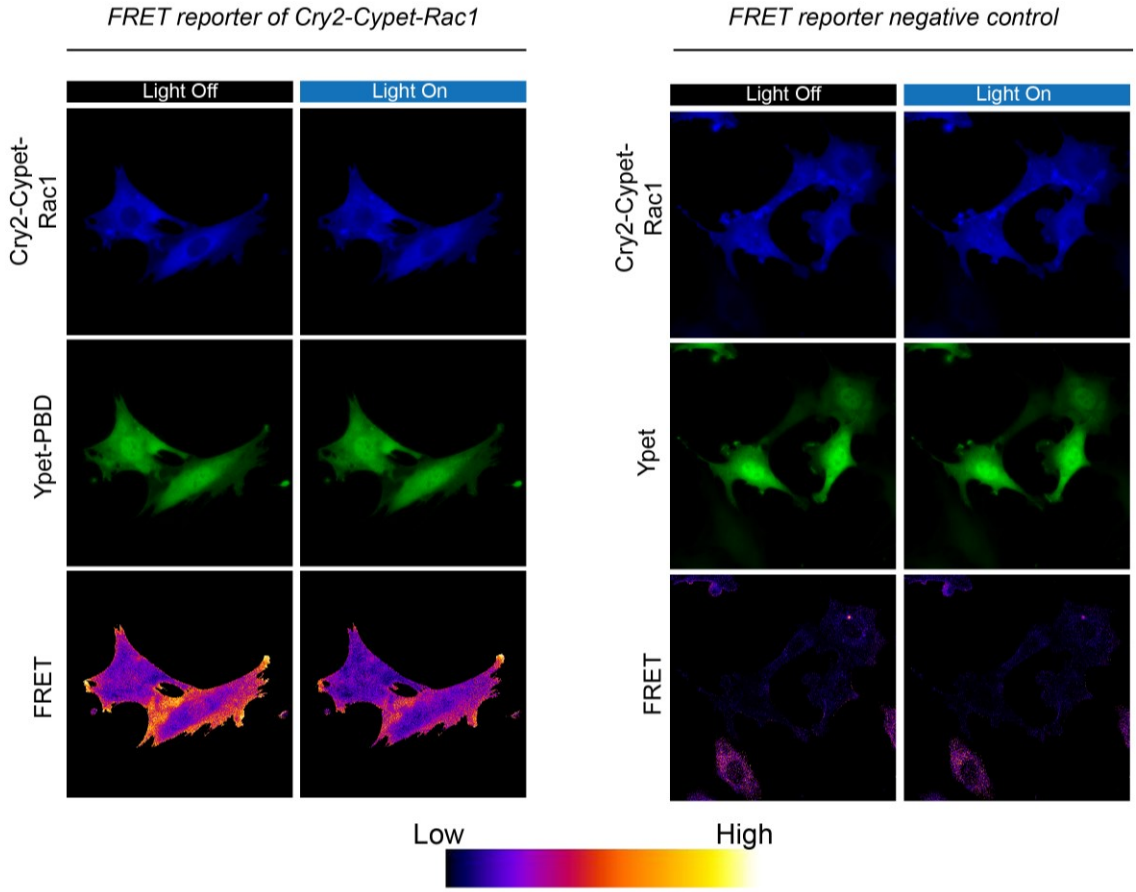

Figure 4.13 Rac1 FRET signal in fibroblasts. A) Coexpression of Cry2-Cypet-Rac1 with Ypet-PBD shows high Rac1 activity at the cell periphery and in cell protrusions. Blue light activation appears to reduce FRET signal and thus Rac1 activation levels. B) A control FRET pair with Ypet lacking a PBD gives negligible FRET signal in both dark and light conditions, suggesting that the FRET signal observed in (A) is due to the specific Rac1:PBD interaction.

4.3 Discussion

The Rho GTPases Rac1, RhoA, and Cdc42 have been demonstrated to be central regulators of key biological processes and have been widely studied. Nevertheless, there is a near complete lack of understanding and appreciation for the role of multimerization in the activation cycle of these important proteins. Motivated by *in vitro* findings of the effects of oligomerization on GTPase activity, we demonstrated that the three main GTPases could all be induced to translocate to the plasma membrane upon Cry2 clustering, and that while Rac1 and Cdc42 clustering induced weak morphological signs of activation, RhoA clustering induced robust morphological contractile phenotypes and measurable increases in GTP vs GDP loading.

Since Rho GTPases share a common activation mechanism, we focused on the well-characterized Rac1 to investigate why clustering induces translocation and activation, and – given the similarities – why we observe differences in the ability to activate different Rho GTPases through clustering. Our data point to a mechanism whereby GEF binding in the clustered state directly induces GDI dissociation and lipid tail exposure, inducing membrane translocation. Interestingly, our results showed that removal of the C-terminal cysteine necessary for lipid modification induces strong nuclear localization, likely mediated by the polybasic domain on the Rac1 C-terminal tail. Removal of corresponding cysteines within RhoA and Cdc42 does not alter the cytoplasmic distribution of these proteins, but these fusions are not able to translocate to the membrane upon clustering (Figure 4.7), indicating that the lipid tail is required for translocation and is likely the main mediator of membrane localization. Interestingly, we also often observe notable nuclear translocation of clustered Cry2-mCh-Rac1(wild-type) protein, suggesting that Rac1 multimerization and/or activation may play a role in nuclear transport and function, a finding corroborated by recent reports (*19, 20*). However, relatively little is understood about Rac1 function within the nuclear compartment.

Further experimentation must be undertaken to verify our working model and to investigate whether removing the autoinhibitory arginine within the Rac1 and Cdc42 C-terminal tails can enable strong light-inducible clustering and activation of these Rho GTPases. In addition, it would be interesting to know whether Rho GTPase clustering is an endogenous mode of activation as well, or whether this shared property is an artifact of the common activation cycle and signaling architectures of these proteins.

4.4 Methods

Cloning and viral production

All constructs and mutants were constructed using the CPEC method (*21*). DNA encoding human Rac1, RhoA, and Cdc42 were obtained from Dr. G. Steven Martin (UC Berkeley). Plasmids encoding the DH-PH domain of Tiam were a gift from Dr. Chris Voigt (MIT). FRET plasmids encoding Cypet and Ypet were obtained from Dr. Patrick Daugherty (UC Santa Barbara). The PAK1 binding domain (PBD) was obtained from Addgene (www.addgene.org, Plasmid # 13723). A list of constructs generated for this chapter can be found in Appendix A. Virus was packaged as described (*22*), in the presence of 3 μg/mL doxycycline to repress transgene expression. Stable cell lines were created through infection and puromycin selection.

Cell culture

HEK 293Ts were cultured on polystyrene plates in Iscove's Modified Eagle Medium (Corning cellgro, Manassas, VA) with 10% fetal bovine serum (FBS) (Life Technologies) and 1% penicillin/streptomycin (P/S) (Life Technologies) at 37°C and 5% CO_2. NIH 3T3 fibroblasts were cultured in DMEM (Corning cellgro) supplemented with 10% bovine calf serum (BCS) and 1% P/S. Stable cell lines expressing the Cry2-GTPases were maintained in 100 ng/mL doxycycline to repress expression, as high levels of sustained Cry2-GTPase expression impaired cell growth. Doxycycline was withdrawn 24 h before experiments, and serum was reduced to 2%.

Live Cell Imaging

Time lapse microscopy of activated Cry2 fusions in HEK 293Ts was performed using a BX51WI microscope (Olympus Corporation, Center Valley, PA) equipped with Swept Field Confocal technology (Prairie Technologies, Inc., Middleton, WI). Clustering visualization in 293Ts was carried out at room temperature. Simultaneous blue light exposure and mCherry imaging was accomplished by imaging in both 488 nm and 561 nm laser channels, 1 exposure per 2-5 seconds, with 488 nm laser varied between 0.1 and 100% power. Given the minute-timescale of the dissociation kinetics of Cry2 clustering, this intermittent pulsing was considered a sufficient approximation of continuous exposure and was necessary to avoid extensive photobleaching of the mCherry fluorophore. Images were also acquired on a Zeiss LSM 710 AxioObserver confocal microscope with full incubation chamber in conjunction with the Zeiss ZEN software. Experiments were carried out at 37°C and in 5% CO_2. mCherry was visualized with 561 nm laser excitation through a 40x or 63x oil immersion objective, and blue light activation was achieved using either the 450 nm or 488 nm laser. FRET imaging was also performed with the Zeiss LSM 710. Cells with strong expression of the two FRET components were chosen for imaging. Cells expressing Ypet strongly were sighted using weak excitation with the 514 nm laser. Donor and acceptor images were acquired using the 450 nm and 514

lasers, respectively. Care was taken to not image Cypet before image acquisition, as 450 nm light activates Cry2.

ELISA

Cry2-mCh-Rac1 expressing NIH 3T3 cells were seeded in 6 well plates at 70,000 cells per well and serum starved over 3 days. After 24 hrs in serum free medium supplemented with 1 ng/mL doxycycline, cells were exposed to 30 s of blue LED light. The samples were processed, and the levels of GTP-loaded (active) Rac1 were determined using the G-LISA Rac1 Activation Assay Biochem Kit (Cytoskeleton, Inc., Denver, CO) according to manufacturer instructions. This ELISA-based assay uses the differential binding of GDP- vs GTP-loaded Rac1 to the binding domain a Rac1 effector to determine the relative levels of only active Rac1 in a sample.

Image Analysis

Stacks of timelapse images were assembled in ImageJ (http://rsbweb.nih.gov/ij/). Clusters were then counted in each frame of the timelapse in CellProfiler (www.cellprofiler.com).

FRET Analysis

Ratiometric FRET signal was calculated through a custom script in ImageJ, which processed the images as follows:

1. Bleedthrough of donor emission and acceptor emission into the FRET channel upon donor excitation was quantified using cells expressing only one of the FRET pairs. After background subtraction, the ratio of bleedthrough divided by the intensity of the donor or acceptor was defined by α and β, respectively.
2. Cells co-expressing the donor and acceptor were imaged, and images for donor emission, acceptor emission, and FRET emission were acquired.
3. Background fluorescence intensities for the FRET acquisition were measured and subtracted from each (donor, acceptor, FRET) channel.
4. A binary cell mask was created by thresholding the acceptor image. Each channel was then multiplied by this mask, yielding non-zero pixel values only for the region representing the cell.
5. FRET signal was then measured with the following algorithm:

$$FRET = \frac{[FRET] - \alpha \times [Donor] - \beta \times [Acceptor]}{[Donor]}$$

Where $[FRET]$, $[Donor]$, and $[Acceptor]$ are the background-subtracted intensities measured for the FRET, donor, and acceptor channels.

4.5 Acknowledgements

I would like to thank Atri Choksi, Colin Mesuda, and Shalmalee Pandit for their technical assistance in generating the constructs tested and described in this chapter.

4.6 Appendices

4.6.1 Appendix A

List of constructs generated for Chapter 4

Construct Name	***Backbone***	***Description***
Cry2-mCh-Rac1	CLPIT retroviral vector	Full length wild-type Rac1 fused to the C-terminus of Cry2-mCh
Cry2-mCh-Rac1 (W56F)	CLPIT retroviral vector	GEF-binding deficient Rac1 fused to the C-terminus of Cry2-mCh
Cry2-mCh-Rac1 (Y32A)	CLPIT retroviral vector	GEF-catalysis deficient Rac1 fused to the C-terminus of Cry2-mCh
Cry2-mCh-Rac1 (D65A)	CLPIT retroviral vector	GEF-catalysis deficient Rac1 fused to the C-terminus of Cry2-mCh
Cry2-mCh-Rac1 (R186K)	CLPIT retroviral vector	Putative Arg-finger-deficient Rac1 fused to the C-terminus of Cry2-mCh
Cry2-mCh-Rac1 (C189A)	CLPIT retroviral vector	Prenylation-deficient Rac1 fused to the C-terminus of Cry2-mCh
Cry2-mCh-Rac1(C189A, R186K)	CLPIT retroviral vector	Prenylation, Arg-finger deficient Rac1 fused to Cry2-mCh
Cry2-mCh-Rac1(C189A, R186K, K183Q)	CLPIT retroviral vector	Prenylation, Arg-finger deficient Rac1(K183Q) fused to Cry2-mCh
Cry2-mCh-Rac1(C189A, K183Q)	CLPIT retroviral vector	Prenylation deficient Rac1(K183Q) fused to Cry2-mCh
Cry2-mCh-Cdc42	CLPIT retroviral vector	Full length wild-type Cdc42 fused to the C-terminus of Cry2-mCh
Cry2-mCh-Cdc42(R186K)	CLPIT retroviral vector	Arg-finger-deficient Cdc42 fused to the C-terminus of Cry2-mCh
Cry2-mCh-Cdc42(R186K,C188A)	CLPIT retroviral vector	Arg-finger, prenylation deficient Cdc42 fused to the C-terminus of Cry2-mCh
Cry2-mCh-Cdc42(C188A)	CLPIT retroviral vector	Prenylation deficient Cdc42 fused to the C-terminus of Cry2-mCh
Cry2-mCh-RhoA	CLPIT retroviral vector	Full length wild-type RhoA fused to the C-terminus of Cry2-mCh
Cry2-mCh-RhoA(Δ190-193)	CLPIT retroviral vector	Prenylation, C-tail deficient RhoA fused to the C-terminus of Cry2-mCh
Cry2-Cypet-Rac1	CLPIT retroviral vector	Cry2-Rac1 FRET donor
Cry2-Cypet-Rac1(R186K)	CLPIT retroviral vector	Arg-finger deficient Cry2-Rac1 FRET donor
Ypet-PBD	CLPIT retroviral vector	Rac1 FRET acceptor
Ypet	CLPIT retroviral vector	FRET acceptor control
Tom20-GFP-TIAM	CLPIT retroviral vector	Mitochonrdria localized GFP-TIAM

4.7 References

1. A. B. Jaffe, A. Hall, Rho GTPases: biochemistry and biology. *Annual review of cell and developmental biology* **21**, 247 (2005).
2. A. J. Ridley, H. F. Paterson, C. L. Johnston, D. Diekmann, A. Hall, The small GTP-binding protein rac regulates growth factor-induced membrane ruffling. *Cell* **70**, 401 (1992).
3. A. J. Ridley, A. Hall, The small GTP-binding protein rho regulates the assembly of focal adhesions and actin stress fibers in response to growth factors. *Cell* **70**, 389 (1992).
4. C. D. Nobes, A. Hall, Rho, Rac, and Cdc42 GTPases regulate the assembly of multimolecular focal complexes associated with actin stress fibers, lamellipodia, and filopodia. *Cell* **81**, 53 (1995).
5. S. Etienne-Manneville, A. Hall, Rho GTPases in cell biology. *Nature* **420**, 629 (2002).
6. V. S. Kraynov *et al.*, Localized Rac Activation Dynamics Visualized in Living Cells. *Science* **290**, 333 (2000).
7. M. Machacek *et al.*, Coordination of Rho GTPase activities during cell protrusion. *Nature* **461**, 99 (2009).
8. Y. I. Wu *et al.*, A genetically encoded photoactivatable Rac controls the motility of living cells. *Nature* **461**, 104 (2009).
9. D. M. Dietz *et al.*, Rac1 is essential in cocaine-induced structural plasticity of nucleus accumbens neurons. *Nat Neurosci* **15**, 891 (2012).
10. X. Wang, L. He, Y. I. Wu, K. M. Hahn, D. J. Montell, Light-mediated activation reveals a key role for Rac in collective guidance of cell movement in vivo. *Nat Cell Biol* **12**, 591 (2010).
11. S. K. Yoo *et al.*, Differential Regulation of Protrusion and Polarity by PI(3)K during Neutrophil Motility in Live Zebrafish. *Developmental Cell* **18**, 226 (2010).
12. A. Levskaya, O. D. Weiner, W. A. Lim, C. A. Voigt, Spatiotemporal control of cell signalling using a light-switchable protein interaction. *Nature* **461**, 997 (2009).
13. M. Yazawa, A. M. Sadaghiani, B. Hsueh, R. E. Dolmetsch, Induction of protein-protein interactions in live cells using light. *Nat. Biotech.* **27**, 941 (2009).
14. X. X. Zhou, H. K. Chung, A. J. Lam, M. Z. Lin, Optical Control of Protein Activity by Fluorescent Protein Domains. *Science* **338**, 810 (2012).
15. L. J. Bugaj, A. T. Choksi, C. K. Mesuda, R. S. Kane, D. V. Schaffer, Optogenetic protein clustering and signaling activation in mammalian cells. *Nature methods* **10**, 249 (2013).
16. B. Zhang, Y. Gao, S. Y. Moon, Y. Zhang, Y. Zheng, Oligomerization of Rac1 gtpase mediated by the carboxyl-terminal polybasic domain. *J Biol Chem* **276**, 8958 (2001).
17. Y. Gao, J. Xing, M. Streuli, T. L. Leto, Y. Zheng, Trp56 of Rac1 Specifies Interaction with a Subset of Guanine Nucleotide Exchange Factors. *Journal of Biological Chemistry* **276**, 47530 (2001).
18. R. Dvorsky, M. R. Ahmadian, *Always look on the bright site of Rho: structural implications for a conserved intermolecular interface*. R. Dvorsky, M. R. Ahmadian, Eds., (2004), vol. 5, pp. 1130-1136.
19. E. Hinde, K. Yokomori, K. Gaus, K. M. Hahn, E. Gratton, Fluctuation-based imaging of nuclear Rac1 activation by protein oligomerisation. *Sci. Rep.* **4**, (2014).

20. K. Sandrock, H. Bielek, K. Schradi, G. Schmidt, N. Klugbauer, The Nuclear Import of the Small GTPase Rac1 is Mediated by the Direct Interaction with Karyopherin α2. *Traffic* **11**, 198 (2010).
21. J. Quan, J. Tian, Circular Polymerase Extension Cloning of Complex Gene Libraries and Pathways. *PLoS ONE* **4**, e6441 (2009).
22. J. H. Yu, D. V. Schaffer, Selection of novel vesicular stomatitis virus glycoprotein variants from a peptide insertion library for enhanced purification of retroviral and lentiviral vectors. *Journal of virology* **80**, 3285 (2006).

Chapter 5

Probing Cell-fate Decisions with Optogenetic Neurogenesis

5.1 Introduction

There is great interest within the field of regenerative medicine to understand how precise signaling cues regulate cellular fate and function. This information, in turn, can be used to manipulate and direct cells down particular lineages for the end goal of cell replacement therapies. Of acute interest are efforts to direct neurogenesis, where the understanding and implementation of neural differentiation programs holds promise for mitigating or reversing the effects of Alzheimer's, Parkinson's, ALS, and other neurodegenerative diseases.

The Wnt pathway has been reported to mediate a number of critical events in neurogenesis, including cell proliferation, differentiation, adhesion, polarity, and morphogenesis (*1*). In the canonical Wnt pathway, the key signaling molecule is β-catenin, a transactivating transcription co-factor constitutively localized in the cytoplasm and at the cell membrane in complex with cadherins. In the absence of Wnt signal, cytoplasmic β-catenin binds an Axin/APC scaffold along with GSK-3β (*2*). GSK-3β constitutively phosphorylates β-catenin, which recruits an E3 ubiquitin ligase and ultimately results in constitutive ubiquitination and proteosomal degradation of the cytoplasmic fraction of β-catenin. In the canonical Wnt pathway, upon Wnt binding to its receptors Frizzled (Fzd) and LRP6, GSK-3β is phosphorylated and inactivated, thereby suppressing β-catenin degradation and allowing cytoplasmic accumulation of the β-catenin signaling molecule. β-catenin then translocates to the nucleus in a concentration-dependent, importin-independent manner, where it binds to TCF/LEF and acts as a transcriptional activator for its many target genes (*3*).

There is uncertainty, however, in the precise role β-catenin plays in neuronal differentiation of adult progenitor cells. *In vivo* overexpression studies have demonstrated effects on either cell proliferation or neuronal differentiation (*4-7*), while in vitro studies suggest a context dependent effect of β-catenin (*5, 6, 8-10*). One possibility is that the differential effects of β-catenin depend on signaling strength or timing of the β-catenin molecule. Though independent overexpression studies *in vivo* have suggested both proliferative and differentiating effects of β-catenin, closer inspection reveals experimental differences, such as promoter strength, that may well induce β-catenin at differing transcriptional and signaling levels (*4-8*). *In vitro*, β-catenin function has been linked to FGF2 presence, but FGF2 has also been shown to

enhance β-catenin signaling levels through a mechanism distinct from that of Wnt regulation, allowing for potential synergistic Wnt/FGF activation of β-catenin (*8*). Thus, an unexamined variable in neural progenitor differentiation remains β-catenin signaling levels.

Optogenetic activation of β-catenin signaling holds promise as a powerful tool to interrogate the dependence of the neurogenic program on precise β-catenin dynamics. We have previously shown the ability to tunably regulate β-catenin signaling with light by clustering the LRP6 endodomain fused to the *Arabidopsis* Cry2 protein, which forms protein oligomers upon light illumination (Chapter 2). In this chapter, we first establish the neurogenic influence of strong β-catenin activation in the rat adult hippocampal neural progenitor cell (NPC) model. Then, we optimize both the Cry2-LRP6c optogenetic tool as well as the illumination apparatus to allow for light-induced neuronal differentiation, and we demonstrate the tunability of differentiation as a function of input light modulation.

5.2 Results

To determine the dependence of adult rat hippocampal neural progenitor cells (NPCs) (*11*) on activation of β-catenin signaling, we exposed rat NPCs in culture to a 5 day differentiation protocol in which we modulated the β-catenin pathway through addition of GSK-3 inhibitor CHIR-99021 (CHIR). Cells grown in 0.5% FBS were given 3 μM CHIR for Day 0-1, Days 0-2, Days 0-3, Days 0-4, or Days 0-5 (Figure 5.1A). Immunostaining on Day 5 revealed a marked increase in βIII-tubulin (neuronal) staining corresponding with increased duration of β-catenin signaling. These data suggest that strong β-catenin activation can profoundly influence cell fate decisions for differentiation into a neuronal phenotype. In parallel, we assayed whether cells must immediately receive the β-catenin signal upon withdrawal of proliferative conditions (20 ng/mL FGF2). Here, cells were grown in 0.5% FBS for 0, 1, 2, 3, or 4 days before supplementation with 3 μM CHIR. Neurogenesis was strongest when CHIR was added on day 1 of the 5 day differentiation protocol, and it progressively decreased with increasing delay before β-catenin activation (Figure 5.1B, quantified in Figure 5.2). Notably, however, differentiation was still observed even in samples grown for 3 or 4 days in 0.5% FBS before CHIR addition, suggesting that NPCs may remain primed for neurogenesis despite the extended presence of non-neuronal differentiation conditions.

To further examine the neurogenic effect of CHIR, adult neural stem cells were differentiated in 0.5% FBS and varying CHIR concentrations from 0-3 μM (Figure 5.3A,B). Strong neurogenesis was observed at the 1 μM and more so at the 3 μM levels. As the reported IC_{50} for CHIR 99021 is 10 nM, these data suggest that robust β-catenin activation is required to bias neurogenesis in differentiating adult neural stem cells.

With the knowledge that strong β-catenin activation directly yields neurogenesis, we set out to characterize the dependence of neuronal differentiation on the dynamics of β-catenin signaling using our Cry2-mCh-LRP6c optogenetic tool (Chapter 2). However, numerous initial attempts to differentiate Cry2-mCh-LRP6c-expressing NPCs failed. Illumination experiments were carried out for 5 days, with NPCs seeded in 96 well plates and placed on top of custom-built illumination setups as depicted in Figure 5.4. As experiments reached day 2 or 3, cells began looking unhealthy or dead, though many survived. Staining revealed minimal neurogenesis, and the βIII-tubulin-positive cells that did appear were small and stained weakly. We hypothesized that either: 1) the cells were overexposed to blue light illumination; 2) the signal from the Cry2-mCh-LRP6c construct was insufficient to induce differentiation; or 3) Cry2 clustering is incompatible with neural stem cells and induces cellular toxicity after several days of activation.

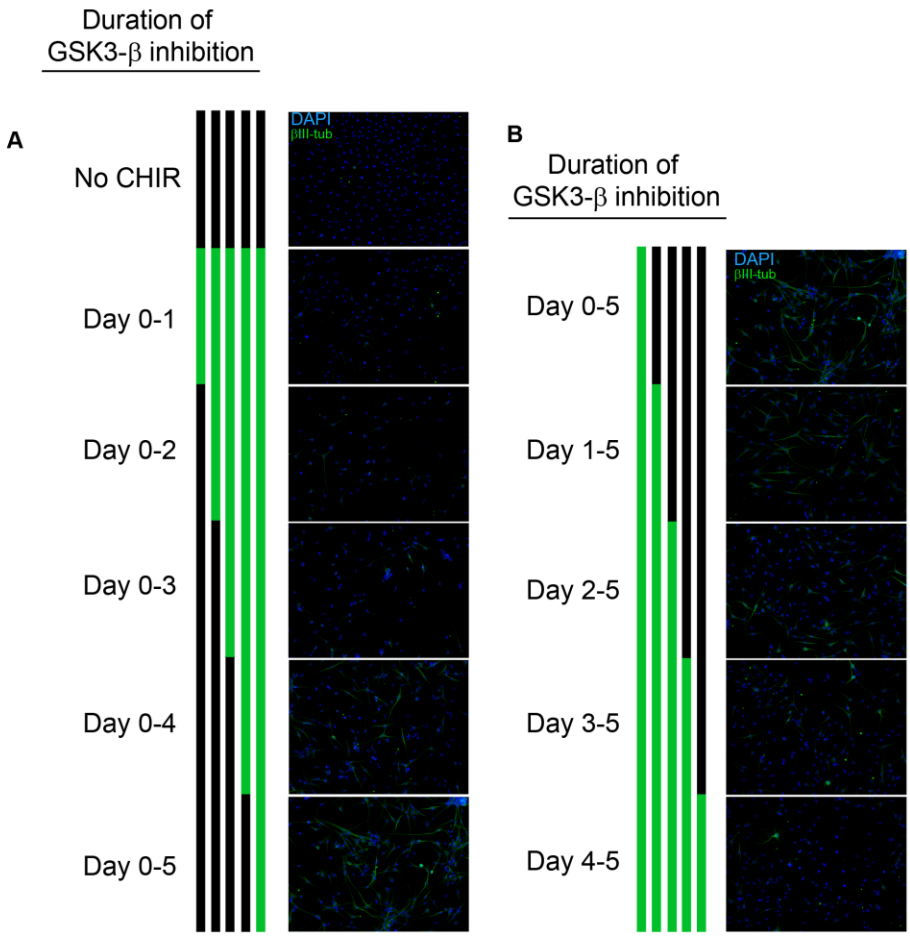

Figure 5.1 β-catenin activation induces neurogenesis in neural progenitor cells (NPCs). A) Addition of GSK-3 antagonist CHIR99021 (CHIR, 3 μM) induces strong neurogenesis upon 5 days of treatment. Treatment for fewer days yields weaker neurogenesis. B) NPCs retained neurogenic potential when CHIR was administered with varying delays before administration. Green bars indicate duration of CHIR treatment.

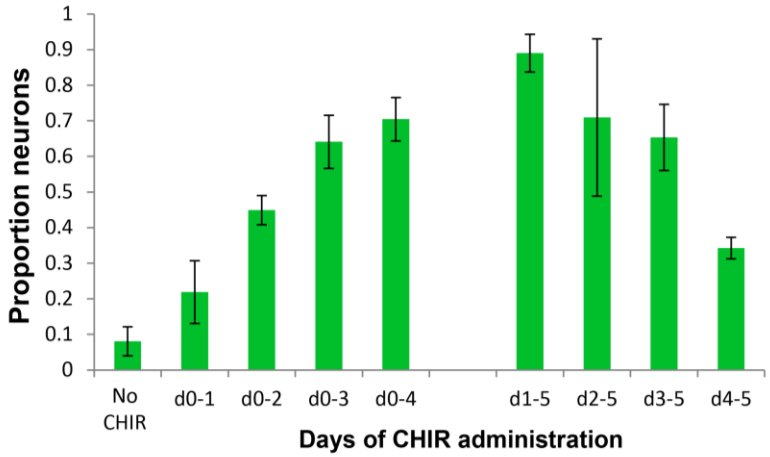

Figure 5.2 β-catenin signaling duration can tune NPC neurogenesis. Graph shows quantification of Figure 5.1.

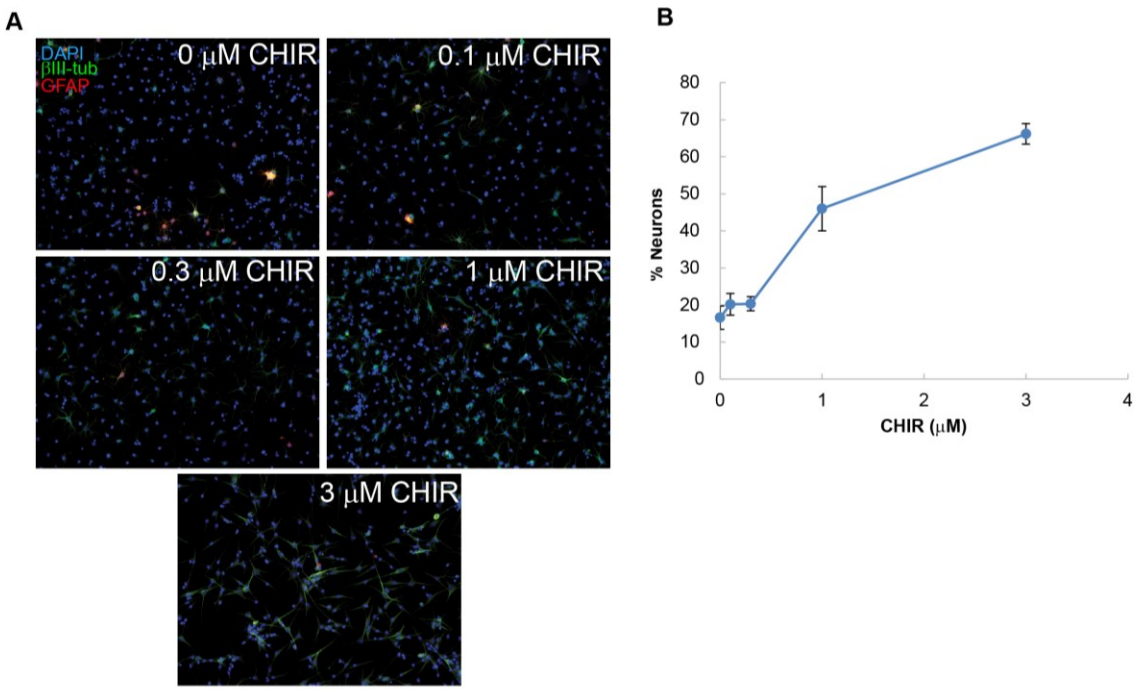

Figure 5.3 Strong β-catenin activation is required for induced neurogenesis in NPCs. A dose response curve shows strong neurogenesis induced by micromolar levels of CHIR, as evidenced by enhanced βIII-tubulin staining for immature neurons after 5 days of 1 and 3 μM CHIR administration (A). Neurogenesis is quantified in (B).

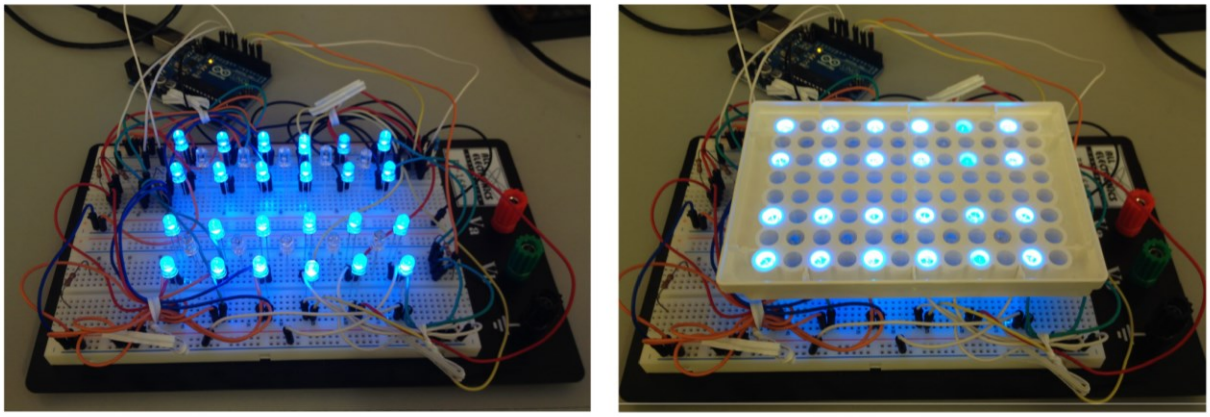

Figure 5.4 LED arrays used for illumination experiments. Clear-bottom 96-well plates were seeded with cells in wells directly above the LEDs. Elevating cell-containing plates above the LEDs and diffusing the incoming LED light with diffuser paper were key modifications necessary for cell survival and optogenetic induction of neurogenesis.

To address the first possibility, we modified the illumination devices shown in Figure 5.4. First, we placed two additional clear-bottom, white-walled 96-well plates in between the plate directly on top of the LEDs and the NPC experimental plate. This was done to lessen the light intensity seen by the cells, as well as to allow the light to diffuse more before encountering the cells for more even illumination. To diffuse the light even more and eliminate intense LED hotspots, we introduced a translucent diffuser paper between the cell plate and the plate stack below it, and we verified the even blue light illumination across each illuminated well. Upon illuminating NPCs with 1 blue light pulse per 5 seconds over 5 days with this modified setup, we noticed significantly less cell death over the course of the experiment, and the illuminated cells were indistinguishable from the ones maintained in dark (data not shown).

To address the concern of an insufficiently strong β-catenin signal from our Cry2-mCh-LRP6c construct, we looked to modify the fusion protein to enhance its signal. One straightforward modification is depicted in Figure 5.5A. Removal of the mCherry gave reproducibly stronger β-catenin signal in response to light. A representative experiment is shown in Figure 5.5B. The signal was typically 2-3 fold higher in transient expression experiments in 293Ts. The enhanced signal may either be due to tighter clustering of LRP6c tails within Cry2 clusters, or perhaps due to enhanced expression levels of the shorter Cry2-LRP6c fusion.

The Cry2-LRP6c fusion was sufficiently potent to strongly photoactivate β-catenin even at single genomic copy expression levels within cells, a result not obtainable with the original Cry2-mCh-LRP6c construct (Figure 5.6). 293Ts harboring the 7x TGP GFP reporter of

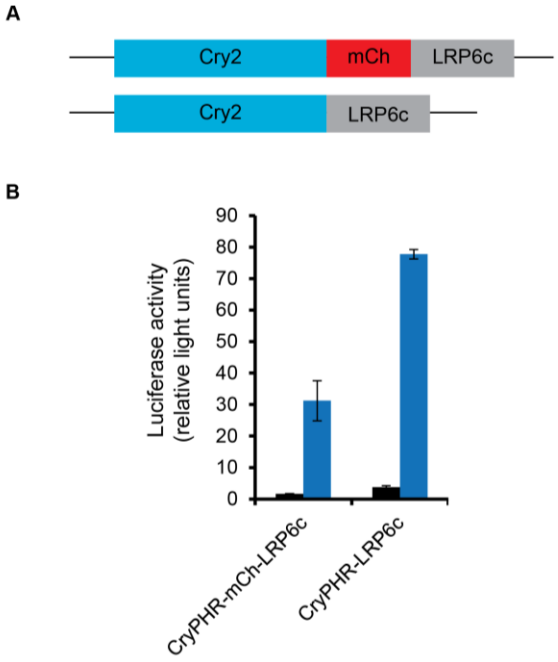

Figure 5.5 Removal of mCherry facilitates stronger light induced β-catenin signal. A) The original Cry2-mCh-LRP6c construct was compared against a construct lacking the mCherry fluorescent protein. B) A representative experiment shows the stronger light-induced signal generated by the shorter, non-fluorescent construct. Graphs show means ± 1 s.d., n = 3 biological replicates.

β-catenin activity were transduced with retrovirus encoding Cry2-LRP6c or Cry2-mCh-LRP6c at an MOI = ~0.1-0.25. After overnight illumination, cells were trypsinized and analyzed for GFP reporter expression. Figure 5.6A shows that only illuminated Cry2-LRP6c-infected cells exhibit reporter expression over background, displaying a shoulder of GFP expression in the flow plot. The small population of cells represented by the shoulder is due to both a noisy reporter baseline (Figure 5.6B), with a fraction of even uninfected cells expressing GFP, as well as the fact that a small population of cells was infected in order to ensure single copy integration. Figure 5.6C demonstrates reporter induction between illuminated and unilluminated cells expressing Cry2-LRP6c at single copy. Reporter cells treated with CHIR are shown as a positive control. Figure 5.7 shows this effect through fluorescent imaging. Cells expressing Cry2-mCh-LRP6c at single copy show no notable light-induced β-catenin induction after overnight illumination. In contrast, single copy Cry2-LRP6c illumination gives strong reporter expression. CHIR treated cells show a strong response and were used as a positive control. In sum, the removal of mCherry from the Cry2-LRP6c fusion provides a significant boost in light-induced signaling strength that allows photoactivation of β-catenin signaling at single copy expression within cells.

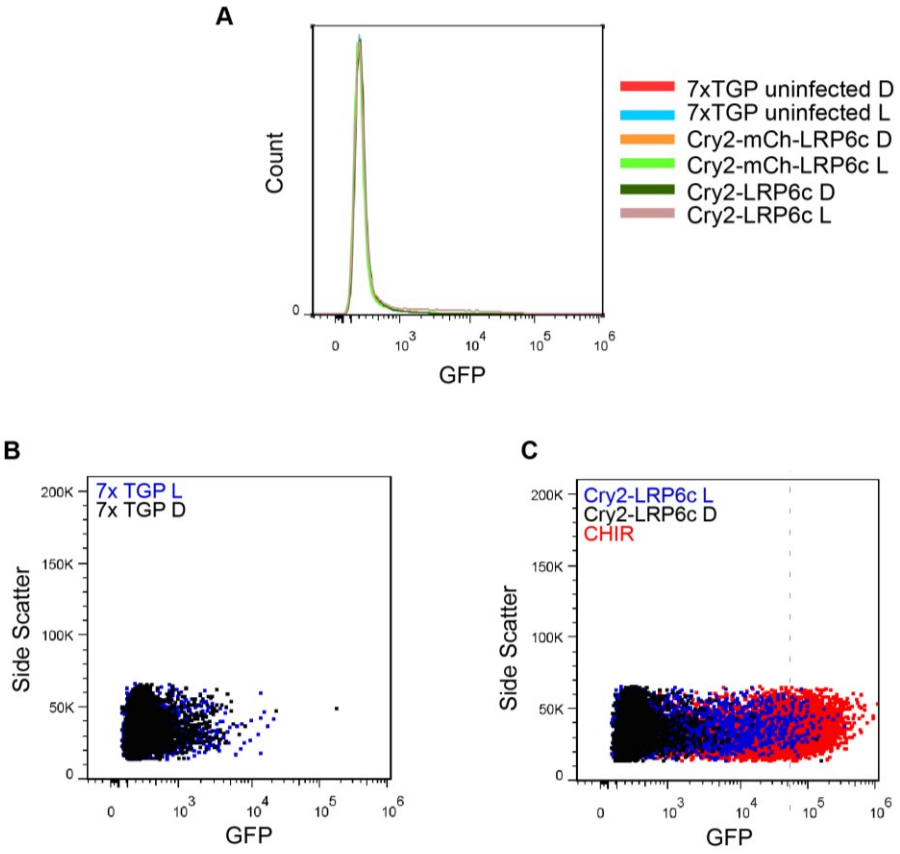

Figure 5.6 Cry2-LRP6c can activate a fluorescent β-catenin reporter in cells harboring a single genomic copy of the construct. A) Comparison of β-catenin-dependent GFP reporter expression in reporter cells transduced with a single copy of Cry2-mCh-LRP6, Cry2-LRP6c, or no construct. Only illuminated cells expressing Cry2-LRP6c exhibit reporter expression. B) Cells expressing only the reporter demonstrate some basal GFP expression, presumably due to basal physiological activation of the pathway. C) Scatter plot representation of GFP reporter expression upon illumination of cells expressing Cry2-LRP6c. Reporter expression induced by 3 μM CHIR is displayed as a positive control.

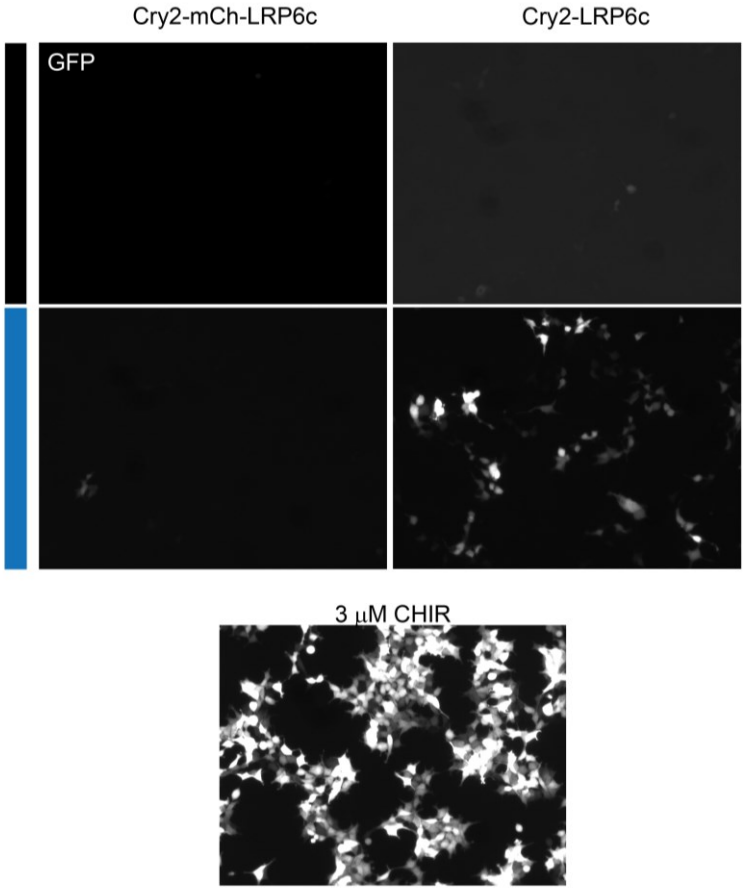

Figure 5.7 Cry2-LRP6c can activate a fluorescent β-catenin reporter in cells harboring a single genomic copy of the construct. Representative images of Figure 5.6 show that the Cry2-mCh-LRP6 construct – at single genomic copy – fails to induce substantial GFP reporter expression at single genomic copy. In contrast, Cry2-LRP6c strongly induces reporter expression under these conditions. The small fraction of activated cells compared to the CHIR activated cells is due largely to only ~10-20% of cells being transduced with Cry2-LRP6c to ensure single copy integration of the construct.

Pursuing the hypothesis that smaller proteins may get expressed at higher concentrations and thus yield more clusters and signal induction, we resolved to explore if we could find a minimal Cry2 clustering domain, or if Cry2PHR was already such a domain. We created two conservative mutations, removing either an alpha helix from the C-terminus or a β-strand from the N-terminus (Figure 5.8A) of Cry2-mCh-LRP6c. Figure 5.8B shows the location of these features on a structure of the PHR domain of *Arabidopsis* Cry1, which shares homology with Cry2 and is the only *Arabidopsis* Cryptochrome structure solved to date. Expression of these constructs within HEK 293T cells yielded no obvious clustering under blue light exposure (Figure 5.9A). To test whether clustering might be happening below the diffraction limit where we would not observe it through fluorescence microscopy, we expressed these constructs within β-catenin luciferase reporter cells. In contrast to the light-induced difference seen with the wild-type Cry2-mCh-LRP6c construct, no signal was observed with the N- or C-terminal mutants, suggesting that the Cry2PHR domain may be the minimal clustering domain and is highly sensitive to further protein truncation.

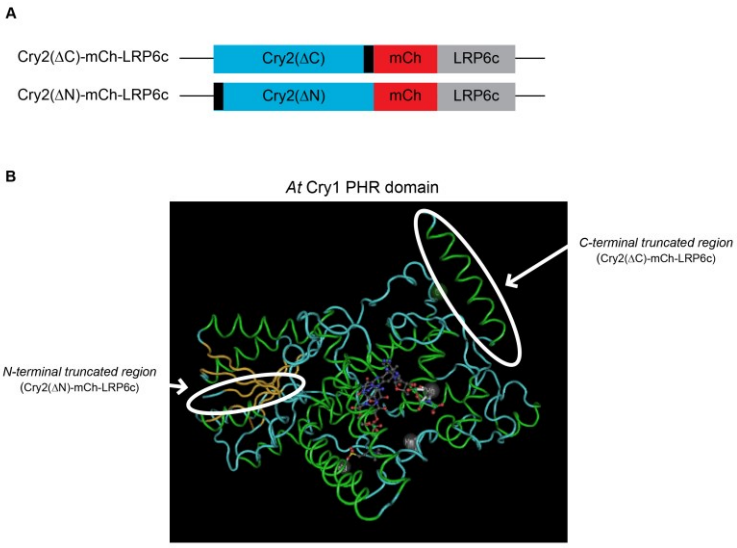

Figure 5.8 Strategies for identifying minimal Cry2 clustering domain. A) C- and N-terminal truncations of Cry2-mCh-LRP6c were generated, removing either a C-terminal α-helix or N-terminal β-strand, respectively (B).

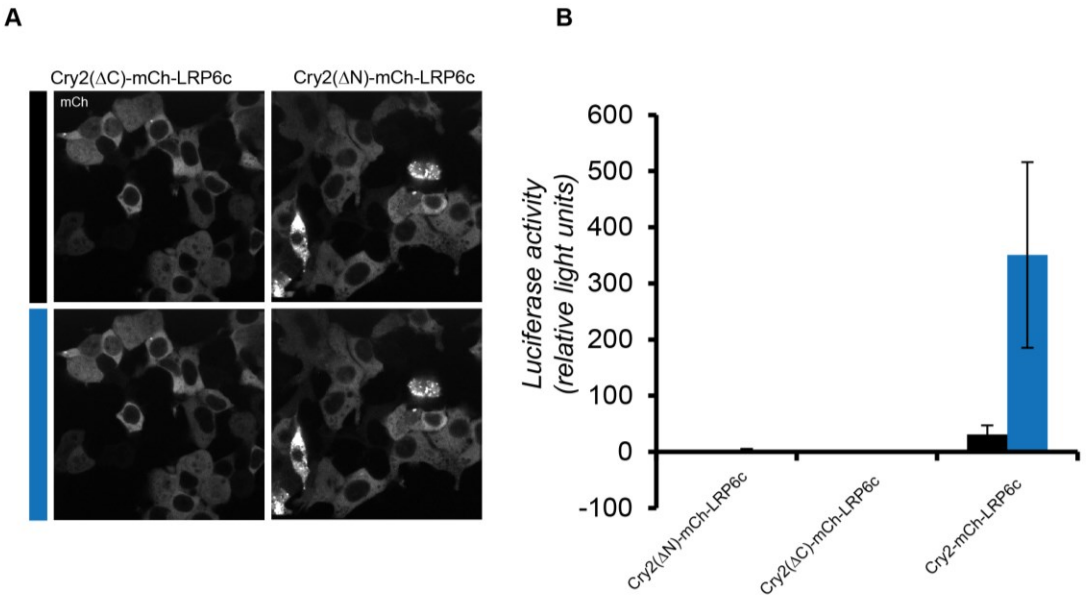

Figure 5.9 Cry2 truncations do not cluster. A) 293Ts expressing the Cry2-mCh-LRP6c truncations described in Figure 5.8 exhibit strong fluorescence, but do not cluster upon light activation. B) To further verify that clustering wasn't occurring, luciferase reporter cells expressing the mutants were illuminated overnight and a luciferase assay was performed to assay β-catenin pathway activation. No signal was observed for either truncation. Graph shows means $\pm$ 1 s.d. for biological triplicates.

As a final strategy for signal enhancement, we attempted to enhance the cytoplasmic protein concentration by exporting the nuclear fraction of the Cry2-LRP6c fusion. We fused the nuclear export sequence (NES) from the HIV Rev protein to the C-terminus of either the Cry2-mCh-LRP6c or the Cry2-LRP6c fusion. Although the Cry2-mCh-LRP6c-NES fusion exhibited enhanced cytoplasmic localization compared to Cry2-mCh-LRP6c (Figure 5.10), no increase in light induced signal was observed by luciferase assay of β-catenin pathway activation (Figure 5.11). Similar results were obtained for the Cry2-LRP6c-NES fusion, except that this fusion expressed high levels of signaling in the dark for reasons we did not investigate. The unaltered signal with increased background in the dark prompted us to abandon the NES variants and continue with the Cry2-LRP6c construct for experimentation.

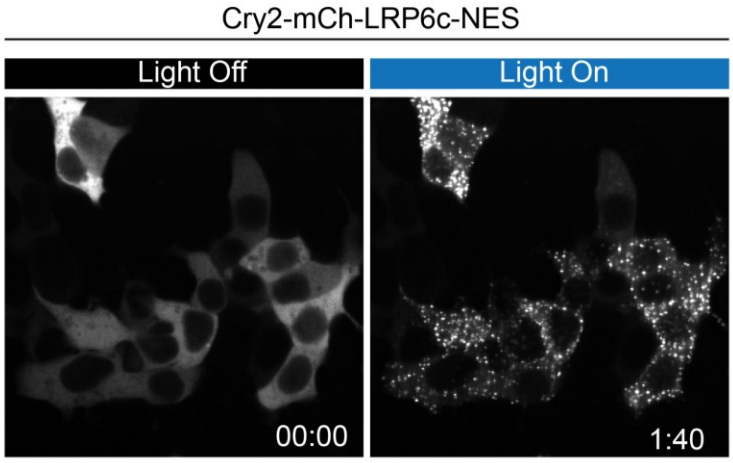

Figure 5.10 A nuclear export sequence (NES) enhances cytoplasmic localization of Cry2-mCh-LRP6c. The Cry2-mCh-LRP6c-NES fusion appears mostly cytoplasmic and retains its ability to cluster under blue light.

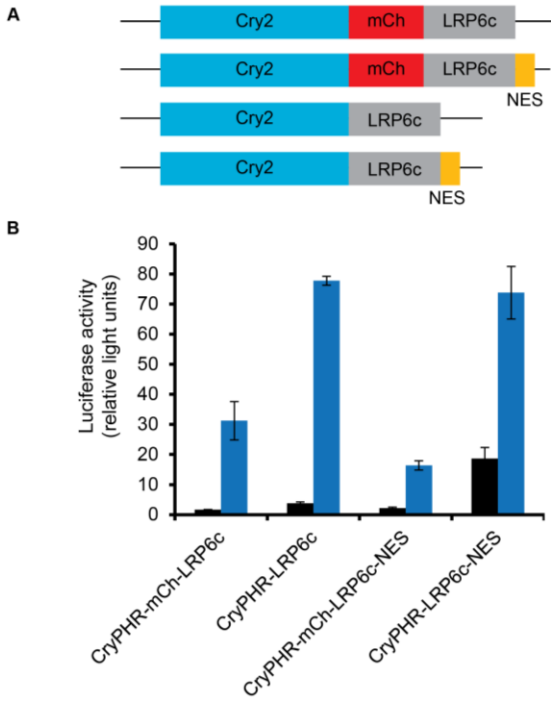

Figure 5.11 Light induced β-catenin signal is not enhanced by addition of an NES on Cry2-mCh-LRP6c or Cry2-LRP6c. A) The NES from the HIV Rev protein was appended to the C-terminus of either the Cry2-mCh-LRP6c or Cry2-LRP6c constructs. B) Reporter cells were transfected with these constructs and illuminated overnight. A luciferase assay reveals that the NES-bearing constructs did not enable enhanced signal generation. Instead, basal signaling was increased in the dark state. Graph shows means ± 1 s.d. of biological triplicates. Data for the non-NES containing constructs as also displayed in Figure 5.5B.

To determine if our hardware and protein modifications would enable light-induced neurogenesis, we infected NPCs with retrovirus encoding Cry2-LRP6c at either an MOI = 3 or at single copy infection levels, in both cases followed by puromycin selection. After five days of a light exposure protocol, we fixed cells and stained them for the immature neuronal marker βIII-tubulin. In all light-administered cases tested, robust neurogenesis was observed, compared to minimal neurogenesis in the absence of light (Figure 5.12). Both cells infected at single copy and those infected MOI = 3 differentiated, both with one pulse every 5 seconds and one light pulse every 10 seconds (Figure 5.13). Light-induced neurogenesis was observed at levels comparable to those obtained by 3 μM CHIR addition (~50-60% of cells stained positive for neurons). Interestingly, neurons produced by light exhibited a flat morphology and typically did not establish strong polarity at the five day timepoint, in contrast to elongated neurons obtained by CHIR addition. This difference is undergoing further study.

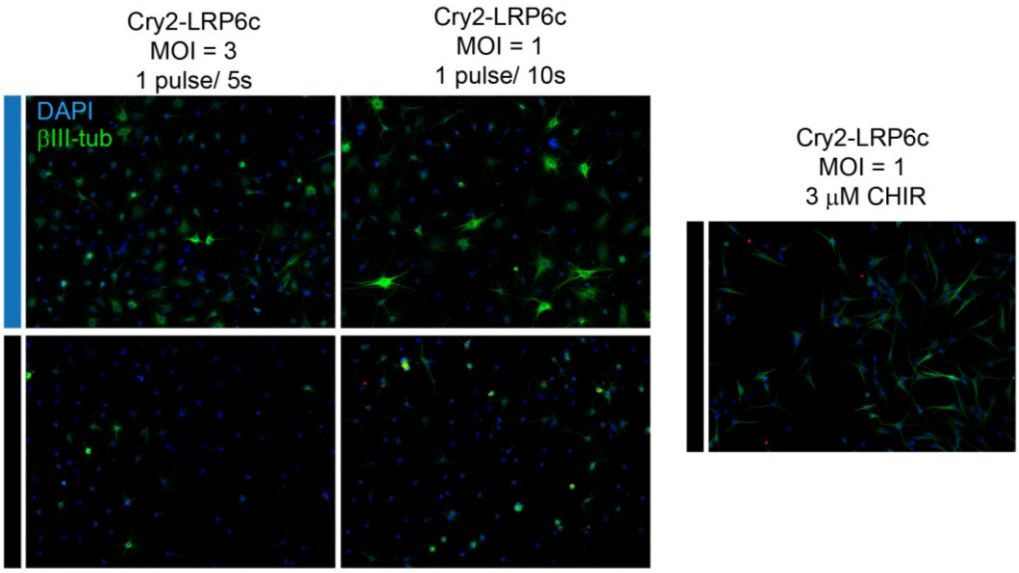

Figure 5.12 Optogenetic neurogenesis of NPCs. NPCs transduced with either single copy or MOI = 3 Cry2-LRP6c exhibited robust neurogenesis upon five days of pulsed blue light illumination. Blue and black bars indicate illuminated and unilluminated samples, respectively. For a positive control of neurogenesis, cells were administered with 3 μM CHIR for 5 days.

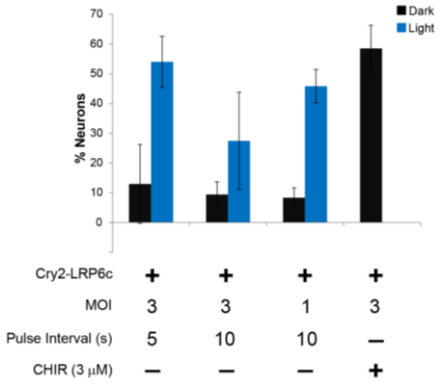

Figure 5.13 Quantification of optogenetic neurogenesis. Neurogenesis was observed in cells infected at both MOI = 3 as well as at single genomic copy. Light pulsing every 5 s gave similar results to pulsing every 10 s. Graph shows mean ± 1 s.d. from biological triplicates for each condition.

Finally, to study how neural stem cell fate changes with varying β-catenin dynamics, we require the ability to tune neurogenesis by tuning the β-catenin signaling input. Two methods for achieving this are either tuning the intensity of the activating blue light, or tuning the duration between activating pulses. Figure 5.14A demonstrates how applying different intensities of blue light over the course of a 5 day differentiation experiment can tune neurogenic levels according to β-catenin signaling input. Figure 5.14B gives representative images of illumination experiments demonstrating an increase in neurogenesis upon increasing the activating pulse frequency between one pulse per hour to one pulse per 5s. Together, these data show that Cry2-LRP6c can indeed be used to strongly regulate neuronal stem cell differentiation, and modulation of the presentation of the activating light source can tune the neurogenic program.

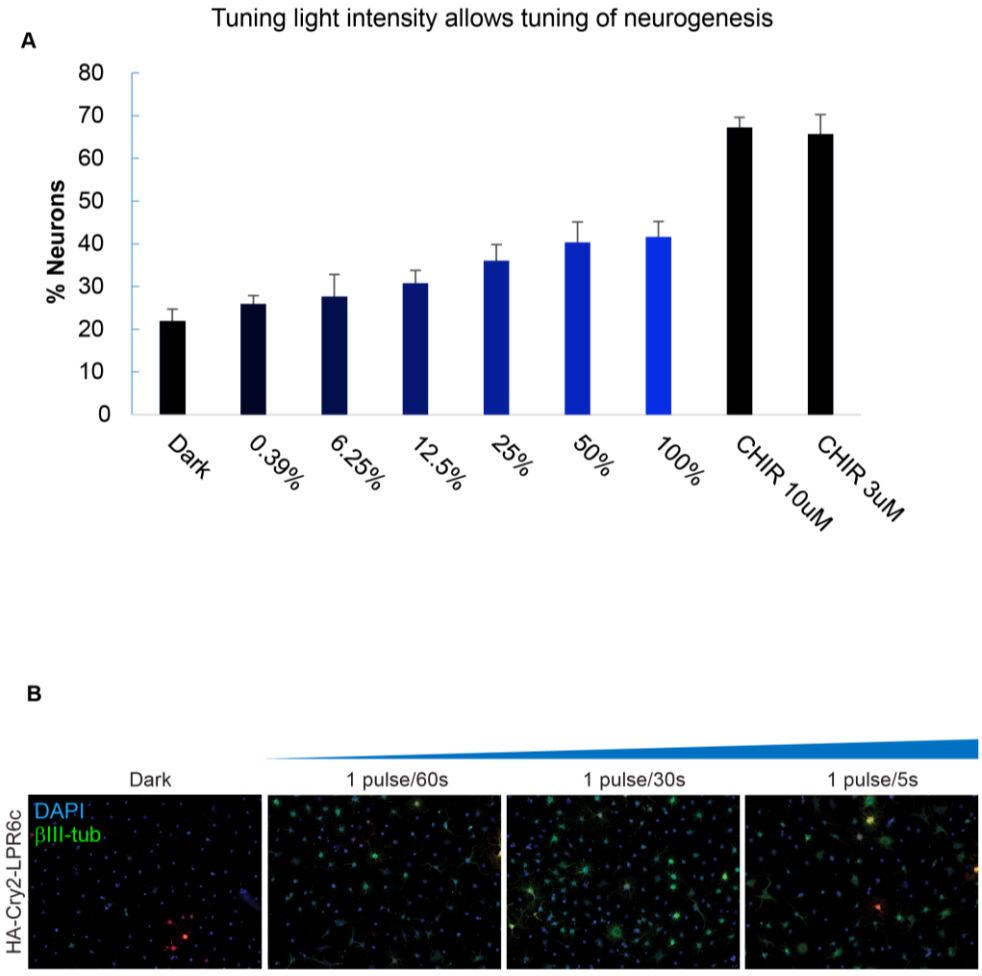

Figure 5.14 Tuning optogenetic neurogenesis. A) NPCs expressing Cry2-LRP6c were differentiated with light of differing intensities. Neurogenesis was a function of pathway activation intensity. Graph shows mean ± 1 s.d. frombiological triplicates for each condition. B) Tuning illumination by varying light pulse frequency can also enable tuning of the neurogenic response.

5.3 Discussion

Understanding the cues directing neurogenesis is an important step in developing therapies that may replenish degenerating pools of neurons typical of many neurological diseases, including Parkinson's, Huntington's, and Alzheimer's diseases. Furthermore, as we understand more about signal transduction within cellular systems, it is becoming clear that the simple presence or absence of an important cue may not be sufficient information to instruct cellular fate; rather, the time-varying dynamics of the signal and signal strength may be an equally key factor (*12*). In this chapter, we have optimized our optogenetic and illumination tools to be compatible with neural stem cell culture and survival and have combined both to enable robust, tunable neurogenesis via light activation.

As there exists controversy in the field over the precise role of β-catenin in neurogenesis, we began our experiments by characterizing the neurogenic effect of strong small molecule activation of the pathway. Though we definitively show a neurogenic influence upon 3-5 days of β-catenin signaling, we cannot rule out pathway-dependent stimulation of proliferation as well. Elucidating the role of early and/or late β-catenin signals of varying strengths on cell proliferation or differentiation will be an interesting early application of optogenetic neurogenesis.

Our initial inability to induce neurogenesis with the Cry2-mCh-LRP6c tool (Chapter 2) motivated us to undertake significant optimization of the experimental system. The consistent increase in light-induced pathway activation with the Cry2-LRP6c vs. the Cry2-mCh-LRP6c fusion (Figure 5.5) may be due to either closer proximity of LRP6c tails in the absence of the mCherry, or perhaps due to an increased intracellular concentration of the smaller protein. Notably, signal increase was enhanced with minimal increase in background signaling in the dark state (Figure 5.5) Though additional engineering efforts were unable to further enhance pathway activation, the stronger signal mediated by mCherry removal alone was sufficient to enable single-genomic-copy modulation of β-catenin signaling (Figure 5.6, Figure 5.7). This is valuable to minimize insult to the cellular system of study. Further, linking a single genomic copy to a cellular phenotype will be valuable for screening strategies for potential directed evolution studies modulating Cry2 properties.

Modifications of the illumination devices proved crucial to successful optogenetic neurogenesis, and this should serve as a caution for all optical perturbations of cellular function, particularly those using blue light activation. Cellular phototoxicity must be considered in optogenetic experiments, particularly ones lasting several days or weeks. Overall, it is advisable to use as little light as possible to achieve the desired outcome/application. Different cells display different levels of sensitivity to extended illumination; while 293Ts may visibly appear unaltered after days of constant LED illumination, NPCs will display extensive cell death. It is also worth mentioning that even in the absence of visible morphological changes, intracellular physiology may well be altered by extensive light activation. In light of this, optogenetics experiments should always be conducted with the minimal light necessary for the desired effect, and appropriate controls and characterizations should be employed to ensure that the observed phenotypes are not an artifact of the experimental illumination.

Additionally, the importance of actively diffusing the incident LED light to provide even illumination across a well should not be understated. Though difficult to see by eye, "hotspots" of light are produced by undiffused LED illumination. In addition to enhanced cytotoxicity from the hotspots, the differences in illumination intensity can lead to differential induced phenotypes across an individual experimental well. Thus, depending where in the well a camera is pointed, disparate conclusions may be drawn from identical experimental conditions. The altered neurogenic potential of different light intensities (Figure 5.14) indicates that subtle changes in light intensity can lead to differential neurogenic induction, an effect that may be seen in individual experimental wells if efforts are not made to ensure even, diffuse illumination.

The ability to induce neurogenesis via Cry2 clustering indicates that Cry2 clusters are not inherently cytotoxic, as may have been hypothesized on account of several pathological conditions that are coincident with large protein aggregates (*13*). Still, it remains unexamined whether *Arabidopsis* Cry2 clusters are entirely orthogonal in a mammalian cellular context. Indeed, the morphology is notably different between Cry2-LRP6c and CHIR-induced neurons, which display a flattened and multipolar vs. elongated phenotype, respectively. As an example, the human E3 ubiquitin ligase COP1 has been shown to interact with *Arabidopsis* Cry2 in a light-promoted manner (*14*). More characterization must be undertaken to understand which, if any, cellular components interact with Cry2 clusters, and whether these interactions introduce artifacts into the system of study. Once these interactions are understood, protein engineering approaches may be undertaken to disrupt these interactions and enhance the orthogonality of the Cry2 module.

Now that we have established optogenetic neurogenesis, precise characterization, tuning, and interrogation of the neurogenic program is possible. Establishing the dependence of fate choices on signal strength and profile are the immediate next goals. Identifying other, earlier markers of neural differentiation will allow finer dissection of when and how the fate decision is made. Additionally, the striking difference between neuronal morphology in CHIR vs. light treated cells during 5-day differentiation may yield insights into how the GSK3 complex regulates neurogenesis, or alternatively into how Cry2 interacts with mammalian cells. Finally, recent work by Nusse and colleagues suggests a role of sub-cellular localization of Wnt signaling regulating cellular identity in asymmetric cell division (*15*). Using subcellular patterned photoactivation, spatial considerations of β-catenin signaling in the processes of NPC differentiation and proliferation may now also readily be examined.

5.4 Methods

Cloning and viral production

All constructs were cloned using the CPEC method and as described in Chapter 2. Constructs for viral packaging were subcloned into the MMLV retroviral vector CLPIT, which provides tetracycline repressible transgene control. Virus was packaged as described (*16*), in the presence of 3 μg/mL doxycycline to repress transgene expression. Lentiviral plasmids encoding the 7x TFP and 7x TGP luciferase and GFP reporters were obtained from Addgene (www.addgene.org, plasmid # 24308 and #24305) and were packaged in HEK 293T cells.

Cell culture

HEK 293Ts were cultured on polystyrene plates in Iscove's Modified Eagle Medium (Corning cellgro, Manassas, VA) with 10% fetal bovine serum (FBS) (Life Technologies) and 1% penicillin/streptomycin (P/S) (Life Technologies) at 37°C and 5% CO_2. Rat hippocampal adult neural stem cells (NSCs) (*11*), were cultured on polystyrene plates coated with poly-ornithine and 5 μg/mL laminin (Life Technologies, Grand Island, NY). NSCs were cultured in Dulbecco's Modified Eagle Medium (DMEM)/F12 (1:1) high-glucose medium containing N-2 supplement (both from Life Technologies) and 20 ng/mL recombinant human FGF-2 (Peprotech, Rocky Hill, NJ). CHIR99021 was obtained from StemRD, Inc. Illumination/differentiation experiments were conducted in 200 uL DMEM/F12 + N2 + 0.5% FBS per one well of a 96-well plate. Stable NSC cell lines were created via 2 h viral infection, after which medium was exchanged to prevent stem cell exposure to residual FBS in the viral aliquots. 16 h after infection, 0.6 μg/mL puromycin was added to select for transduced cells. Selection was monitored in a parallel, untransduced plate. 48-72 h were required for full death of untransduced cells.

Luciferase assay

293T cells harboring the 7x TCF luciferase reporter were seeded in black walled 96-well plates, and 5 ng of expression vector diluted in 150 ng pBluescript was transfected into each well by the calcium phosphate method. 24 hours after transfection, cells were subjected to a light illumination protocol from a custom LED illumination device. Briefly, an LED array was constructed based on the open source electronics Arduino platform (www.arduino.cc). 5 mm blue LEDs (470 nm, 9000 mCandella, 15-20° illumination, www.theledlight.com, # SS5B4SDACY) were placed underneath wells of a 96 well plate and were driven through independent channels by the Arduino. Custom software was written to allow illumination with definable light pulse width, frequency, and intensity. The code can be found in Chapter 2 Appendix A. An example of an illumination device is pictured in Figure 5.4. The plate with cells was aligned above the LED device so that the LEDs illuminated directly underneath individual wells, but the plate was elevated 2 platewidths above the LEDs and a sheet of diffuser paper (Anchor Optics, # AX27421) was placed underneath the cell plate to give even illumination across the well. 500 ms blue light pulses were administered every 10 s or as defined. After 16

hours of illumination, cells were lysed, and luciferase was measured with the Luc-screen Firefly Luciferase Gene Reporter System (Life Technologies).

Immunostaining.

Upon completion of a differentiation experiment conducted in a 96 well plate, cells were fixed and immunostained with great care to avoid cell detachment. Briefly, medium was removed so that approximately 100 μL remained within a well, avoiding complete washout. 4% paraformaldehyde (PFA) was supplemented up to 400 μL, yielding a final fixing concentration of 3% PFA. After 10 minutes, five ¾ washes with PBS were performed to remove PFA. Cells were then blocked for 1 h in 5% donkey serum (DS), after which they were supplemented with primary antibody against βIII-tubulin (Covance MRB-435P 1:1000, or Sigma T8578 1:1000). After overnight incubation at 4°C, wells were washed with five ¾ PBS washes and incubated in PBS with 5% DS, FITC-conjugated secondary antibodies (Jackson Immunoresearch, 1:250), and DAPI (1:2000). After 1 h incubation with gentle shaking at RT, cells were washed with five ¾ PBS washes. Cells were retained in 200 μL PBS per well for imaging.

Imaging

Time lapse microscopy of activated Cry2 fusions in HEK 293Ts was performed using a BX51WI microscope (Olympus Corporation, Center Valley, PA) equipped with Swept Field Confocal technology (Prairie Technologies, Inc., Middleton, WI). Imaging was carried out at room temperature. Simultaneous blue light exposure and mCherry imaging was accomplished by imaging in both 488 nm and 561 nm laser channels, 1 exposure per 2-5 seconds, with 488 nm laser varied between 0.1 and 100% power. Given the minute-timescale of the dissociation kinetics of Cry2 clustering, this intermittent pulsing was considered a sufficient approximation of continuous exposure and was necessary to avoid extensive photobleaching of the mCherry fluorophore. For imaging differentiation experiments, the Molecular Devices ImageXpress Micro high content imager was used with DAPI and FITC filter cubes.

Image Analysis

Stacks of timelapse images were assembled in ImageJ (http://rsbweb.nih.gov/ij/). For immunostaining quantification, image channels were combined and nuclei were counted in CellProfiler (www.cellprofiler.com). Brightness levels were adjusted equally among all channels in Adobe Photoshop, and neuron quantification was performed manually from a subset of representative images from each experimental well. Numbers of neurons were divided by total nuclei numbers to obtain the percentage of cells that differentiated into neurons. Three fields were analyzed per 96-well plate, and three biological replicates were averaged per experimental condition.

Flow Cytometry

293T cells harboring the 7x TGP reporter were infected at MOI ~ 0.25 with retrovirus encoding the Cry2-LRP6c construct. After 3 days incubation to allow for protein expression, cells were seeded in 35 mm plates and illuminated overnight with a 19 LED array (ledlight.com, cat. # 28345) administered at one 500 ms pulse per 10 s. Cells were imaged for fluorescent GFP reporter expression and were subsequently trypsinized, resuspended in PBS, and fluorescence was analyzed quantitatively with flow cytometry using the FC500 flow cytometer (Beckman Coulter). Flow cytometry data was analyzed using the FlowJo software.

5.5 Acknowledgements

I would like to thank Alyssa Rosenbloom, Atri Choksi, Colin Mesuda, Diane Klein, and Nicole Repina for technical help in many of the experimental protocols.

5.6 References

1. W. J. Nelson, R. Nusse, Convergence of Wnt, beta-catenin, and cadherin pathways. *Science* **303**, 1483 (2004).
2. A. Kikuchi, Regulation of beta-catenin signaling in the Wnt pathway. *Biochem Biophys Res Commun* **268**, 243 (2000).
3. R. T. Moon, A. D. Kohn, G. V. De Ferrari, A. Kaykas, WNT and beta-catenin signalling: diseases and therapies. *Nat Rev Genet* **5**, 691 (2004).
4. D. C. Lie *et al.*, Wnt signalling regulates adult hippocampal neurogenesis. *Nature* **437**, 1370 (2005).
5. T. Kuwabara *et al.*, Wnt-mediated activation of NeuroD1 and retro-elements during adult neurogenesis. *Nat Neurosci* **12**, 1097 (2009).
6. Q. Qu *et al.*, Orphan nuclear receptor TLX activates Wnt/beta-catenin signalling to stimulate neural stem cell proliferation and self-renewal. *Nat Cell Biol* **12**, 31).
7. D. Zechner *et al.*, [beta]-Catenin signals regulate cell growth and the balance between progenitor cell expansion and differentiation in the nervous system. *Developmental Biology* **258**, 406 (2003).
8. N. Israsena, M. Hu, W. Fu, L. Kan, J. A. Kessler, The presence of FGF2 signaling determines whether beta-catenin exerts effects on proliferation or neuronal differentiation of neural stem cells. *Dev Biol* **268**, 220 (2004).
9. D. Fang *et al.*, Phosphorylation of Î²-Catenin by AKT Promotes Î²-Catenin Transcriptional Activity. *Journal of Biological Chemistry* **282**, 11221 (2007).
10. W. Y. Kim *et al.*, GSK-3 is a master regulator of neural progenitor homeostasis. *Nat Neurosci* **12**, 1390 (2009).
11. F. H. Gage *et al.*, Survival and differentiation of adult neuronal progenitor cells transplanted to the adult brain. *Proceedings of the National Academy of Sciences of the United States of America* **92**, 11879 (1995).
12. J. E. Purvis, G. Lahav, Encoding and Decoding Cellular Information through Signaling Dynamics. *Cell* **152**, 945 (2013).
13. M. Bucciantini *et al.*, Inherent toxicity of aggregates implies a common mechanism for protein misfolding diseases. *Nature* **416**, 507 (2002).
14. I. Ozkan-Dagliyan *et al.*, Formation of Arabidopsis Cryptochrome 2 Photobodies in Mammalian Nuclei: APPLICATION AS AN OPTOGENETIC DNA DAMAGE CHECKPOINT SWITCH. *Journal of Biological Chemistry* **288**, 23244 (2013).
15. S. J. Habib *et al.*, A Localized Wnt Signal Orients Asymmetric Stem Cell Division in Vitro. *Science* **339**, 1445 (2013).
16. J. H. Yu, D. V. Schaffer, Selection of novel vesicular stomatitis virus glycoprotein variants from a peptide insertion library for enhanced purification of retroviral and lentiviral vectors. *Journal of virology* **80**, 3285 (2006).

Chapter 6

Conclusion

In the study of cell signaling and cell fate decisions, significant knowledge has been gained through experiments employing pharmacological perturbations and genetic modifications, which have allowed us to identify key molecules important in signaling networks regulating various cellular processes. As our abilities to observe cells and tissues has advanced, however, we are understanding that protein signals instruct biological processes in more complex ways than just through their presence or absence. The dynamics of a signal – or its time varying protein concentration, activity, or localization – can strongly inform and instruct cellular function. Although observation of these dynamic phenomena has been enhanced through various techniques including fluorescent protein imaging, we have lacked the ability to manipulate – and thus to fully understand – how signaling dynamics can regulate cellular systems.

The engineering of plant and microbial photosensory proteins to regulate biological processes has attracted significant interest within the past decade, and its implementation to regulate neurons within complex networks has transformed the field of neurobiology. In studying cell signaling and cell fate choices, optogenetic perturbation conceptually offers the ideal methodology to study how cells respond to dynamic signaling perturbations. The first published efforts were described in late 2009, and several optogenetic tools have been published since. However, the field has not reached a consensus on which optical tools to use, partially due to varied modes of activation for individual signaling nodes, but also due to significant shortcomings with current approaches, including the necessity of an exogenously supplied chromophore, cell-type dependent expression and function, and non-modularity.

In this dissertation, I have described my work developing a novel mode of optogenetic protein activation that avoids the above limitations, and moreover can be entirely encoded on a single peptide chain, reducing experimental complexity. *Arabidopsis* Cryptochrome 2 (Cry2) had been demonstrated to cluster upon light activation within plants, but we have demonstrated that this ability is retained within mammalian cells, using only the shorter Cry2 photolyase homology region (PHR) domain lacking its C-terminal tail. As in plants, the mechanism of clustering is unknown, as are the identities of other necessary components necessary. A remaining open question is if the Cry2 clusters interact with endogenous mammalian components in clustered or unclustered form, and if these interactions might impact the host cellular physiology.

Regardless, we have shown that Cry2 clustering within mammalian cells can reversibly cluster protein fusions, and this clustering can activate target signaling nodes and networks and can regulate cellular function and fate choices in a manner tunable by light. Promisingly, our ability to achieve these results – particularly ones requiring long-term illumination, such as neurogenesis – indicates that non-specific Cry2 impact on cellular physiology may be minimal, and that prolonged exposure of cells to large Cry2 aggregates may be non-toxic.

In addition to clustering exogenously expressed and overexpressed signaling proteins, which may in some instances enhance basal signaling levels or otherwise disturb endogenous signal homeostasis, our demonstration that Cry2 can be used to physically cluster endogenous signaling proteins may now enable optical perturbation of fully endogenous signaling machinery, reducing experimental noise and artifacts often associated with protein overexpression necessary for many current techniques. And since the intracellular targets of the CLICR method are determined by the binding adapter used, this technique is highly modular and definable by the experimenter. We anticipate this advance will find broad utility, particularly for those instances where even low-level expression of a signaling molecule is problematic.

The discovery that the three best studied GTPases Rac1, RhoA, and Cdc42 are sensitive to clustering was intriguing and points to the utility of Cry2 to uncover modes of regulation not previously known. Whether Rho GTPase cluster-induced activation occurs in the native cellular setting is unclear and has never been described. It is possible that current imaging methods have been insufficiently sensitive to distinguish GTPase clustering for these proteins. Nevertheless, our results with Cry2 clustering clearly demonstrate a strong oligomerization effect on translocation and activation, and our sensitive methods for activation detection may also allow interrogation as to whether GTPase multimerization occurs to regulate Rho GTPase signaling within the native Rho GTPase population. It will also be interesting to investigate whether other important intracellular enzymes possess a similar ability for cluster-induced regulation, perhaps pointing to a widely generalizable signaling strategy to achieve signal activation and/or enhancement.

Finally, achieving tunable neurogenesis through light-tunable β-catenin activation in neural progenitor cells encourages our efforts and demonstrates our ability to regulate biological processes by inputting signaling profiles into a computer which then communicates this program to cells with light. Technological advances in illumination devices will enable more sophisticated illumination patterns in both time and space, allowing more complex and multiplexed analysis both in cell culture and in living animals. Importantly, the necessary optimizations to our protein and hardware design teach important lessons on the role that phototoxicity may play in these experiments, but also that these limitations may be overcome with careful characterization and control of our test systems.

The ability to fully encode Cry2 in the DNA, the lack of exogenous chromophore, the modularity, the single peptide chain nature, the strong expression and function across numerous cell types, and the demonstrated ability to tunably regulate cellular function make Cry2 oligomerization an exciting optogenetic modality that we expect will find broad application across the bioscience community. Our described results were accomplished using the wild-type Cry2 protein. Looking forward, there is great potential for protein engineering approaches to deliver interesting Cry2 variants with altered clustering or de-clustering kinetics, variants that may be more orthogonal within the mammalian cellular context, and variants that respond to altered light sensitivities allowing combinatorial control of multiple signaling pathways. We anticipate that these and other modifications will further empower optogenetic approaches to precisely probe biological systems, enabling a more complete understanding of how protein signaling regulates processes from cell fate decisions to tissue development and organization, as well as the dysregulation of these processes in disease.